AN ABSTRACT OF THE DISSERTATION OF

Chien-Chih Huang for the degree of Doctor of Philosophy in Materials Science presented on July 30, 2008.

Title: Structure and Piezoelectric Properties of Lead-Free Bismuth-Based Perovskite Solid Solutions

Abstract approved: _____

David P. Cann

A new group of lead free piezoelectric perovskite solid solutions, (1-*x*)Bi(B'B")O_3-*x*ABO_3, were obtained via solid-state processing techniques. The solubility of unstable perovskite Bi(B'B")O_3 compounds into stable perovskite compounds was found to be related to the tolerance factor of the ABO_3 perovskite endmembers. The morphotropic phase boundary (MBP) in perovskite solid solutions based on (1-x)Bi($Zn_{1/2}Ti_{1/2}$)O_3-x$BaTiO_3$ has been measured at x≈0.9 by x-ray diffraction (XRD). Most of the work in this thesis was focused on the structure and electrical behavior of Bi($Zn_{1/2}Ti_{1/2}$)O_3 (BZT) solid solutions with different ABO_3 end members.

Dielectric characterization revealed that the trend of transition temperature T_m as a function of composition for BZT-ABO_3 solid solutions can be described by two types. In the first type, T_m decreased linearly or non-linearly until a second phase appeared, e.g. BZT-($Bi_{1/2}K_{1/2}$)TiO_3. In the second type, T_m decreased to a minimum

(usually below room temperature) and then increased as BZT content increased, e.g. BZT-$BaTiO_3$. In addition, with substitution of Li for Na in $Bi(Zn_{1/2}Ti_{1/2})O_3$-$NaNbO_3$ the diffuseness of the transition peak decreased and transition temperature increased. Hysteresis measurements indicated that the ferroelectric state of $NaNbO_3$, $(Bi_{1/2}K_{1/2})TiO_3$ and $BaTiO_3$ can be induced or enhanced with small amounts of BZT. However, added BZT content resulted in the transition from a normal ferroelectric state to quasi-relaxor state. The ternary system $BiScO_3$-$Bi(Zn_{1/2}Ti_{1/2})O_3$-$BaTiO_3$ was also studied in terms of structure and dielectric behavior.

Structure and Piezoelectric Properties of Lead-Free Bismuth-Based Perovskite Solid Solutions

by

Chien-Chih Huang

A DISSERTATION

Submitted to

Oregon State University

in partial fulfillment of
the requirements for the
degree of

Doctor of Philosophy

Presented July 30, 2008

Commencement June 2009

Doctor of Philosophy dissertation of Chien-Chih Huang presented on July 30, 2008.

APPROVED:

Major Professor, representing Materials Science

Director of the Materials Science Program

Dean of the Graduate School

I understand that my dissertation will become part of the permanent collection of Oregon State University libraries. My signature below authorizes release of my dissertation to any reader upon request.

Chien-Chih Huang, Author

ACKNOWLEDGEMENTS

First of all, I would like to express my deep gratitude for the continuous support, academic suggestion and enormous beer provided by my advisor, Dr. David Cann, throughout this research. I would also like to thank my committee members Dr. William Warnes, Dr. Jamie Kruzic, Dr. Philip Watson and Dr. Leonard Forbes for their valuable instructions and advices which inspired me to think in different ways.

Throughout this work, I am very fortunate in having opportunities to work with many great people. I would like to thank Prof. Naratip Vittayakorn for his insightful advice and a lot of support in this study. I would also like to express my sincere gratitude to Dr. Xiaoli Tan for his guidance in experiment. And of course, I would like to thank all members in our group for working and drinking hard together.

Most of all I would like to thank people who take care of me, especially my parents and three sisters. I would never finish this study without their encouragement and full support. I owe everything I have and everything I have become to my family whose love and support cannot be overstated. Finally thank you Yi-Chen for standing by me and giving me warm regards through it at all.

TABLE OF CONTENTS

TABLE OF CONTENTS (Continued)

TABLE OF CONTENTS (Continued)

TABLE OF CONTENTS (Continued)

TABLE OF CONTENTS (Continued)

Page

LIST OF FIGURES

LIST OF FIGURES (continued)

LIST OF FIGURES (continued)

LIST OF FIGURES (continued)

LIST OF TABLES

CHAPTER 1

Motivation and Objective

1.1 Motivation

Perovskite $Pb(Zr,Ti)O_3$ (PZT) and PZT–based ceramics are widely used for many industrial applications due to their superior performance in piezoelectric, dielectric and pyroelectric applications. However, recently there have been environmental concerns with PZT related to the toxicity of lead oxides which are volatile during processing. Consequently, this has motivated the search for lead free piezoelectric materials with piezoelectric properties comparable to PZT with a reduced environmental impact. Furthermore, the legislations of European Union such as Waste from Electrical and Electronic Equipment (WEEE), Restriction of Hazardous Substances (RoHS) and End-of Life Vehicles (ELV) restrict the use of lead in equipment. Although piezoelectric materials are currently outside of this restriction due to the difficulty in finding a suitable substitution which can compare with lead, a global lead free policy is foreseeable in the future. Therefore, several lead free piezoelectric ceramics such as $BaTiO_3$-based ceramics[1], Bi layered structures[2], alkaline niobate perovskites[3] and Bi-based perovskites[4-9] are actively being studied.

The origin of the enhanced piezoelectric response in perovskite PZT is the result of lone pair electrons in the Pb^{2+} hybrid orbitals[10] and the existence of a morphotropic phase boundary (MPB) between two ferroelectric phases.[11] Therefore, Bi^{3+} is an excellent candidate for the substitution of Pb in the PZT system since it has a similar electronic structure and there are already numerous Bi-based perovskite

ceramics that can be used in lead free solid solutions[5-9] or contain some degree of Pb[13-16]. Through systematic research, a number of MPB systems based on $Bi(M)O_3$-$PbTiO_3$ ($M=Ti^{4+}$, Sc^{3+}, Zn^{2+}, Nb^{5+}…) which show high transition temperature and excellent piezoelectric properties has been discovered.[13,15] However, most still contain more than 60 mole% Pb. Therefore replacing Pb with another suitable endmember will be the main focus of this research.

The excellent piezoelectric properties of PZT are a direct result of (i) the high polarizability of Pb^{2+} hybrid orbitals (ii) the strong ferroelectric nature, and (iii) the presence of an MPB. The purpose of this research is to develop Bi-based perovskite compounds which exhibit strong ferroelectric properties and an MPB by manipulating composition. The primary objectives of this research are are given in the following section.

1.2 Objective

The first step of this research is to stabilize perovskite phase which contains as much as possible high polarizable Bi^{3+} ion. In order to investigate the formation mechanism of Bi perovskite, a list of perovskite stability of binary system for $Bi(B'B'')O_3$-ABO_3($B'=Zn^{2+}$, Ni^{2+}, Sc^{3+}, Y^{3+}, Ga^{3+}; $B''=Ti^{4+}$) for different stable none lead perovskite ABO_3 end members were studied. The stability of perovskite structure can be described as tolerance (t), given in equation (1.1):

$$t = \frac{r_a + r_o}{\sqrt{2}(r_b + r_o)} \tag{1.1}$$

Where r_A, r_B, and r_o are the ionic radii of A, B and O site, respectively. Based on tolerance factor, a relationship between tolerance factor and solubility of $Bi(B'B'')O_3$ in stable ABO_3 perovskite was discussed.

In order to obtain a good piezoelectric material, an MPB, a strong ferroelectric nature, large dielectric constant and high transition temperature are desired. The summary of recent MPB compositions related to Bi-based perovskite is shown in figure 1.1. One can conclude that the MPB will appear near a tolerance factor of t=0.99-1.01 in lead-based systems. This inspired the synthesis of a range of MPB compositions by manipulating the composition of $Bi(B'B'')O_3$-ABO_3 solid solutions in this research. The behavior of a ferroelectric can be judged from dielectric measurements and the polarization hysteresis as function of the electric field. Complex perovskite structures like $(A`A``)BO_3$ or $A(B`B``)O_3$ will result in relaxor behavior due to insufficient driving force for ordering derived from the ionic valence and ionic radius. In order to understand the mechanisms behind the transition from relaxor ferroelectric to normal ferroelectric in Bi-based perovskites, the effects of doping and thermal processing will be investigated.

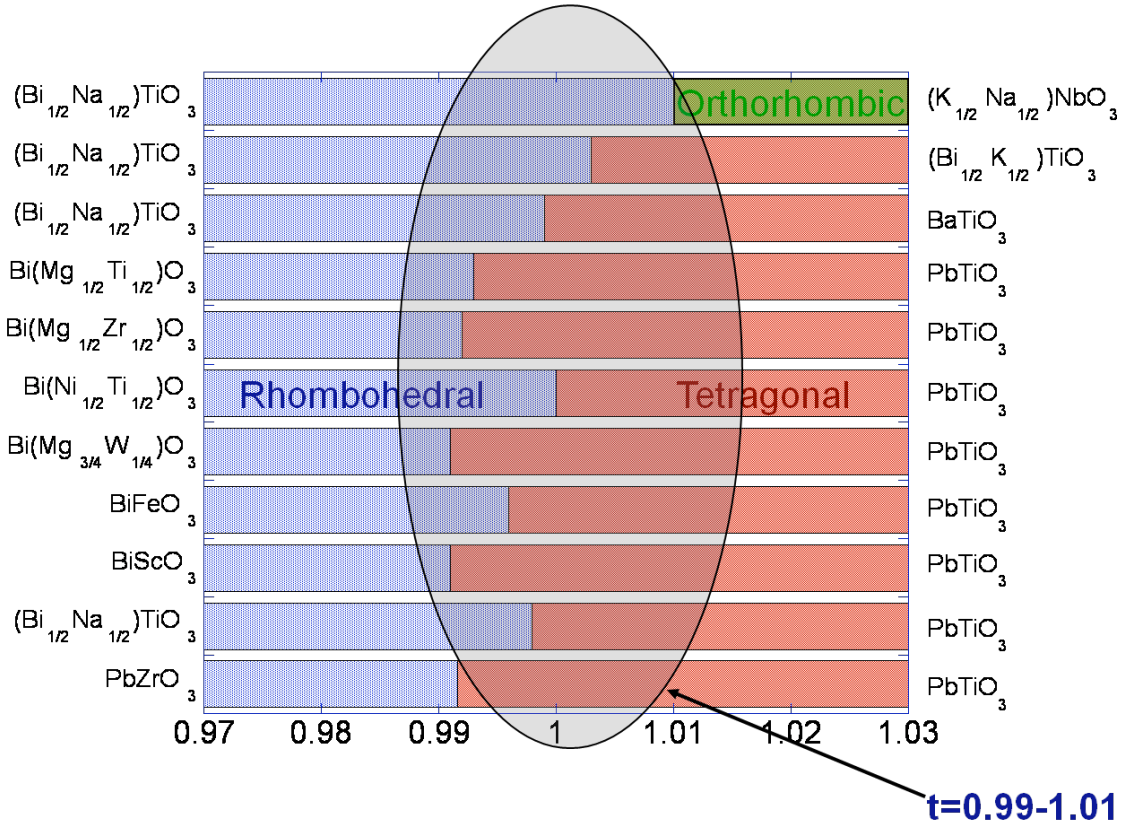

Figure 1.1 Recent MPB compositions related to Bi-based perovskite

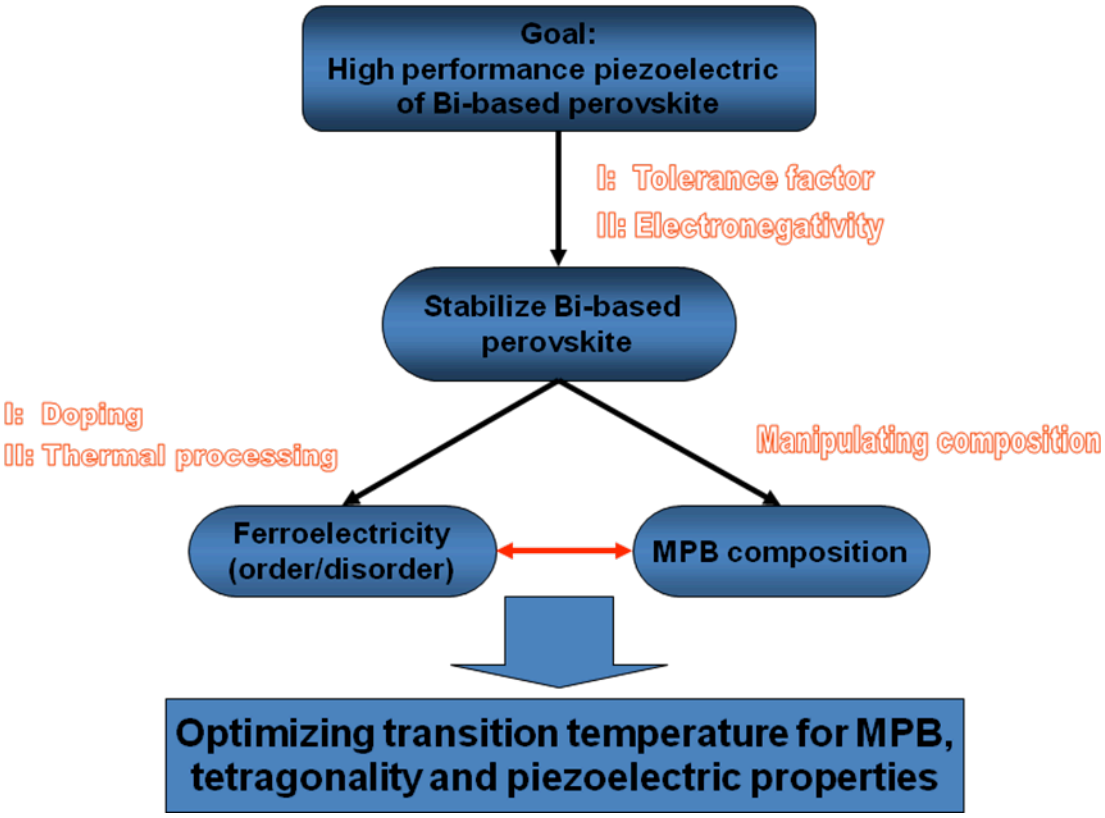

Figure 1.2 The plan of this study

1.3 References

1. Z. Yu, C. Ang, R. Guo, and A. S. Bhalla, J. Appl. Phys **92**, 1489 (2002).
2. R. J. Cava, T. Siegrist, W. F. Peck, Jr., J. J. Krajewski, B. Batlogg and J. Rosamilia, Appl. Rev. **44**, 9746 (1991).
3. I. P. Raevski and S. A. Prosandeev, J. Phys. Chem. Solids **63**, 1939 (2002)
4. C. F. Buhrer, J. Chem. Phys. **36**, 798 (1962).
5. T. Takenaka, K. Maruuama, and K. Sakata, Jpn. J Appl. Phys. **30**, 2236 (1991).
6. Y. Hiruma, R. Aoyagi, H. Nagata and T. Takenaka, Jpn. J Appl. Phys. **44**, 5040 (2005).
7. H. Nagata, T. Takenaka, Jpn. J Appl. Phys. **36**, 6055 (1997)
8. A. Sasaki, T. Chiba, Y. Mamiya and E. Otsuki, Jpn. J. Appl. Phys. **38**, 5564 (1999).
9. Y. Y. Tomashpol'skii, E. V. Zubova, K. P. Burdina and Y. N. Venevtsev, Soviet Phys **13**, 859 (1969).

CHAPTER 2

Introduction

2.1 Piezoelectricity

Piezoelectric effect was first discovered in 1880 by Pierre and Jacques Curie[1] during their research on the effect of pressure on the generation of charge in quartz. Originated from the microscopic structure of the solid, the piezoelectricity is the effect that can transform electrical energy into mechanical energy or vice versa. There are two different effects, direct and indirect effect, which can describe this phenomenon. In direct piezoelectric effect, shown in Figure 2.1a, ceramics with certain structure become electrically polarized when the stress is applied. This phenomenon is linear and can be reversible. For indirect effect, or called converse piezoelectric which is shown in figure 2.1b, the geometric strain is generated proportional to an applied electric field. Owing to these effects, piezoelectric crystals have a bunch of applications in sensors, actuators, generators, ultrasound, etc.[2, 3].

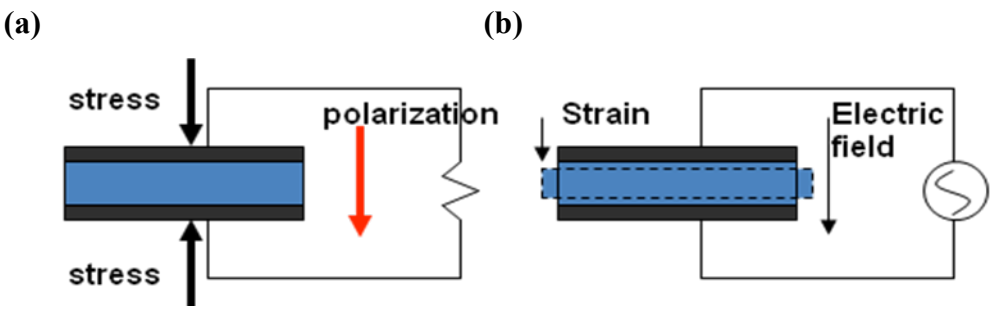

Figure 2.1 Direct (a) and indirect (b) effect of piezoelectric properties

The direction of the induced polarization depends on the direction of the applied stress on the crystal which can be demonstrated in Figure 2.2. When the stress in the y-direction is applied on the stress-free unit cell in Figure 2.2a, the movement of atoms will result in the shift of the centers of mass of A atoms and B atoms away from each other along y axis, as illustrated in Figure 2.2b. The polarization is generated along y axis in this case. However when the stress is applied in the x direction which is shown in Figure 2.2c, there is no induced polarization along this direction since there is no net displacement of centers of mass of A atoms and B atoms.

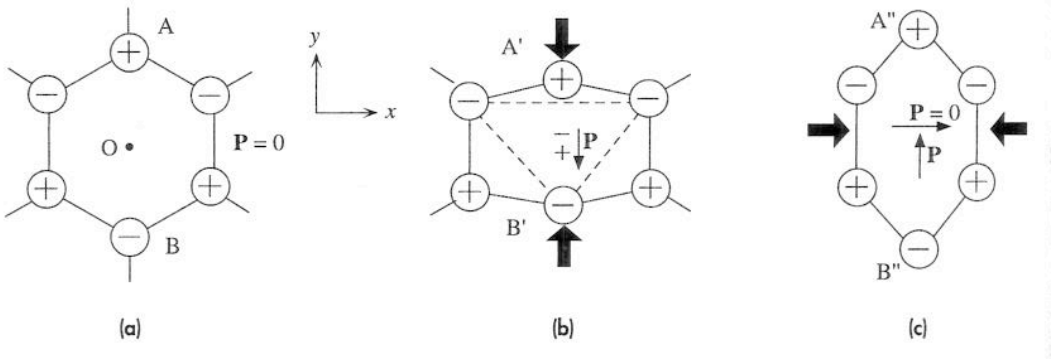

Figure 2.2 A hexagonal unit cell has no center symmetry which has (a) no applied stress (b) stress in y-axis and (b) stress in x-axis[4]

In solids, an applied stress in one direction can induce polarization in other directions. Therefore the indirect and converse piezoelectric effect can be written in equations (2.1) and (2.2) as following:

Direct effect:

$$P_i = d_{ij} T_j \tag{2.1}$$

Indirect effect:

$$S_{ij} = d_{ij} E_i \tag{2.2}$$

Where T is stress (N/m^2) and S is strain. Both S and T are second rank tensor. P is polarization and E is electric field. And d_{ij} is piezoelectric coefficient which is related to crystal structure.

Another common way to measure the strength of the piezoelectric effect is the electromechanical coupling factor *k*. This factor is the measurement of the fraction of electrical energy converted to mechanical energy. The coupling factor can be written in equation (2.3):

$$k^2 = \frac{\text{output mechanical energy}}{\text{input electrical energy}}$$

Or (2.3)

$$k^2 = \frac{\text{output electrical energy}}{\text{input mechanical energy}}$$

Because there is always energy loss during the conversion, e.g. energy loss due to friction, k^2 is always smaller than 1. The *k* value for quartz is 0.1, for $BaTiO_3$ ceramic is 0.4, and for $Pb(Zr, Ti)O_3$ ceramic is 0.5-0.7. The *k* values for single crystal $BaTiO_3$ and $Pb(Zr, Ti)O_3$ can even be greater than 0.9 [5].

2.2 Ferroelectricity

2.2.1 Ferroelectric

Similar to ferromagnetic materials which possess a spontaneous magnetization, ferroelectricity occurs in certain crystal structures which can be polarized even in the absence of applied field. The polarization comes from the separation of positive and negative charges in the crystals which is a result of crystal distortions from a

crystallographic phase transition. Figure 2.3 demonstrates the crystal distortions of a $BaTiO_3$ crystal at different temperatures. When the temperature is below 130°C, the separations of the centers of mass of the negative charges, O^{2-}, and positive charges, Ba^{2+} and Ti^{4+}, in the $BaTiO_3$ crystal results in the ferroelectric behavior. However, when the temperature is over 130°C, the crystal retains cubic symmetry and there is no net polarization. The temperature which ferroelectric property is lost is called Curie temperature (T_c).

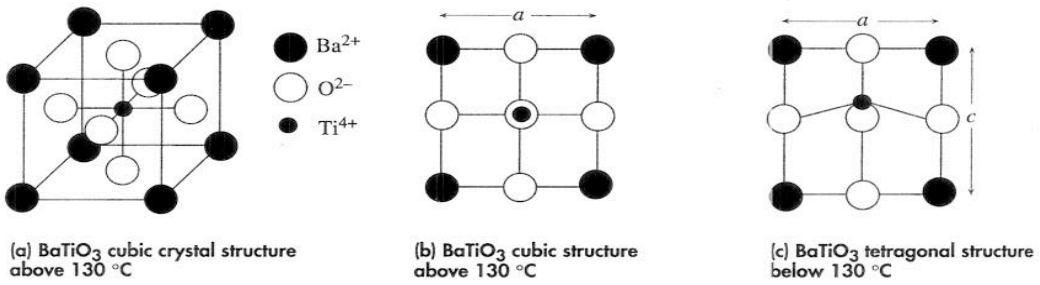

Figure 2.3 Crystal distortions of $BaTiO_3$ unit cell above and below 130°C[4]

Rochelle salt ($KNaC_4H_4O_6 \cdot 4H_2O$) was the first known ferroelectric which was discovered by Valasek[6]. After his research, a large number of crystals which possess ferroelectric behavior has been discovered. Since the ferroelectric property comes from crystal distortions, it is reasonable to relate the appearance the ferroelectric properties to the host crystallographic point group. Table 2.1 demonstrates the classification of crystallographic point groups in terms of the center of symmetry (COS) and polar axis. There are a total of 32 point groups for all possible crystals[7]. Only crystals which lack center of symmetry (COS) can have the piezoelectric effect. Within these piezoelectric point groups, only 10 of them possess a polar axis which can be indicated as the ferroelectric point groups. Since ferroelectric crystals are part

of the members of piezoelectric groups and can enhance the piezoelectric effect via a domain wall contribution, ferroelectric materials are excellent starting materials for the development of new piezoelectric materials.

Table 2.1 Classification of crystallographic point group in terms of center of symmetry (COS) and polar axis

Polar	COS	Cubic		Hexagonal		Tetragonal		Trigonal		Ortho	Mono	Tri
Non-Polar	$\bar{1}$	m3m	m3	6/mmm	6/m	4/mmm	4/m	$\bar{3}$m	$\bar{3}$	mmm	2/m	$\bar{1}$
	1	432	23	622	$\bar{6}$	422	$\bar{4}$	32		222		
		$\bar{4}$3m		$\bar{6}$m2		$\bar{4}$2m		Piezoelectric point groups				
Polar				6mm	6	4mm	4	3m	3	mm2	2	1
				Ferroelectric point groups							m	

The polarization is used for measuring the degree of ferroelectricity. As a ferroelectric is polarized, a region with the same polarizations vectors, called domain, is formed. These domains will initially nucleate randomly with the polarizations vectors along one of the symmetry allowed direction. With increasing electric field, domains oriented favourably to the applied electric field will grow at the expense of those domain oriented unfavourably. Upon the application of the different directional electric field, the polarization vectors within the domain can be reoriented. This example of polarization as a function of applied electric field (abbreviated as P-E loop) is shown is figure 2.4.

The P-E (or called D-E) hysteresis loop can be obtained after a ferroelectric crystal is subjected to electric fields. In figure 2.4, the value of the remnant polarization, P_r, is used to measure ferroelectricity. This value was obtained once the

applied electric field has been removed. The spontaneous polarization, P_s, is obtained by extrapolation at high electric field back to zero field. In ceramics, P_s is larger than P_r due the smaller domain size and internal stress of grain compared to single crystal. For single crystal, since P_s is almost the same with P_r square shaped loop can be obtained. The energy required to reorient the polarization vectors is called coercive field, E_c. Generally, ceramics with higher values of P_r is preferable.

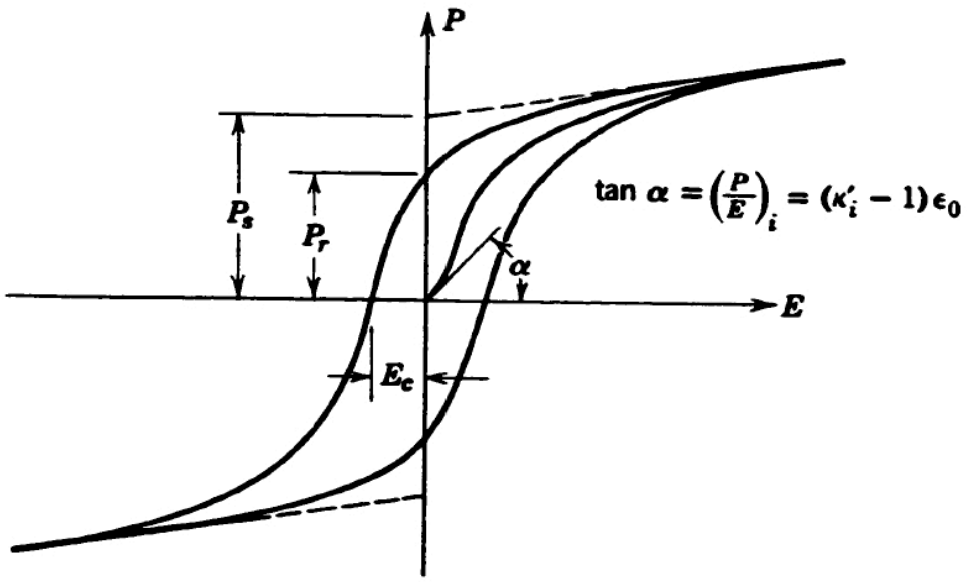

Figure 2.4 A typical ferroelectric hysteresis loop.[8]

2.2.2 Relaxor Ferroelectric

Relaxor ferroelectrics are a group of materials which were first discovered in the 1950's by Smolenskii *et al*.[9] The best starting point for the discussion of the difference between a normal ferroelectric and a relaxor is considering the behavior around the Curie point which is illustrated in figure 2.5.

Considering the dielectric behavior at the Curie point, for a normal ferroelectric, when the temperature is above Curie temperature, T_c, the dielectric constant follows linear relation called Curie-Weiss law which is shown in equation (2.4). In contrast to the sharp first order dielectric transition peak as a function of temperature for a normal ferroelectric, relaxor ferroelectrics exhibit a broad and frequency dependent maximum dielectric permittivity. In relaxor ferroelectrics, the dielectric constant does not follow Curie-Weiss behavior above the ferroelectric transition temperature, but, instead follows the so-called quadratic Curie-Weiss law[10, 11] which is shown in equation (2.5).

Normal Ferroelectric: $$\frac{1}{\varepsilon} = \frac{T - T_C}{C} \qquad (2.4)$$

Relaxor Ferroelectric: $$\frac{\varepsilon'_{max}}{\varepsilon'(f,T)} = 1 + \frac{(T - T_m(f))^{\gamma}}{2\delta_{\gamma}^2} \quad (1 \leq \gamma \leq 2) \qquad (2.5)$$

Where ε_{max} is the permittivity at T_m. The parameter of γ is degree of dielectric relaxation, where $\gamma = 1$ corresponds to a normal first-order ferroelectric phase transition. Larger values of γ express more relaxor-ferroelectric behavior of transition. The value of δ_r represents the degree of diffuseness for transition peaks. Both γ and δ_r were determined from the slope and intercept of $\ln(\varepsilon'_m / \varepsilon')$ versus $\ln(T-T_m)$.

Considering the polarization at the Curie point, the decrease of polarization to zero is relatively rapid in ferroelectric materials compared to relaxor ferroelectric materials. The gradual decrease of the polarization in relaxors can be extended to the

temperature above T_m but the polarization decays to zero at temperatures below T_m. At temperatures below T_m, relaxors can also show non-linear P-E behavior. However the remnant polarization is much smaller than in normal ferroelectrics when the temperature is close to T_m.

Generally, these kinds of materials may undergo transitions between the following states. (i) When the temperature above T_m, the paraelectric (PE) state occurs, and (ii) upon cooling they gradually transform into an ergodic relaxor (ER) state with a random distribution of polar nano-regions (PNRs). Generally the transition temperature from PE to ER state is the so-called burns temperature (T_B) and is lower than T_m. It must not be confused with a structural transformations temperature since at T_B there is no macroscopic structure change. (iii) An intermediate non-ergodic state (true relaxor state) with short range ordered polar nano-regions appeared once the temperature is low enough. (iv) When a strong electric field is applied to the non-ergodic state, the ferroelectric state appears.[12] On the basis of ordered PNRs, the relaxor ferroelectric shows unique properties from dipolar glasses and normal ferroelectrics.

.

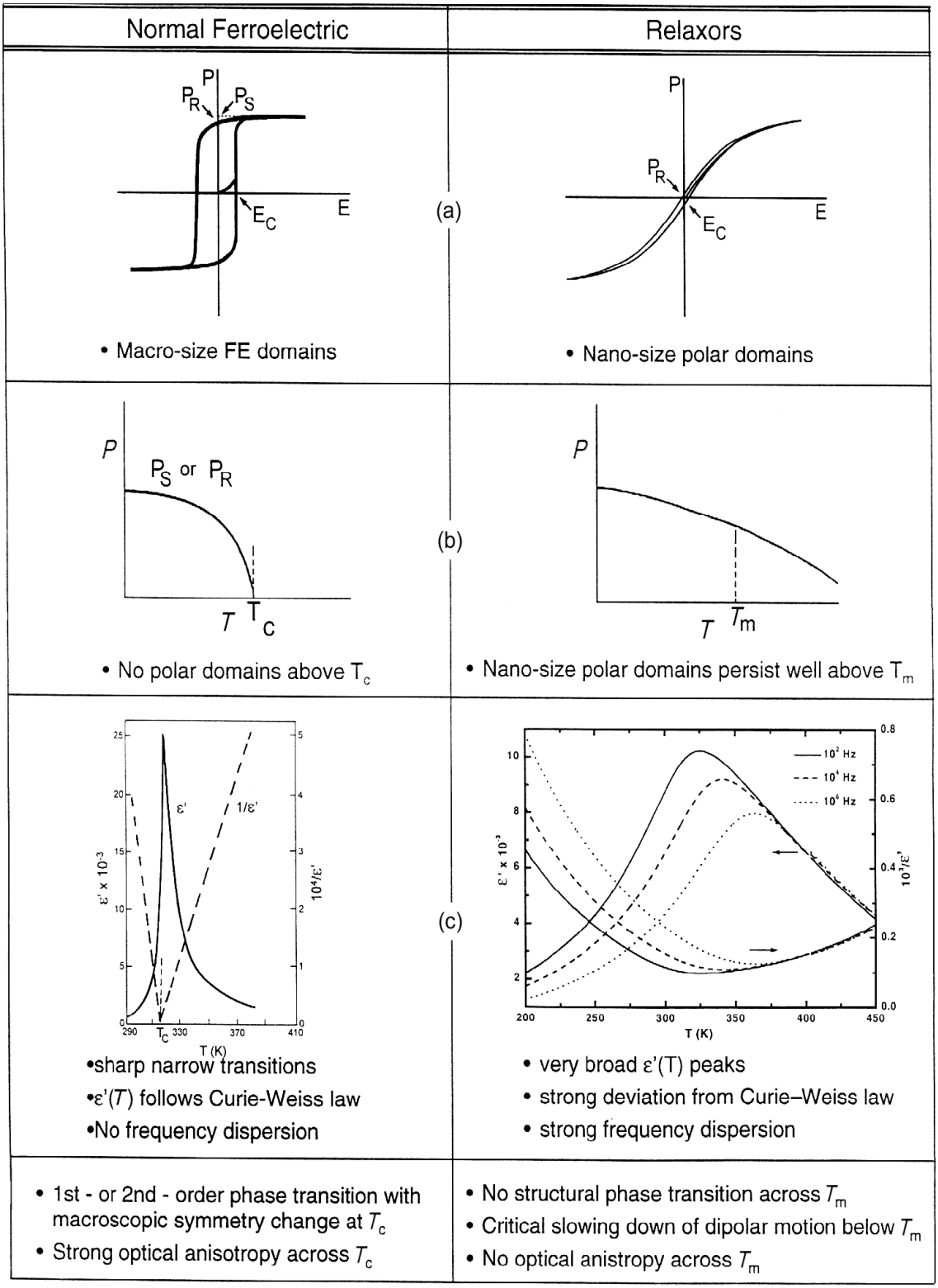

Figure 2.5 Comparisons of normal ferroelectric and relaxor ferroelectric[13]

2.3 Perovskite Materials

The perovskite structure, written as $\mathbf{A^{XII}B^{VI}X_3}$, is one of the most versatile crystal structures. The A site is in 12-fold coordination with large cations, the B site is in 6-fold coordination with smaller cations, and the X sites are 6-fold coordinated anions. The crystal structure is shown in figure 2.6. Through manipulating composition of each site, it can be used as a catalyst, capacitor, magnetic material, magnetoresistive material, non-linear optical material or even a superconductor[3]. Furthermore, most piezoelectric and ferroelectric materials are derived from the perovskite structure.

The perovskite structure can tolerate a wide range of compositional variation. The simple ternary perovskite can be divided into $A^{1+}B^{5+}O_3$, $A^{2+}B^{4+}O_3$, $A^{3+}B^{3+}O_3$ types and oxygen and cation deficient phases. An example for $A^{1+}B^{5+}O_3$ types perovskite is $KNbO_3$. This type oxide is of particular interest due to its ferroelectric properties. The $A^{2+}B^{4+}O_3$ type probably contains the largest number of perovskite type compounds. The best compounds known of this type are titanates due to the ferroelectric properties that barium and lead compounds exhibit. The last type of ternary perovskite, $A^{3+}B^{3+}O_3$, includes $BiFeO_3$ and $LaAlO_3$ which generally possess a lower symmetry structure like rhombohedral or orthorhombic.

In addition to the simple ternary perovskite, the perovskite structure can also allow complex charge compensated compositions. Most of the materials in the complex perovskite families are known to be relaxor ferroelectric. The general formula for the complex perovskites can be written as $\mathbf{(A'A'')^{XII}(B'B'')^{VI}X_3}$**.** Where

the average valence of the A site and B site follows the same rules for simple ternary perovskites.

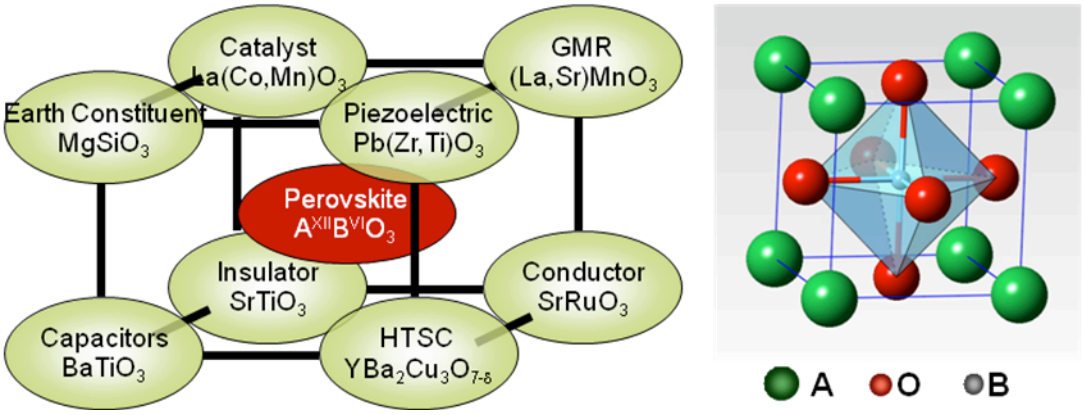

Figure 2.6 ABO_3 perovskite-type unit cell and applications

2.3.1 Stability of Perovskite

The most import parameter that dominates the stability of a crystal structure of ionic compounds is the ionic radius which can be explained by lattice energy based on thermodynamics. The lower lattice energy that can be obtained, the more stable the structure is. The lattice energy can be written as:

$$E_{lattice}=E_{static}+E_{vibrational} \quad (2.6)$$

Since $E_{static}>>E_{vibrational}$ at room temperature and low pressure, the effect of vibration to the lattice energy can be negligible. Thus, the equation (2.6) can be written as[14].

$$E_{lattice}=E_{electrostatic}+E_{repulsion}+E_{other} \quad (2.7)$$

In general, the electrostatic term accounts for 70-90% of lattice energy and the repulsion energy are 10-20%[14]. Therefore, we just need to consider the electrostatic term here:

$$E_{electrostatic} = NMZ^{+}Z^{-}e^{2}/r_{AB} \quad (2.8)$$

Where N is the number of particles, generally taken as Avogadro's number, M is the Madelung number which is a constant related to certain structure, Z^{+} and Z^{-} are the charges of cations and anions, e is the charge on the electron and r_{AB} is the distance between cations and anions. So it can be seen the ionic radius is crucial important for the lattice energy.

In early 1920s, Goldschmidt proposed a simple geometrical relationship between cations and anions which can be used to describe the stability of the perovskite structure. The phase stability can be described as a tolerance factor expressed as following equation.

$$t = \frac{r_a + r_o}{\sqrt{2}(r_b + r_o)} \quad (2.9)$$

Where r_a, r_b and r_o are ionic radius of ion in A, B and O sites respectively. For a given composition, if t is between 0.88-1.09 there is a high probability that it will be stable in the perovskite structure. For ideal cubic, the tolerance factor is equal to 1. Generally, perovskites with the tolerance factor higher than one will assume tetragonal symmetry and for tolerance factors less than 1 the structure will have rhombohedral or orthorhombic symmetry.

However, the tolerance factor alone is not sufficient to describe the stability of perovskite. For example, the tolerance factor for $BiGaO_3$ is equal to one, however the structure is not stable in perovskite form. In order to describe the stability of perovskite in different valance of A and B site, Muller and Roy proposed to plot a "structural map", which utilizes the ionic radii of A and B as coordinates to study the distribution of different structures for many ternary structural families, including $A^{1+}B^{5+}O_3$, $A^{2+}B^{4+}O_3$, $A^{3+}B^{3+}O_3$ systems[3,15]. The structural map is shown in figure 2.7.

Another factor used to complement tolerance factor is the electronegativity difference between substituent cation and anions given as:

$$\Delta EN = \frac{(\chi_{A-O} + \chi_{B-O})}{2} \qquad (2.10)$$

This factor describes ionic character of bonding in the compound. Larger electronegativity differences with higher degree of ionic bonding result in more stable perovskite structures. These models provide a useful way for synthesizing perovskite compounds.[3,15,16,17]

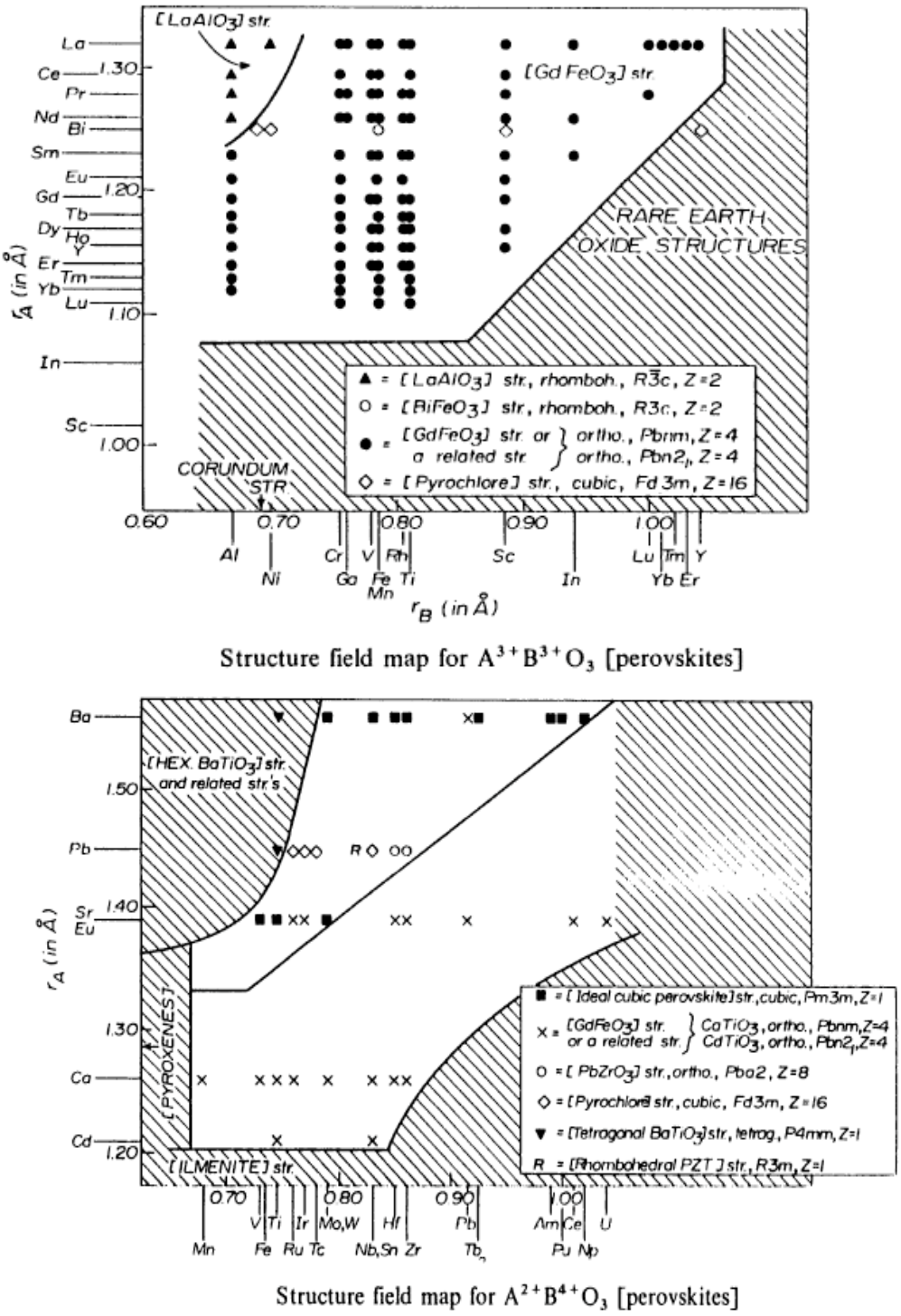

Structure field map for $A^{3+}B^{3+}O_3$ [perovskites]

Structure field map for $A^{2+}B^{4+}O_3$ [perovskites]

Figure 2.7 Structure map of $A^{3+}B^{3+}O_3$ and $A^{2+}B^{4+}O_3$ perovskites[3]

2.3.2 Order/Disorder Perovskite

In the context of this work, the presence of order/disorder indicates the compositional disorder on one of the cation sublattices. Compositional disorder means the disorder in arrangement of different ions on the crystallographically equivalent sites. Most complex perovskite exhibit relaxor behavior and are composed of aliovalent ions located on one crystallographic site, e.g. $Pb(Mg^{2+}_{1/3}Nb^{5+}_{2/3})O_3$ (PMN) or $Pb(Sc^{3+}_{1/2}Ta^{5+}_{1/2})O_3$(PST). Recently, there have been some reports about isovalent compositions which can also show relaxor behavior, e.g. $Ba(Zr^{4+}_{x}Ti^{4+}_{1-x})O_3$[18]or $Ba(Ti^{4+}_{x}Sn^{4+}_{1-x})O_3$[19]. However the degree of disorder for these relaxor compounds can be modified through proper thermal processing or doping. The degree of order/disorder in a perovskite can have great influence on the ferroelectric properties.

Followed by the first model to describe the relaxor behavior proposed by Smolenskii,[20] there have been numerous theories reported for explaining the behavior of the relaxor. Although there is still no theory that can completely explain all of the relaxor behavior, for some specific cases the most widely accepted models are those proposed by Cross[21], Randall[22] and Davies[23]. All of their models are based on the concept of order/disorder regions in different size and shape interfere with each other and result in broad and frequency dependent dielectric properties.

In the thermodynamic view, the ground state of a composition should be compositionally ordered since the electrostatic and elastic energy can be minimized by ordering of the ions of different size and valence. In the kinetic view, the ordered state must be accompanied with ionic diffusion. The diffusion rate is controlled by temperature and the different mass and valence state for ions on one site. There are

four different cation order/disorder schemes that can be considered for complex perovskites.

(i) The ratio of different ions on B site is 1:1 and the difference in mass and the valance of the ions is large enough to drive the ions into a long range ordered state rapidly, e.g. $Pb(Mg_{1/2}W_{1/2})O_3$. This kind of material typically shows normal ferroelectric or anti-ferroelectric properties.

(ii) The ratio of different ions in B site is 1:1 and the difference in mass and valance of the ions is moderate. An ordered state in this case can only be achieved by long time annealing, e.g. $Pb(Sc_{1/2}Nb_{1/2})O_3$ and $Pb(In_{1/2}Nb_{1/2})O_3$. This kind of material can exhibit normal ferroelectric after long annealing times.

(iii) The 1:2 ratio of different ions on the B site, e.g. $Pb(Mg_{1/3}Nb_{2/3})O_3$, shows interesting behavior with nano-scale ordered regions. The most convincing model to describe the ordering of $A(B'_{1/3}B''_{2/3})O_3$ type perovskite is called the "random site" model which was proposed by Davies and Akbas[21]. In their model, one of the B-sublattices is occupied exclusively by B^{5+} ions while the other one contains a random distribution of $B^{2+}$and B^{5+} ions in a 2:1 ratio so that the local stoichiometry is preserved. The random site model is illustrated in figure 2.8.

(iv) There are very limited reports about A site ordering in complex perovskites. One possible example is $(Na_{1/2}La_{1/2})(Mg_{1/3}Nb_{2/3})O_3$.[24] The reason may come from the difficulties of ordering cations in twelve fold coordination since large AO_{12} polyhedra cannot alternate with small AO_{12} polyhedra without large strains.[25] In addition, there are no reports about long range ordering in B site in which the ratio is not 1:1 or 1:2.

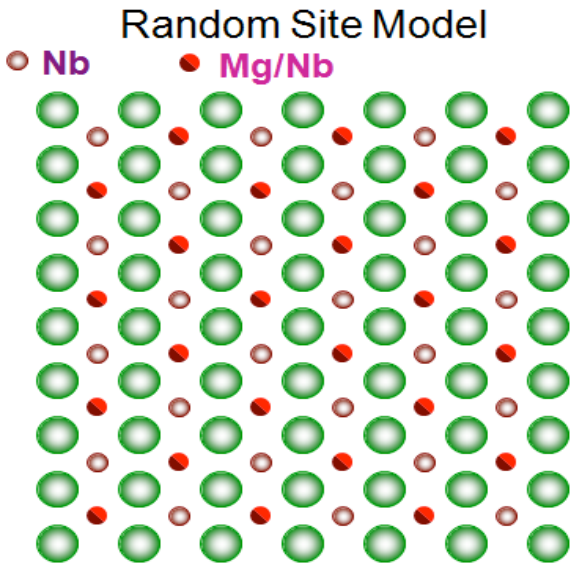

Figure 2.8 Random site model for $A(B'_{1/2}B''_{2/3})O_3$ perovskite

2.3.3 Morphotropic Phase Boundary (MPB)

An MPB can be obtained from the compositional boundary between two different phases which can be achieved by controlling the ratio of each perovskite component. The most famous case for MPB research is lead zirconate-titanate, $Pb(Zr_xTi_{1-x})O_3$ (PZT). The vertical phase boundary is between the $PbTiO_3$ (tetragonal symmetry) and $PbZrO_3$ (Rhombohedral symmetry) at a composition close to x=0.5, as shown in figure 2.9, where the materials exhibit the outstanding piezoelectric and dielectric properties.[5] The origin of the high piezoelectric response in MPB can be explained by a high degree of freedom of the electric dipoles within the boundary which can be easily oriented via an electric field. Recent structural studies also

indicate an intermediate phase at a composition at the MPB which possesses a monoclinic distortion which is responsible for the enhancement of piezoelectric and dielectric properties[26].

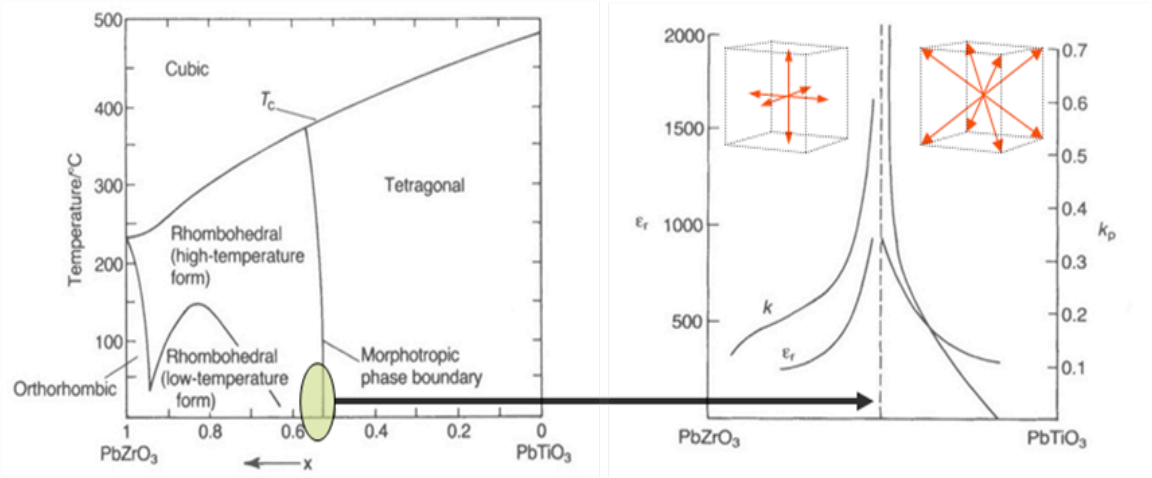

Figure 2.9 Phase diagram and piezoelectric properties for $Pb(Zr_xTi_{1-x})O_3$[5]

In addition to PZT, MPB systems can also be found in relaxor-$PbTiO_3$ solid solutions. For example, the (1-x)$Pb(Sc_{1/2}Nb_{1/2})O_3$-x$PbTiO_3$ (PSN-PT) system shows an MPB at x=0.4 and has a large piezoelectric coefficient of d_{33}=450 pC/N with a T_C=260°C.[27] The binary (1-x)$Pb(Yb_{1/2}Nb_{1/2})O_3$-x$PbTiO_3$ (PYN-PT) shows an MPB at x=0.5 and has a piezoelectric coefficient d_{33}=250 pC/N with a T_C=370°C.[28] Based on these results of high performance piezoelectric materials, an MPB provides an import way to improve the piezoelectric and dielectric properties.

2.4 Bi-based Perovskite

The origin of the enhanced piezoelectric response in perovskite PZT is the result of lone pair electrons in the Pb^{2+} hybrid orbitals[29] and the existence of a morphotropic phase boundary (MPB) between two ferroelectric phases. Therefore, Bi^{3+} is an excellent candidate for the substitution of Pb in the PZT system since it has a similar electronic structure which leads to large polarization and there are already numerous Bi-based perovskite ceramics that can be used in solid solutions. In addition, Bi based compounds have relative higher transition temperatures which may be suitable for wide temperature application. Finally, Bi is non-toxic and its compounds already have been used in numerous medical and cosmetic applications.

2.4.1 6s Lone Pair Electrons in Trivalent Bismuth

A lone pair is an electron pair without bonding or sharing with other atoms which can be found in the outmost electron shell in atoms. The existence of the lone pair repulsive force applied to other bonding schemes generally causes a distortion of the structure. Elements from the bottom of Group 13 (Tl), Group 14 (Pb, Sn) and Group 15 (Bi) contain the asymmetric electron densities often referred to as a lone pair. The perovskite compounds containing Bi^{3+} and Pb^{2+} ions show structural distortions which can induce the ferroelectric properties. The Bi^{3+} ion's off-center distortion was confirmed by comparison of high temperature phase of $BiCrO_3$ and $LaCrO_3$[30,31], since the ionic size of La^{3+} and Bi^{3+} is similar but the distortion of Bi-compounds is much larger than in the La-compounds. The higher distortion has been explained by the highly polarized $6s^2$ lone pair Bi^{3+} ion which is illustrated in figure

2.10. The $6s^2$ lone pair has also been used to explain the different behavior between $PbTiO_3$ and $BaTiO_3$[29]. From the conventional theory, $6s^2$ electron pairs in Pb are considered to form a lone pair, filling an orbital created through the self-hybridization of the 6s and 6p orbitals which results in structural distortions[32]. However this theory cannot explain the non-distorted structure of PbS. Recently, through *ab initio* calculations using density-functional theory on PbO, Watson *et al*.[33] proposed that the lone pair is the result of the interaction between Pb 6*s* and the oxygen 2*p* orbital. In addition, Seshadri and Hill[34] showed electronic structure calculations of the low-temperature monoclinic phase of the perovskite $BiMnO_3$ which indicated the hybridization of Bi 6*s* and O 2*p*. All of the results illustrate the importance of the existence of lone pairs in Bi and Pb and their influence on structural distortions.

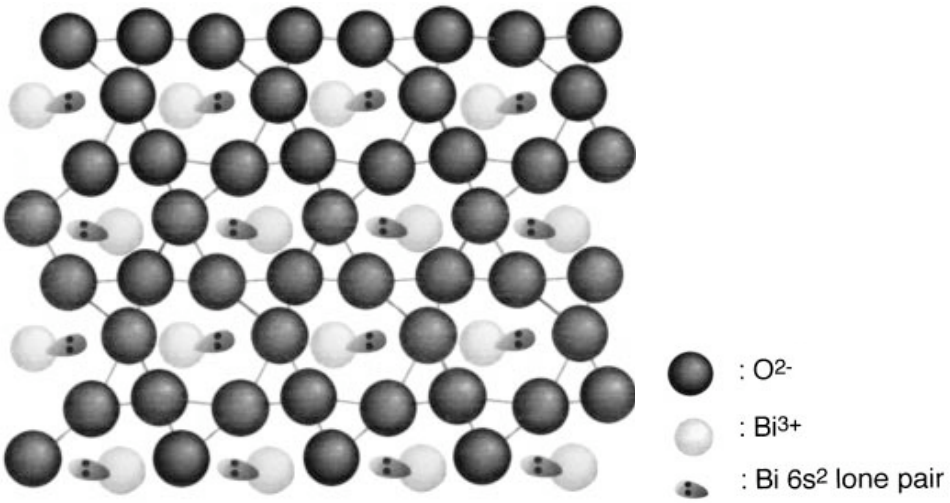

Figure 2.10. Illustration of structure distortions due to Bi lone pair.[31]

2.4.2 $(Bi_{1/2}A_{1/2}')BO_3$ Type Perovskites and Solid Solutions

The origin of ferroelectrity results from not only from B site transition metals with inert-gas electron structure (S^2P^6) in the ground state, for example Ti^{4+}, Zr^{4+}, Nb^{5+}, Ta^{5+}, but also the unshared lone pair of A site 6s electrons which is stereochemically active, for example Pb^{2+}, Bi^{3+}. Due to these considerations, Smolenskii *et al* developed a group of new bismuth alkaline-based perovskites, $(Bi_{1/2}K_{1/2})TiO_3$ (BKT) and $(Bi_{1/2}Na_{1/2})TiO_3$ (BNT), which posses ferroelectric properties[35]. They also found that $(Bi_{1/2}K_{1/2})ZrO_3$ (BKZ) and $(Bi_{1/2}Na_{1/2})ZrO_3$ (BNZ) can be stabilized in a perovskite phase and BKZ was recently confirmed to be in orthorhombic symmetry[36]. However there are no further reports related to BKZ and BNZ. Recently, high pressure synthesis of $(Bi_{1/2}Ag_{1/2})TiO_3$ further expanded the research on $(Bi_{1/2}A_{1/2}')BO_3$ type perovskites[37].

After Smolenskii's research, there has been an extensive study done by Takenaka *et al* on lead free BKT and BNT based solid solutions like $BaTiO_3$–BNT, BNT–BKT and $BaTiO_3$–BKT[38-40]. Moreover, dielectric and piezoelectric properties of a solid solution based on the $BaTiO_3$-BNT-BKT ternary system near the morphotropic phase boundary (MPB) were recently discussed[41]. Properties of the BNT and BKT compounds, as well as their solid solutions will be briefly reviewed below.

Bismuth Sodium Titanate, $(Bi_{1/2}Na_{1/2})TiO_3$ (BNT), is a perovskite with rhombohedral symmetry which lattice parameter a = 3.98 Å , α = 89.67° at room temperature[25]. A transformation to tetragonal symmetry occurs between 200-340 °C, followed by a transition to cubic symmetry above 540 °C.[42] The BNT powder is very stable in a moist environment and can be kept in air for a month without any change in

the DTA data[25]. The dielectric constant of BNT is approximately 500 at room temperature and rises to a maximum value of 2000 around 300 °C[43]. The P-E hysteresis measurements confirmed the existence of ferroelectricity of the rhombohedral phase for BNT and a paraelectric state in the cubic phase. However there is a debate about dielectric behavior of the tetragonal phase in BNT. Recent studies suggested that the paraelectric behavior can appear in the tetragonal phase of BNT[43].

There have been many reports on lead free piezoelectric materials based on BNT solid solutions. The properties of BNT and BKT based solid solutions are listed in table 2.2. The dielectric and piezoelectric properties of a solid solution based on three components of $BaTiO_3$–$(Bi_{1/2}Na_{1/2})TiO_3$–$(Bi_{1/2}K_{1/2})TiO_3$ near the morphotropic phase boundary (MPB) has attracted considerable attention[44]. The electromechanical coupling factor, k_{33}, of 0.56 and piezoelectric constant, d_{33}, of 183 pC/N was obtained in 0.852BNT−0.120BKT−0.028BT. These values were relatively high among lead-free piezoelectric ceramics and the T_C near the MPB was higher than 300 °C. Another ternary system,$(Bi_{1/2}Na_{1/2})TiO_3$–$(Bi_{1/2}K_{1/2})TiO_3$- $(Bi_{1/2}Li_{1/2})TiO_3$, also showed high T_c and large piezoelectric properties[46].

Bismuth Potassium Titanate, $(Bi_{1/2}K_{1/2})TiO_3$ (BKT), is a perovskite with tetragonal symmetry which lattice parameter is a = 3.913 Å , *c* = 3.993 at room temperature. The transition temperature from tetragonal to cubic is around 380°C[35,49]. There is also a second-phase transition temperature T2, that is, from tetragonal to pseudo cubic, existed at about 270°C[49]. The P-E loop exhibits hysteresis up to 320 °C

indicating the ferroelectric nature at room temperature. Like BNT, BKT powders are also inert to moisture.

The investigation of BKT based solid solutions is sparse compared to BNT due the poor sinterability. The high c/a in BKT which results in difficulties of poling has also limited the application of BKT. In order to improve the properties of BKT, Hiruma *et al*. reported the increase of the density of BKT ceramics through a hot pressed method.[50] Sasaki *et al*. reported an enhancement of piezoelectric and ferroelectric properties through solid solution with BNT.[51] The properties of BNT and BKT based solid solutions are listed in table 2.2.

Table 2.2 Dielectric and piezoelectric properties of BNT and BKT based solid solution.

	ε	Loss	K_p	d_{33}(PC/N)	T_c (^oC)	T_d (^oC)	Ref.
BNT-BT	580	0.013	0.192(K_{31})	125(d_{31})	288	-	38
BNT-BKT	825	0.03	0.22	150	290	210	45
BNT-BKT-BT	770	0.034	0.367	183	290	100	44
BNT-BKT-BLT	1550	0.034	0.401	216	350	160	46
BKT-BST	870	0.04	0.15	110	296	-	47
BKT-BBT	837	0.05	0.23	140	297	-	47
BKT-KN	800	0.3	0.15	-	-	-	48

LBT: (Li0.5Bi0.5)TiO3; BT: BaTiO3; SBT: (Sr0.7Bi0.2)TiO3; BBT: (Ba0.7Bi0.2)TiO3; KN: KNbO3; Td: depolarization temperature.

2.4.3 $Bi(B'_{1/2}B''_{1/2})O_3$ Type Perovskites and Solid Solutions

The existence of an MPB gave rise the performance of PZT. However due to the increasing demand for high T_c piezoelectric materials which can be used in high temperature environments, such as internal vibration sensors or fuel injection nozzles which require operation as high as 300°C,[52] a class of new high temperature MPB systems was needed. Recently Eitel *et al.* proposed a new class of materials in which $PbTiO_3$ is alloyed with Bi-based perovskite[53]. Guided by an empirical crystallographic approach, there are a number of MPB systems based on $Bi(B'_{1/2}B''_{1/2})O_3$-$PbTiO_3$ ($B'=Mg^{2+}$, Zn^{2+}, Ni^{2+}, Sc^{3+}, $B''=Nb^{5+}$, Ta^{5+}, W^{6+})[53-57]that have been discovered. Even with compositions that do not exhibit an MPB[58-60], e.g. $Bi(Zn_{1/2}Ti_{1/2})O_3$-$PbTiO_3$, there are still interesting properties such as an enhancement in the tetragonality (c/a ratio) or a high T_C for this kind of system. The Curie temperature compositional dependence of $PbTiO_3$ with $Bi(B_{1/2}'B_{1/2}'')O_3$ additions is shown is figure 2.11.

Considering the high T_c piezoelectric properties, to date there is no relaxor-$PbTiO_3$ MPB system can exhibit higher T_C than PZT (~386°C) except for the $Bi(B'_{1/2}B''_{1/2})O_3$-$PbTiO_3$ system. Guided by the tolerance factor shown in equation 1.6, Eitel *et al*. noted that there is a general trend between the transition temperature and the tolerance factor of $Bi(B'_{1/2}B''_{1/2})O_3$ endmember[53]. When $PbTiO_3$ is mixed with a smaller tolerance factor endmember, the transition temperature will become higher. The curie temperature of $PbTiO_3$-based MPBs versus the end member tolerance factor is shown in figure 2.12. For the (1-x)$BiScO_3$-x$PbTiO_3$ (BS-PT) solid solution, the tolerance factor for $BiScO_3$ is 0.907 (based on 6-fold correction) which is much lower than $PbTiO_3$. The MPB was found at x=0.64 which separates the rhombohedral and

tetragonal phase. A transition temperature is around 450°C which is much higher than PZT. Poled ceramics showed coupling factors of K_p=0.56 and piezoelectric coefficients of d_{33}=460 pC/N. Based on the first principle study done by Iniguez *et al.*,[62] the origin of the exceptional piezoelectric properties in BS-PT can be related to the hybridization between Bi/Pb-6*p* and O-2*p* orbitals which provided ferroelectric instability.

For some compositions within the $Bi(B'_{1/2}B''_{1/2})O_3$-$PbTiO_3$ system which do not show an MPB, a strong structural distortion and high ferroelectric to paraelectric transition temperature still can be observed. For the (1-x)$Bi(Zn_{1/2}Ti_{1/2})O_3$-x$PbTiO_3$ (BZT-PT) solid solution[58,59], the transition temperature is higher than 700°C for x=0.6. Moreover, the enhanced tetragonality (c/a ratio) can be up to 2.11 for this composition. Another composition which substitutes W for Ti, $Bi(Zn_{3/4}W_{1/4})O_3$-$PbTiO_3$ (BZW-PT),[60] also demonstrated the similar behavior with BZT-PT which showed an enhanced c/a ratio. There is an interesting point needed to be addressed, this behavior is not shown in the similar composition of $Bi(Mg_{3/4}W_{1/4})O_3$-$PbTiO_3$ (BMW-PT)[57] in which the c/a ratio decreased with increasing BMW content. The valence of Mg and Zn are the same and the ionic radius is very similar (Mg^{2+}=0.86Å, Zn^{2+}=0.88Å). Therefore it is reasonable to relate this strong structural distortion to the existence of Zn. Recently, based on the first principle study done by Grinberg *et al.*,[62] they found that the hybridization between Zn-4*s* and 4*p* and O-2*p* orbitals allowed the formation of short, covalent Zn-O bonds which result in large displacement between A-site and B-site.

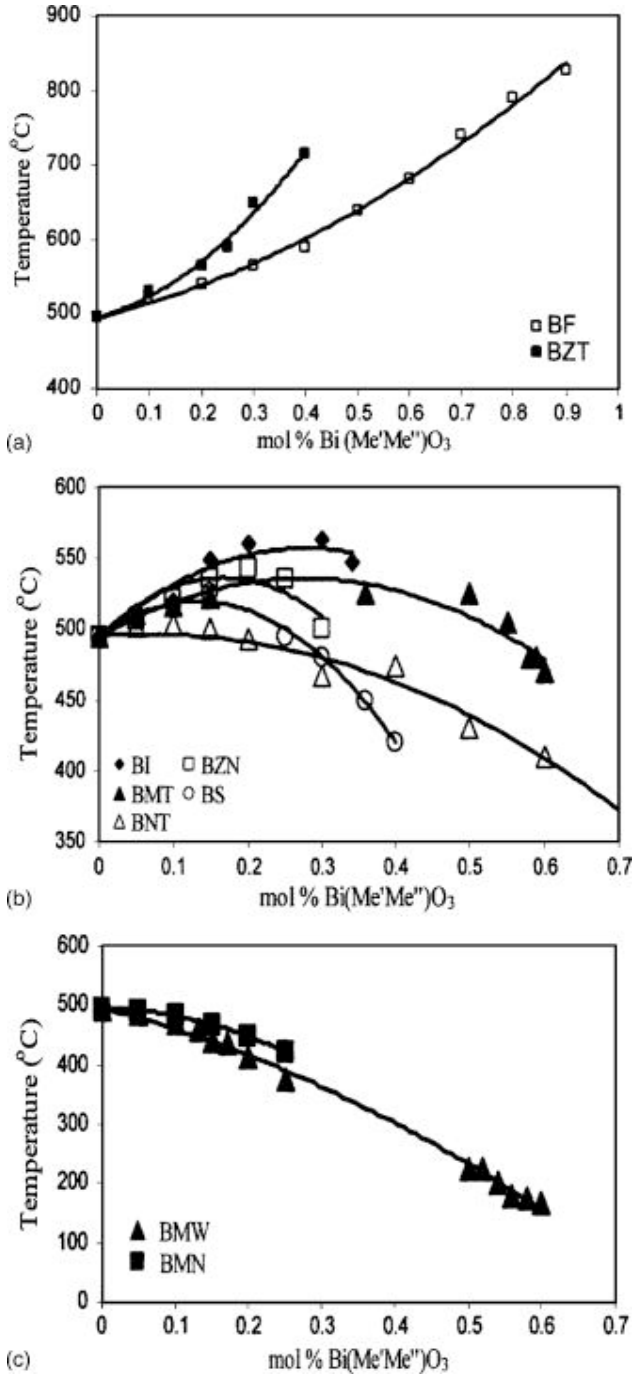

Figure 2.11 Curie temperature compositional dependence of $PbTiO_3$ with $Bi(B_{1/2}'B_{1/2}'')O_3$additions for (a) $BiFeO_3$ (BF) and $Bi(Zn_{1/2}Ti_{1/2})O_3$(BZT); (b) $Bi(Zn_{2/3}Nb_{1/3})O_3$ (BZN), $BiInO_3$(BI), $BiScO_3$ (BS), $Bi(Ni_{1/2}Ti_{1/2})O_3$ (BNT), and $Bi(Mg_{1/2}Ti_{1/2})O_3$ (BNT); and (c)$Bi(Mg_{2/3}Nb_{1/3})O_3$ (BMN) and $Bi(Mg_{3/4}W_{1/4})O_3$ (BMW).[61]

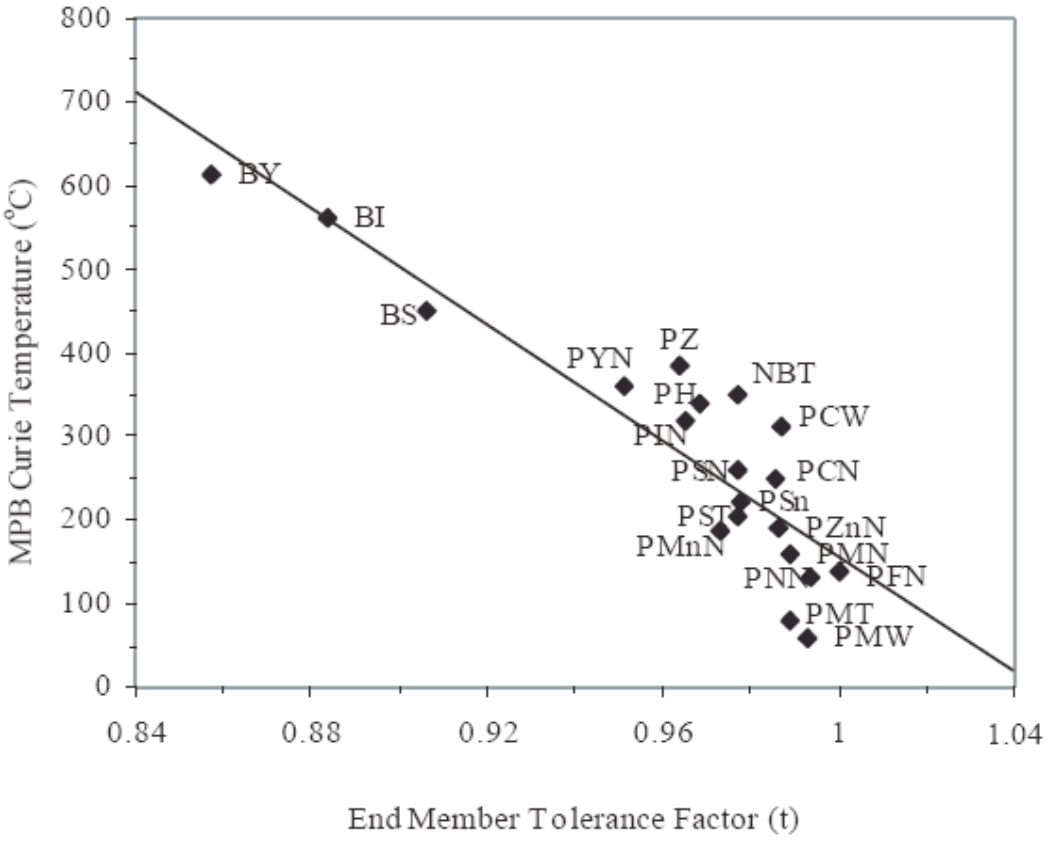

Figure 2.12 Curie temperature of $PbTiO_3$-based MPBs versus end member tolerance factor.[53]

2.5 References

1. P. Curie & J. Curie, "Developement by Pressure of Polar Electricity in Hemihedral Crystals with Inclined Faces," Bulletin de la SocieteMineralique de France, 3 90 (1880).
2. K. Uchino, Ferroelectric Devices, Marcel Dekker,Inc., New York (2000).
3. A. S. Bhalla, R. Guo, R. Roy, Mat. Res. Innovat. 4 3 (2000).
4. S. O. Kasap, Electronic Materials and Devices, McGraw-Hill, New York (2006).
5. B. Jaffe, W. R. Cook, H. Jaffe, Piezoelectric Ceramics, Academic Press, New York, (1971).
6. J. Valasek, Phys. Rev. 17, 475 (1921).
7. V. K. Pecharsky and P. Y. Zavalij, Fundamentals of Powder Diffraction and Structure Characterization of Materials, Kluwer Academic, Boston (2003).
8. W. D. Kingary and W. R. Cook, Introduction to Ceramics, Wiley and Son Inc., New York, (1976).
9. G. A. Smolenskii and A. L. Agranovskaya, Sov. Phys.-Tech. Phys.,1380 (1958).
10. C. A. Randall, A. S. Bhalla, T. R. Shrout, and L. E. Cross, J. Mater. Res. 5, 829 (1990).
11. B. S. Kang, S. K. Choi, Solid State Commun. 121, 441 (2002).
12. A. A. Bokov, Z.-G. Ye, J. Mater. Sci. **41,** 31(2006).
13. G. A. Samara and E. L. Venturini, Phase Transitions 79, 21 (2006).

14. A. Navrotsky, Physics and Chemistry of Earth Materials, Cambridge University, Cambridge (1994).

15. O. Muller, R. Roy, The Major Ternary Structural Families, Springer-Verlag, New York (1974).

16. A. Halliyal, T. R. Gururaja, U. umar and A. Safari, IEEE 6th International Sympoosium on Application of Ferroelectrics, 437 (1986).

17. N. Wakiya, N. Ishizawa, K. Shinozaki and N. Mizutani, Mater. Res. Bull. 30, 1121 (1995)

18. A. Simon, J .Ravez and M. Maglione, J. Phys.:Condens.Matter16, 963 (2004).

19. N. Yasuda, H. Ohwa and S . Asano, Jpn. J. Appl. Phys. 35, 5099 (1996).

20. G. A. Smolenskii, Jpn. J. Appl. Phys. 28 (1970).

21. D. Viehland, S. J. Jang, L. E. Cross and M. Wuttig, J. Appl. Phys. 68, 2916 (1990).

22. C. A. Randall and A. S. Bhalla, Jpn. J. Appl. Phys. 29, 327 (1990).

23. P. K. Davies and M. A. Akbas, J. Phys. Chem. Solids 61, 159 (2000).

24. R. Tarvin, P. K. Davies, J. Am. Ceram. Soc. 87,859 (2004).

25. V. A. Isupov, Ferroelectrics 315, 123 (2005).

26. R. Guo, L. E. Cross, S. -E. Park, B. Noheda, D. E. Cox and G. Shirane, Phys Rev. Lett. 84, 5423 (2000).

27. S. W. Choi, T. R. Shrout, S. J. Jang & A. S. Bhalla, Ferroelectrics100, 29 (1989).

28. C. Duran, S. Trolier-McKinstry and G. L. Messing, Journal of Electroceramics 10, 47 (2003).

29. R. E. Cohen, *Nature***358**, 136 (1992).

30. F. Sugawara, S. Iida, Y. Syono, and S. Akimoto, J. Phys.Soc. Jpn. 25, 1553 (1968).

31. T, Atou,H. Chiba, K. Ohoyama,Y. Yamaguchi.Y. Syono,J.Solid State Chem. 145, 639 (1999).

32. L.E. Orgel, J. Chem. Soc. 1959, 3815 (1959).

33. G.W. Watson, S.C. Parker, G. Kresse, Phys. Rev. B, 8481 59 (1999).

34. R. Seshadri and N. A. Hill Chem. Mater.13, 2892 (2001).

35. G. A. Smolenskii, V. A. Isupov, A. I. Ggranovskaya and N. N. Krainik, Soviet Physics Solid State 2, 2651 (1961).

36. K. Prasad, Lily, K. Kumari and K.L. Yadav, J. Phys. Chem. Solids 68, 1508 (2007).

37. J.-H. Park, P. M. Woodward, J. B. Parise, R. J. Reeder, I. Lubomirsky and O. Stafsudd, Chem. Mater. 11, 177 (1999).

38. T. Takenaka, K. Maruyama, K. Sakata, Jpn. J. Appl. Phys. 30 Part 1 (9B), 2236 (1991).

39. A. Sasaki, T. Chiba, Y. Mamiya, E. Otsuki, Jpn. J. Appl. Phys. 38 Part 1 (9B), 5564 (1999).

40. Y. Hiruma, H. Nagata, T. Takenaka, J. Ceram. Soc Jpn, S. 112(5), S1125 (2004).

41. H. Nagata, M. Yoshida, Y. Makiuchi, T. Takenaka, Jpn. J. of Appl. Phys. 42(12), 7401 (2003).

42. J. A. Zvirgzds, P. P. Kapostins, J. V. Zvirgzde, T. V. Kruzina, Ferroelectrics 40, 75 (1982).

43. East, J.; Sinclair, D. C. J. Mater. Sci. Lett. 16, 422 (1997).

44. T. Takenaka, H. Nagata, J. Eur. Ceram. Soc. 25, 2693 (2005).

45. S. Zhao, G. Li, A. Ding, T. Wang, Q. Yin, J. Phys. D: Appl. Phys.39, 2277 (2006).

46 . Y. Yuan, S. Zhang, X. Zhou, J. Liu, Jpn. J. Appl. Phys. 45, 831 (2006).

47. Thomas R. Shrout&Shujun J. Zhang, J Electroceram 19, 111(2007).

48. T. Wada, K. Toyoike, Y. Imanaka and Y. Matsuo, Jpn. J. Appl. Phys. 40, 5703 (2001).

49. V. V. Ivanova, A. G. Kapyshev, Y. N. Venevtsev and G. S. Zhdanov, Izv. Akad. Nauk SSSR 26, 354 (1962).

50. Y. Hiruma, R. Aoyagi, H. Nagata and T. Takenaka, Jpn. J. Appl. Phys. 44, 5040 (2005).

51. A. Sasaki, T. Chiba, Y. Mamiya, E. Otsuki, Jpn. J. Appl. Phys. 38, 5564 (1999).

52. R. C. Turner, P. A. Fuierer, R. E. Newnham, T. R. Shrout, Appl. Acoust. 41, 299 (1994).

53. R. E. Eitel, C. A. Randall, T. R. Shrout, P. W. Rehrig, W. Hackenberger, and S. -E. Park, Jpn. J. Appl. Phys. 40, 5999 (2001).

54. C. A. Randall, R. Eitel, B. Jones and T. R. Shrout, J. Appl. Phys.95, 3633 (2004).

55. D. I. Woodward, I. M. Reaney, R. E. Eitel and C. A. Randall, J.appl. phys. 94, 3313 (2003).

56. S. M. Choi, C. J. Stringer, T. R. Shrout and C. A. Randall, J. Appl. Phys. 98, 034108 (2005).

57. C. J. Stringer, R. E. Eitel, T. R. Shrout and C.A. Randall, J. Appl. Phys. 97, 024101 (2005).

58. M. R. Suchomel and P. K. Davies, J. Appl. Phys. 96, 4405 (2004).

59. M. R. Suchomel and P. K. Davies, Appl. Phys. Lett. 86, 262905 (2005).

60. D. M. Stein, M. R. Suchomel and P. K. Davies, Appl. Phys. Lett. 89, 132907 (2006).

61. C. J. Stringer, T. R. Shrout, C. A. Randall, I. M. Reaney,J. Appl. Phys. 99, 024106(2006).

62. I. Grinberg, M. R. Suchomel, W. Dmowski, S. E. Mason, Hui Wu, P. K. Davies and A. M. Rappe. Phys. Rev. Lett.98, 107601 (2001).

CHAPTER 3

Experimental Procedures

The experimental procedure and techniques used for the preparation and characterization of the ceramics in this study are described in this chapter. For the compositions of $Bi(B'B'')O_3$-ABO_3 ceramics, the solubility of $Bi(B'B'')O_3$($B'=Zn^{2+}$, Ni^{2+}, Sc^{3+}, Y^{3+}; $B''=Ti^{4+}$) for different tolerance factor ABO_3 end members were studied. The compositions for $Bi(B'B'')O_3$-ABO_3 in this study are shown in figure 3.1. Due to the expected ferroelectric properties and good sinterability of $Bi(Zn_{1/2}Ti_{1/2})O_3$, the solid solutions of $xBi(Zn_{1/2}Ti_{1/2})O_3$-$(1-x)ABO_3$ were made with all of the stable ABO_3 perovskite end members shown in figure 3.1. In order to investigate the influence of solubility for tolerance factor in unstable perovskite, the solid solutions of $BaTiO_3$ were synthesized with all of the unstable $Bi(B'B'')O_3$ perovskite end members. In the ternary system, $BiScO_3$-$Bi(Zn_{1/2}Ti_{1/2})O_3$-$BaTiO_3$ was selected for this study.

Unstable perovskite Stable perovskite

$Bi(B'B'')O_3$ $+ABO_3$

$B'=2+, B''=4+$

$Bi(Zn_{1/2}Ti_{1/2})O_3$	t=0.97
$Bi(Ni_{1/2}Ti_{1/2})O_3$	t=0.98
$Bi(Mg_{1/2}Ti_{1/2})O_3$	t=0.98

$B'=3+$

$BiGaO_3$	t=1.00
$BiScO_3$	t=0.94
$BiYO_3$	t=0.88
$BiYbO_3$	t=0.84

$BaTiO_3$	t=1.06	EN=2.23
$KNbO_3$	t=1.05	EN=2.23
$KTaO_3$	t=1.05	EN=2.28
$Bi_{1/2}K_{1/2}TiO_3$	t=1.04	EN=1.96
$AgNbO_3$	t=1.02	EN=1.68
$K_{1/2}Na_{1/2}NbO_3$	t=1.01	EN=1.96
$Bi_{1/2}Na_{1/2}TiO_3$	t=0.98	EN=1.93
$NaNbO_3$	t=0.97	EN=2.18
$La_{1/2}Zn_{1/2}TiO_3$	t=0.94	EN=2.09

Table 3.1 Compositions of $Bi(B'B'')O_3$-ABO_3 in this study, where t: tolerance factor, EN: difference of electronegativity

3.1 Ceramics Processing

Ceramics of a composition $Bi(B'_{1/2}\ B''_{1/2})O_3$-$ABO_3$ were synthesized by conventional solid state reaction methods. Reagent grade oxide powders which chemical purity and suppliers are listed in Table 3.1 were batched in stoichiometric amounts and vibratory milled with ethanol and yttrium-stabilized zirconia media (Tosoh) for 6h. The dried powders were calcined in crucibles in temperature range from 900°C -950°C for 6h followed by an additional milling and drying step to reduce the particle size down to submicron region. The milled calcined powders were mixed with 3 wt% polyvinyl butyral (PVB) binder and then uniaxially cold-pressed at 150 MPa into 12.7mm diameter pellets. Following binder burnout at 400°C for 3h, the pellets were covered by the powders which have the same compositions with pellets and were sintered in sealed crucibles shown in figure 3.1 between 1020°C-1300°C for 2h. During the sintering, bismuth powders were "sacrificed" to produce the bismuth-rich atmosphere to prevent further bismuth loss from pellets.

Besides the convention ceramics processing method, for the composition of $xBi(Zn_{1/2}Ti_{1/2})O_3$-$(1-x)BaTiO_3$, the $ZnTiO_3$ precursor method were also studied. In this composition, zinc carbonate basic $[ZnCO_3]_2{\cdot}[Zn(OH)_2]_3{\cdot}xH_2O$ (Fluka) was used for synthesizing $ZnTiO_3$. First, the weight ratio of Zn can be obtained by measuring the Zn in TG/DTA spectrometer (Perkin Elmer Instrument) after carbonate basic burned out. According to TG/DTA data, Zn carbonate basic powders were batched in stoichiometric amounts with TiO_2 and then calcined at 800°C for 12h. The calcined $ZnTiO_3$ powders were mixed with $BaCO_3$ and TiO_3 to obtain the composition of $xBi(Zn_{1/2}Ti_{1/2})O_3$-$(1-x)BaTiO_3$.

Table 3.2 Specifications of the component oxide powders used in this study

Chemical	CAS#	Description
$BaCO_3$	513-77-9	99.5%, Fisher# B30-500
$Bi2O_3$	1304-76-3	99.9%, Aldrich Chemicals # 223891
$CaCO_3$	471-34-1	Fisher # C64-500
Cr_2O_3	1308-38-9	98%, Aldrich Chemicals # 393703
Ga_2O_3	12024-21-4	99.999%, All-Chemie LTD
La_2O_3	1312-81-8	99.9%, Aldrich # 21161-3
PbO	1317-36-8	99.9%, Aldrich # 211907-500G
Mn_2O_3	1317-34-6	99%, Aldrich # 377454-250g
NiO	1313-99-1	99.99%, Aldrich # 203882-20g
Nb_2O_5	1313-96-8	99.99%, Aldrich # 208515-500g
K_2CO_3	584-08-7	99%, Aldrich # 209619-500g
Rb_2CO_3	584-09-8	99%, Alfa Aesar # 12893
Sc_2O_3	12060-08-1	99.9%, Alfa Aesear # 11216
Ag_2O	20667-12-3	99%, Alfa Aesar # 11407
Na_2CO_3	497-19-8	Fisher # S78419
$SrCO_3$	1633-05-2	99.9%, Product No.: 472018-500G
SnO_2	18282-10-5	99.9%, Alfa Aesear # 12283
TiO_2	13463-67-7	98.0 - 100.5%, Fisher # AC27737-0010
Y_2O_3	1314-36-9	99.9%, Fisher # 40759
Yb_2O_3	1314-37-0	99.9%, Alfa Aesear # 11191
ZnO	1314-13-2	Fisher # S80249
ZrO_2	1314-23-4	99.9%, Aldrich # 230693

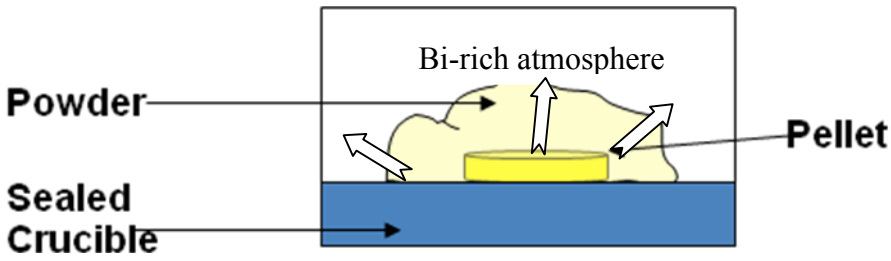

Figure 3.1 Illustration for sealed crucible

3.2 Physical Properties and Structure Determination

3.2.1 Structure Determination

To determine the phase purity and lattice parameters of calcined powder and ceramics samples, the x-ray diffraction technique was performed by x-ray diffractometer (Bruker-AXS D8) in the 2θ scan range of 10°-80°. The source of X-ray employed Cu-Kα radiation, with a tube voltage and current of 40 kV and 40mA, respectively. Room temperature XRD data was collected with step size of 0.02 at a scanning rate of 10^{o} per minute. The peaks of x-ray diffraction pattern were determined and analyzed by EVA software. The lattice parameter calculation was based on least square method according to each peak.

3.2.2 Density Measurement

The densities of ceramics were obtained using the Archimedes method which was described in the following equation[1]:

$$\rho = \frac{w_d}{w_0 - w_i} \qquad (3.1)$$

Where W_d is dry weight and W_i is sample weight in the water. W_0 is the weight of sample after taking out from water.

Before the measurement of W_0, samples were put into the O-ring sealed chamber and vacuated the chamber by rotary pump for 5 mins. After the air was pulled out from pores of samples, the water was introduced into the chamber in order to fill in the pores of samples.

3.2.3 Weight Loss Determination

The weight loss of Bismuth of $Bi(B'_{1/2}\ B''_{1/2})O_3$-$ABO_3$ powders at wide temperature range were determined by TG/DTA spectrometer (Perkin Elmer Instrument) with heating rate of 10^oC under ambient atmosphere. The weight loss as a function of time for the composition $0.15Bi(Zn_{1/2}Ti_{1/2})O_3$-$0.85Bi_{1/2}K_{1/2}TiO_3$ was measured at 1000^oC and 1020^oC for 10h.

3.3 Electrical Measurements

3.3.1 Sample Preparation

Prior to making dielectric measurements, the samples were polished to obtain smooth and parallel surfaces. In order to avoid the fringing field effects, thickness of the samples were polished down to the size of 1mm which makes the thickness less than 1/10 of diameter.

Two different kind of electrodes, Silver and Gold, were applied to samples according the measurement type and temperature range. For dielectric properties as a function of temperature, after polishing, a silver electrode paste

(Heraeus C1000) was applied on the surface and then fired at 600°C for 30 mins with heating rate of 2°C per min. For polarization hysteresis measurements (P-E) and strain as a function of electric field, the samples were sputtered by gold.

3.3.2 Dielectric Properties Measurement

The dielectric measurements were consisted of an LCR meter (Agilent 4284A, Hewlett-Packard Inc.), measurement unit and a desktop computer which was operated by Labview program (National Instrument). For low temperature dielectric measurement, this system was combined with environmental chamber (model 9023 delta design Inc.) which was capable of making dielectric measurements in the frequency range of 100 Hz to 100 kHz and temperature range of 150°C to -150°C. When higher temperature measurements were required, a high temperature measurement cell (NorECS Probostat) was used. This instrument was designed to work from room temperature to 1600°C. The heating rate during measurement is ± 2°C/min in air, while the capacitance and loss were measured using an applied ac voltage of 1 V at frequencies between 100 Hz to 100 kHz. The dielectric constant, ε, was calculated by the following equation[2]:

$$\varepsilon_r = \frac{Ct}{\varepsilon_0 A} \tag{3.2}$$

Where C is the capacitance (Farad), ε_r is the permittivity of free space (8.854 x 10^{-12} F/m), and A and t are the electrode area and thickness of the sample in meters, respectively

3.3.3 Resistivity Measurements

The resistivity is obtained by the technique of complex impedance spectroscopy (CIS). CIS is a powerful technique, which is used to investigate the electrical processes occurring in a material on applying AC input signal. The complex impedance can be written as[3]:

$$Z^*(\omega) = Z'(\omega) - iZ''(\omega) \tag{3.3}$$

Where Z' represents the resistance, Z" is the reactance and ω is the measurement frequency (ω=2π*f*). According to the Debye model the frequency dependence of the impedance can be written as following equation[3]:

$$Z'(\omega) = R_1 + \frac{R_2 - R_1}{1 + \omega^2 \tau^2} \tag{3.4}$$

Where R_1 and R_2 are the high and low frequency resistances, respectively. The relation between resistance and reactance can be expressed in terms of relaxtion time (τ) and is shown in figure.

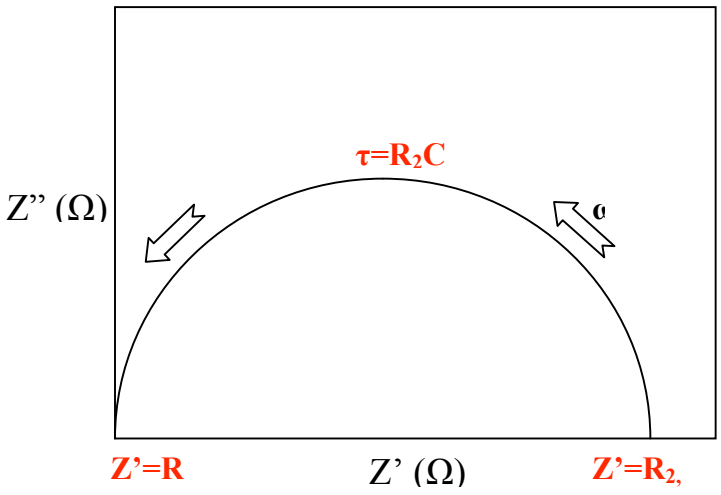

Figure 3.2 Complex impedance plot

3.3.4 Ferroelectric and Piezoelectric Properties Measurement

Polarizations as a function of electric field (P-E loop) at 10 Hz of the gold-sputtered samples were observed using a ferroelectrics test system (Radiant Precision series). The data was obtained and analyzed by vision software (Radiant). During the polarization measurement, an electric field of 10-100 kV/cm based on the coercive fields of the samples was applied. To prevent the breakdown of from the side area of the samples, samples were immersed in silicone oil during the measurement.

The electrical strains at room temperature were obtained by using an optical displacement sensor (MTI-2100) combined with radiant ferroelectric test system. The high field longitudinal piezoelectric constant, d_{33}, was determined from the ratio of maximum strain to maximum field.

Electromechanical coupling factor were determined as a function of composition for all ceramics systems. The techniques used were based on the IEEE Standard on Piezoelectricity (ANSI/IEEE Std.176-1987). The electromechanical properties of poled ceramics were determined by resonance methods using Frequency Response Analyzer (Solartron 1260) and Impedance Analyzer interfaced (Solartron 1296) with Smart software (Solartron). The piezoelectric planar coupling factor (k_p) is defined by the following equation[4]:

$$\frac{1}{(k_p)^2} = 0.398\left(\frac{f_r}{f_a - f_r}\right) + 0.579 \tag{3.5}$$

Where f_r is resonant frequency and f_a is anti-resonant frequency.

3.4 Reference

1. J. S. Reed, Principles of Ceramics Processing, Wiley Interscience, New York (1995)
2. S. O. Kasap, Electronic Materials and Devices, McGraw-Hill, New York (2006).
3. D. C. Sinclair and A. R.West, J. Appl. Phys. 66, 3850 (1989).
4. Electrical Measurement Method for Piezoelectric Ceramic Elements (Standards of Electronic Materials Manufacturers Association of Japan, April 1993) EMAS-6100.

CHAPTER 4

Phase Transitions and Dielectric Properties in $Bi(Zn_{1/2}Ti_{1/2})O_3$-$BaTiO_3$ Perovskite Solid Solutions

Based on article published in Journal of Applied Physics *(in press)*

http://jap.aip.org/

Chien-Chih Huang and David P. Cann

Materials Science, Department of Mechanical Engineering, Oregon State University, Corvallis, Oregon 97331, USA

Abstract

$(1-x)Bi(Zn_{1/2}Ti_{1/2})O3-xBaTiO_3$ polycrystalline ceramics were obtained via solid state processing techniques. The perovskite structure was found to be stable for compositions containing x=0.66 or greater. Based on x-ray diffraction data, a morphotropic phase boundary between tetragonal and rhombohedral perovskite phases was observed at x≈0.9. For compositions rich in $BaTiO_3$, the symmetry of the perovskite phase was tetragonal but with increased $Bi(Zn_{1/2}Ti_{1/2})O_3$ content, the rhombohedral phase appeared. Dielectric characterization revealed that as $Bi(Zn_{1/2}Ti_{1/2})O_3$ content increased, the transition temperature decreased and the transition peak became very diffused. A comparison of the dielectric behavior with other $Bi(Zn_{1/2}Ti_{1/2})O_3$-based solid solutions is also discussed.

4.1 Introduction

Solid solutions of $Bi(Me)O_3$-$PbTiO_3$ perovskites have been widely investigated due their high Curie transition temperature (T_C) and excellent piezoelectric properties.[1-2] In $Bi(Me)O_3$ compounds, the Me can be either a single trivalent cation or two cations with average +3 valance which occupy the octahedral sites. Recently, Eitel *et al.* reported a new piezoelectric material based on $BiScO_3$-$PbTiO_3$ (BS-PT) which showed high piezoelectric properties and a high transition temperature ($T_C \approx 450°C$) at the morphotropic phase boundary (MPB).[2-3] Instead of decreasing tetragonality with increasing $Bi(Me)O_3$ content, Suchomel *et al.* demonstrated an enhanced tetragonality in $Bi(Zn_{1/2}Ti_{1/2})O_3$- $PbTiO_3$ (BZT-PT) solid solutions.[4-5] In this system, the MPB did not appear and the tetragonal phase persisted over all compositions studied until a second phase formed.

Due to environmental concerns, the replacement of toxic Pb in piezoelectric materials is a high priority. Thus there is a great need for a Pb-free piezoelectric material that shows comparable electric properties to Pb-based piezoelectrics. Bi-based perovskites are a good candidate due to the similar electronic structure with Pb.[6-7] However, the smaller size of the Bi cation severely limits the stability of the perovskite structure. Therefore, one approach is to utilize a solid solution with a stable perovskite end member. Thus, $BaTiO_3$ is a good candidate due to a high degree of solid solution with other perovskite phases and a stable tetragonal crystal structure at room temperature.

In previous work, solid solutions within the ternary perovskite system $Bi(Zn_{1/2}Ti_{1/2})O_3$-$BiScO_3$-$BaTiO_3$ (BZT-BS-BT) were investigated.[8] The phase equilibria and dielectric data showed a transition between the pseudo-cubic relaxor behavior to tetragonal normal ferroelectric behavior. The object of this research is focus on the transition temperature and ferroelectric properties of the binary $Bi(Zn_{1/2}Ti_{1/2})O_3$- $BaTiO_3$ (BZT-BT) system. The dielectric properties of the $BiScO_3$-$BaTiO_3$ system will be also discussed as a comparison.

4.2 Experiment

Ceramics of a composition (1-*x*)$Bi(Zn_{1/2}$ $Ti_{1/2})O_3$-*x*$BaTiO_3$ where x=0.66-1 were synthesized by conventional solid state reaction methods. Reagent grade oxide powders of Bi_2O_3 (≥99.9%), ZnO (≥99%), TiO_2 (≥99.9%), and $BaCO_3$(≥99.5%) were batched in stoichiometric amounts and vibratory milled with ethanol and yttrium-stabilized zirconia media for 6h. Precursor method which made $ZnTiO_3$ first and then mixed with other oxides was also adopted to compare with conventional ceramic mixing. The dried powders were calcined in crucibles at 950°C for 12h followed by an additional milling and drying step. The calcined powders were mixed with 3 wt% polyvinyl butyral (PVB) binder and then uniaxially cold-pressed at 150 MPa into 12.7mm diameter pellets. Following binder burnout at 400°C, the pellets were sintered in sealed crucibles between 1100°C-1300°C for 2h. For phase determination, x-ray diffraction (Bruker-AXS D8) was utilized in the 2θ scan range of 10°-80° using sintered ceramics.

Prior to making dielectric measurements, the samples were polished to obtain smooth and parallel surfaces. After polishing, a silver electrode paste (Heraeus C1000) was applied and then fired at 650°C for 30 mins. Polarization hysteresis measurements (P-E) were obtained at a frequency of 10Hz using a ferroelectrics test system (Radiant). The strain as a function of applied electric field was determined by using an optical displacement sensor (MTI-2100). An Agilent 4284A LCR meter was then used to measure the dielectric properties over a wide temperature range.

4.3 Results and Discussion

4.3.1 Crystal Structure of BZT-BT Solid Solutions

Figure 4.1 shows XRD patterns of sintered (1-x)BZT-xBT ceramics at room temperature. Single-phase perovskite was obtained for compositions containing up to 34 mole% BZT. Higher concentrations of BZT resulted in the formation of secondary phases. According to the peak splitting of the {200} reflection, the samples exhibited tetragonal symmetry (*P*4*mm*) between $1 \leq x \leq 0.95$. The tetragonality (or c/a ratio) decreased as the BZT content increased as observed by the merging of the {200} peaks as shown in figure 4.1b. For compositions between $0.8 \leq x \leq 0.66$, the structure was stabilized into pseudo-cubic or rhombohedral symmetry. According to XRD data, a morphotropic phase boundary (MPB) between the tetragonal and rhombohedral phases was observed at a composition close to $x = 0.9$. However the exact MPB composition is difficult to determine. In addition, the precursor method didn't change the results of XRD and solubility of perovskite.

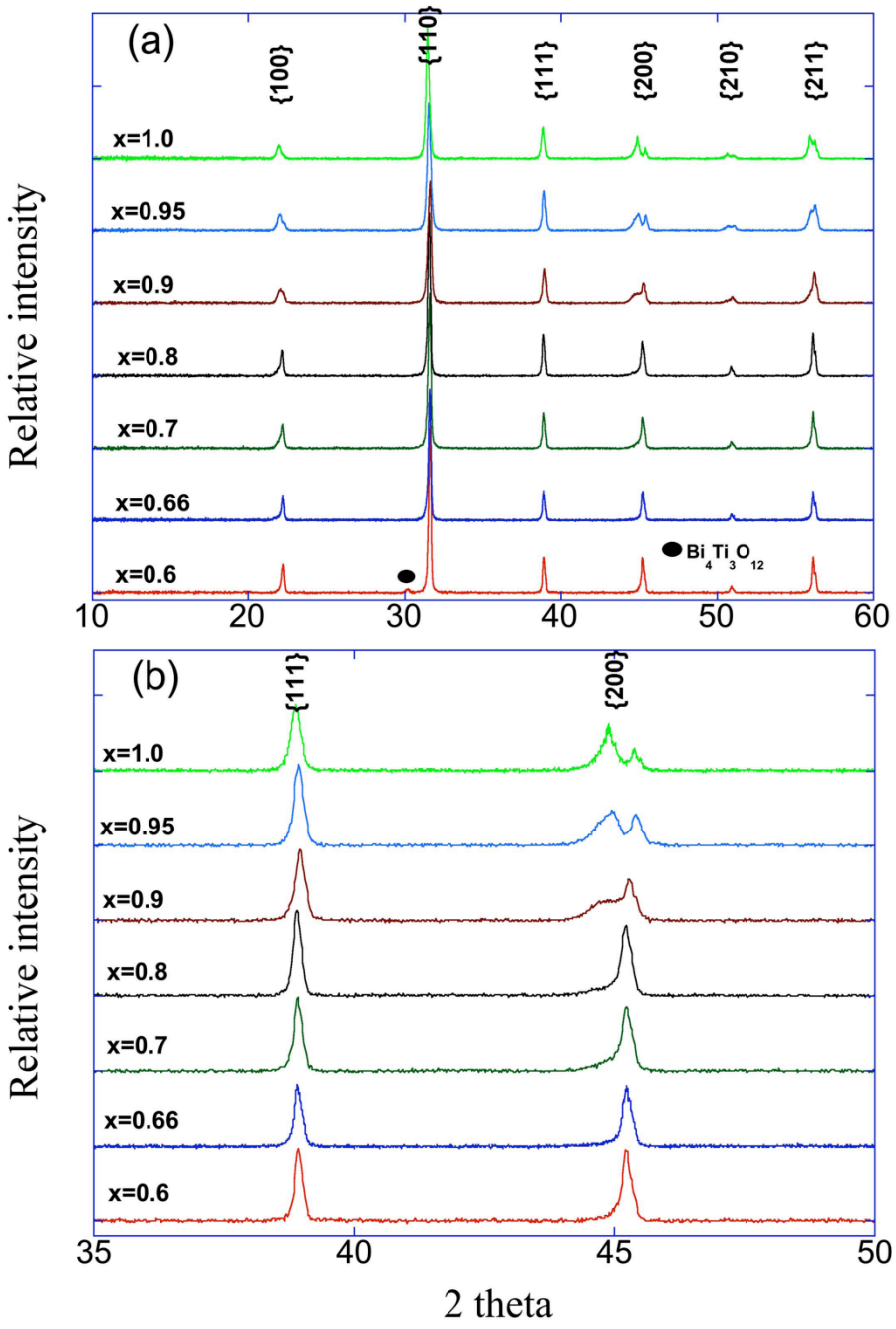

Figure 4.1 XRD diffraction patterns of sintered (1-x)(BZT)-xBT ceramics.

4.3.2 Dielectric Properties of BZT-BT Solid Solutions

In figure 4.2, the dielectric constant as a function of temperature was plotted for the (1-*x*)$Bi(Zn_{1/2}Ti_{1/2})O_3$-*x*$BaTiO_3$ ceramic solid solutions. According to figure 4.2, pure $BaTiO_3$ ceramic showed three distinct transition temperatures at approximately -90°C, 0°C , and 130°C. However, with the addition of only 5% BZT, the transition peaks at 0°C and -90°C vanished and a single phase transition was observed. The dielectric data for the *x*= 0.9 composition shows that the transition temperature is in the vicinity of room temperature. This is consistent with the relatively broad peaks observed in the XRD data (figure 4.1).

Figure 4.3 illustrates the diffuseness of the phase transition in terms of the parameter δ_r and the temperature at which the maximum permittivity was observed (T_m) as a function of composition. The degree of diffuseness (δ_r) can be obtained from the following expression:[10]

$$\frac{\varepsilon_m^{'}}{\varepsilon^{'}(f,T)} = 1 + \frac{(T - T_m(f))^{\gamma}}{2\delta_\gamma^2} \quad (1 \le \gamma \le 2) \qquad 4.1$$

It was observed that the diffuseness increased with increasing BZT content. However the transition temperature T_m exhibited at minimum at *x* = 0.9. Within the tetragonal region, T_m decreased dramatically with increasing BZT content indicating a destabilization of the ferroelectric phase. Within the rhombohedral phase field the transition temperature increased linearly with BZT content. This phenomena is very similar to previous results in the $BiScO_3$-$Bi(Zn_{1/2}Ti_{1/2})O_3$-$BaTiO_3$ ternary system.

The effects of composition on the unit cell parameters and volume is shown in figure 4.4. While the volume decreases as the mole percent of BZT increases, there is an anomalous peak close to the MPB composition at $x = 0.9$. This could be attributed to the coexistence of the rhombohedral and tetragonal phases due to the fact that at this composition the phase transition is very close to room temperature ($T_m \approx 30°C$). It could also be related to structural disorder in the B-cation sublattice due to the limited processing temperatures.

The dielectric properties as a function of frequency for the 0.2BZT-0.8BTcomposition are shown in figure 4.5. The frequency dependence of the transition peaks indicates a strong relaxor behavior for this composition. Moreover, these compositions exhibit a stable dielectric constant and low loss tangent (tan $\delta <$ 0.01) up to high temperatures ($T < 400^{o}C$). It may have potential for high temperature applications.

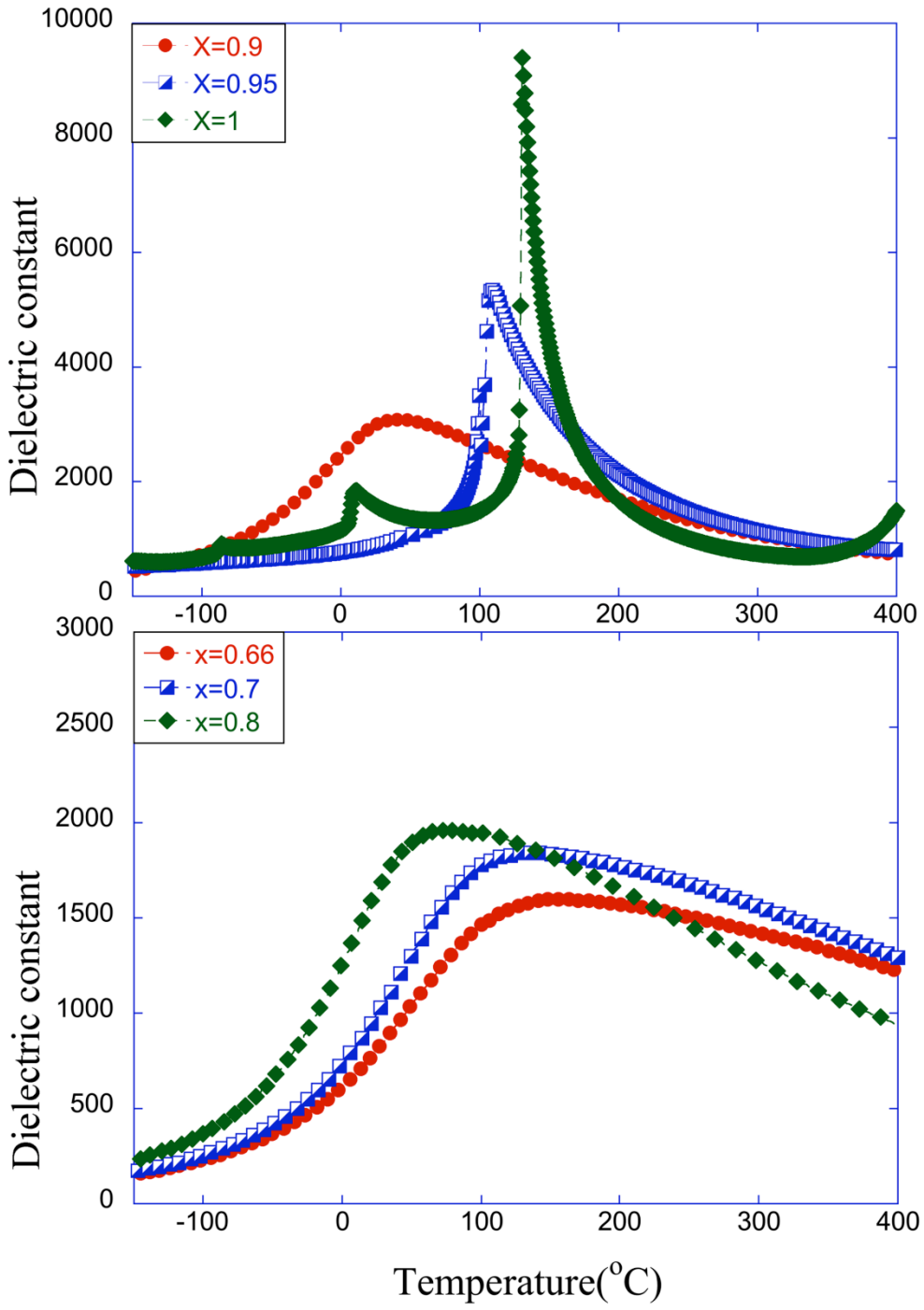

Figure 4.2 Dielectric constant as a function of temperature for (1-*x*)BZT-*x*BT at a measurement frequency of 10 KHz.

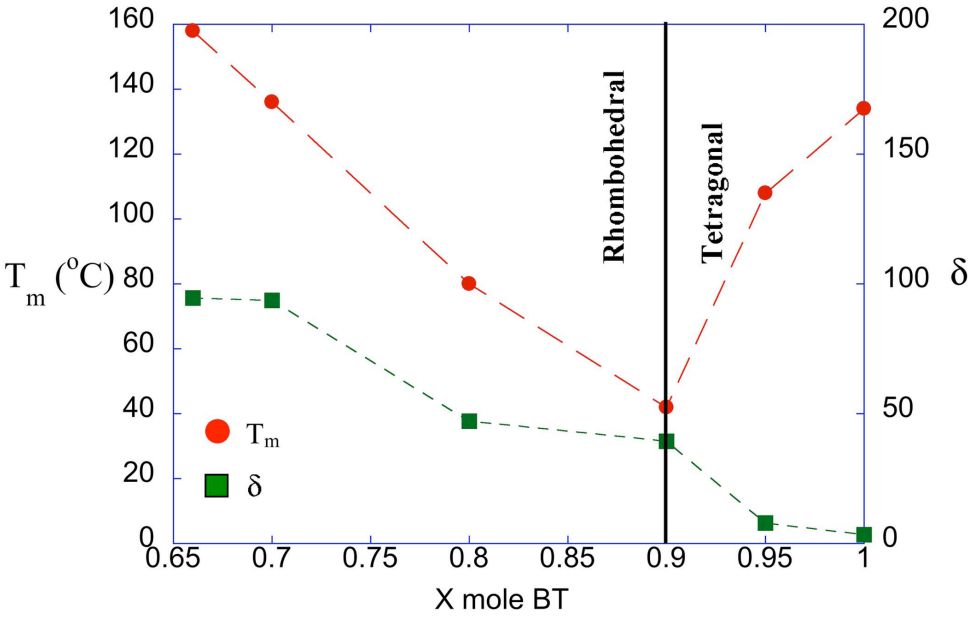

Figure 4.3 T_m and diffuseness δ as a function of $BaTiO_3$ content.

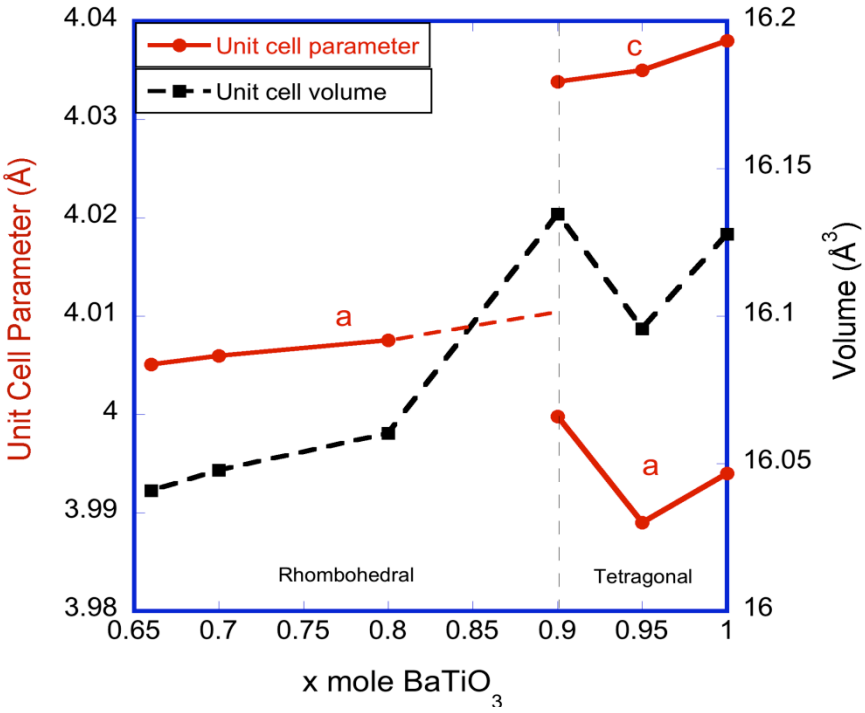

Figure 4.4 Lattice parameter of (*1-x*)BZT-*x*BT

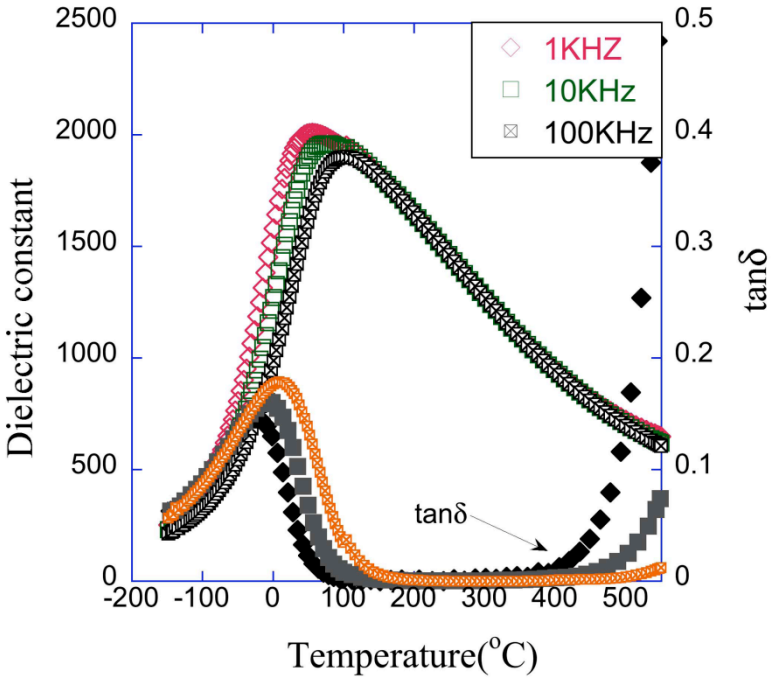

Figure 4.5Dielectric constant and tanδ of 0.2BZT-0.8BT as a function of temperature.

4.3.3 Ferroelectric and Piezoelectric Properties for BZT-BT Ceramics

The polarization hysteresis data at room temperature for (1-*x*)BZT-*x*BT are shown in Figure 4.6. The remnant polarization (P_r) and Coercive field (E_c) were increased to 10.2 μC/cm and 11.3 KV/cm for 0.05BZT-0.95BT compared to pure $BaTiO_3$. However, when more BZT was added the area of hystersis loops decreased dramatically. The absence of clear hysteresis behavior for higher BZT contents can be related to a decreased T_m as shown in figure 4.2. Although T_m increased for x>0.1, the relaxor behavior due to rhombohedral symmetry and possibly degree of higher disorder in the structure resulted in the disappearance of hysteresis loop.

Figure 4.7 shows the strain behavior at room temperature under a bipolar driving electric field from 0 to 60 KV/cm. The slope of the strain-electric field loop

decreased when the BZT content increased. This may due to the loss of normal-ferroelectric behavior which was revealed in figure 4.6. The planar coupling factor (k_p) on (1-x)BZT-xBT ceramics was obtained at room temperature was shown in figure 4.8. The k_p is 0.21 for x=0.95 and further BZT added will result in the vanish of resonant and anti-resonant peaks. This can be explained by the relaxor behavior when more than 10 mole% BZT was added which was shown in figure 4.6.

Figure 4.9 illustrated the resistivity of (1-x)BZT-xBT ceramics. The resistivity increased to the maximum value of 10^{13} Ω at x= 0.8 and then decreased as increasing BZT content. The increased resistivity may relate to higher density for BZT-BT solid solutions.

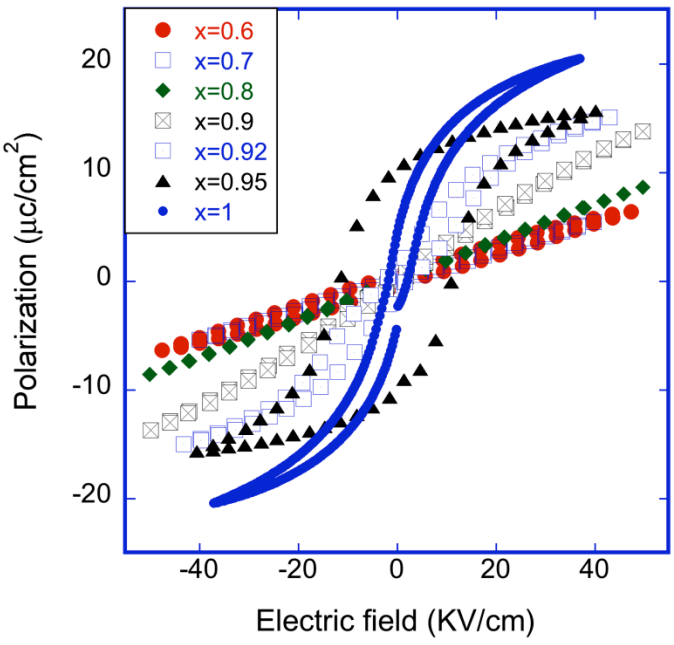

Figure 4.6 P-E hysteresis measurements on (1-x)BZT-xBT ceramics obtained at room temperature

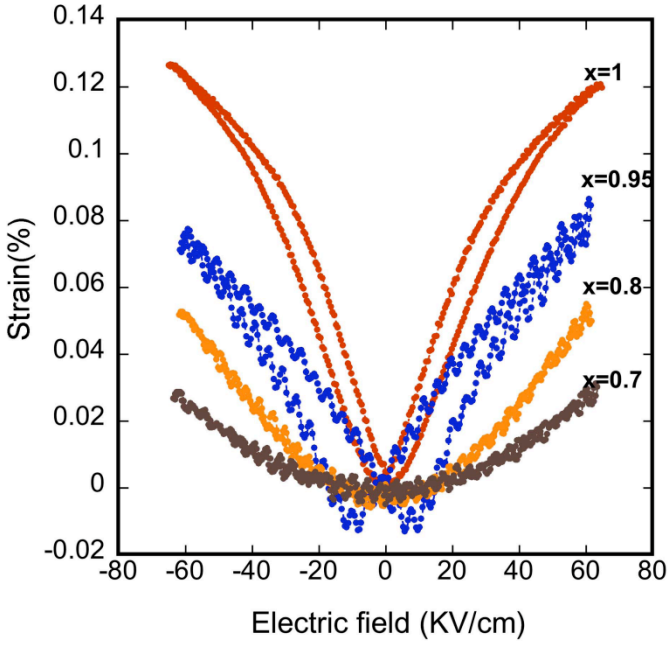

Figure 4.7 Strain-electric field measurements on (1-*x*)BZT-*x*BT ceramics obtained at room temperature

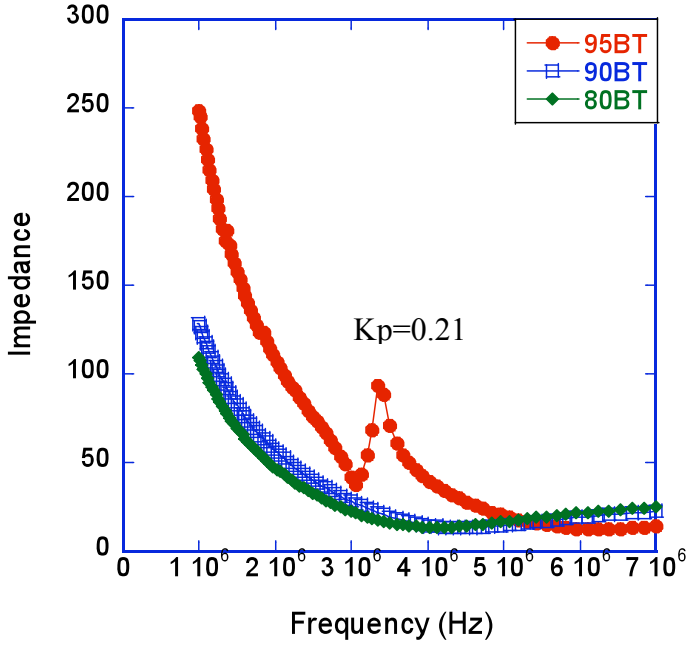

Figure 4.8 Planar coupling factor (k_p) on (1-*x*)BZT-*x*BT ceramics obtained at room temperature

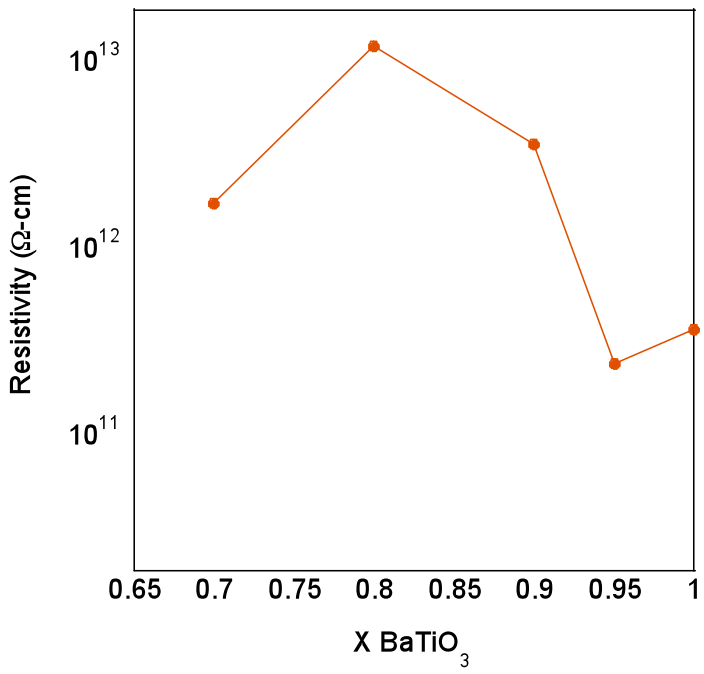

Figure 4.9 Resistivity for x(BZT)-(1-x)$BaTiO_3$

4.3.4 Dielectric Properties for BS-BT and BZT-BT Ceramics

The dielectric constant and loss versus temperature for 0.2(*x*Bi($Zn_{1/2}Ti_{1/2}$)O_3-(1-*x*)$BiScO_3$)-0.8$BaTiO_3$ ceramics are shown in figure 4.10. The transition peak in BS-BT is clearly more diffuse than BZT-BT system. This may indicate that the source of the relaxor behavior is more closely tied to disorder on the B-site. Moreover, though Sc^{3+} is bigger than the average of Zn^{2+} and Ti^{4+}, the transition temperature was the same for BZT-BT and BS-BT. This result is quite different from other $BiMeO_3$-$PbTiO_3$ systems in which the transition temperature is highly dependent upon the size of the B site cations.[1]

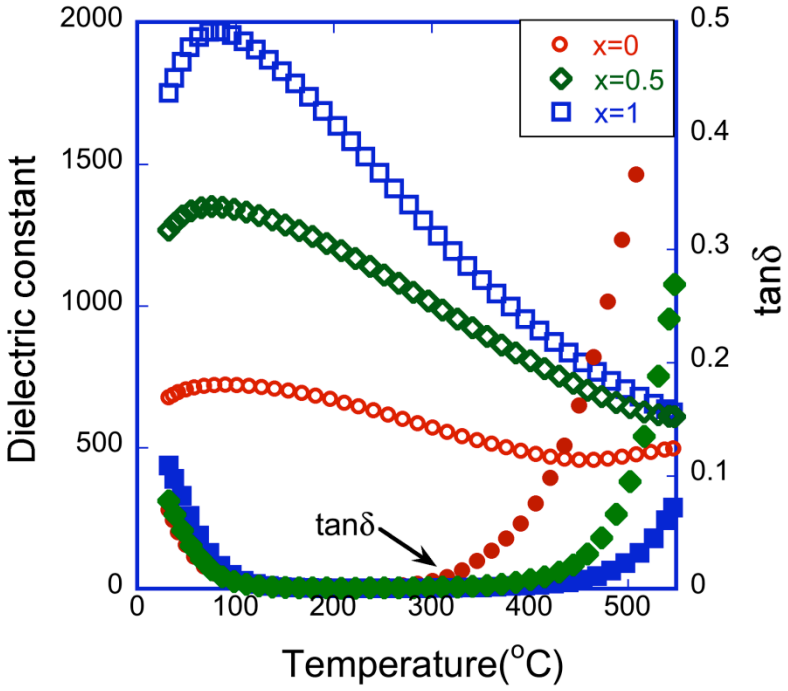

Figure 4.10 Dielectric constant and tanδ versus temperature for 0.2(xBi($Zn_{1/2}Ti_{1/2}$)O_3-(1-x)$BiScO_3$)-0.8$BaTiO_3$ at 10KHz.

4.3.5 Annealing Effect for BZT-BT Ceramics

Figure 4.11 demonstrated the dielectric properties before and after annealing for 0.3BZT-0.7BT ceramics. The peak at T_m remaining the similar value and shape which indicated the absent of long rang ordering. The lack of ordering after annealing may due the complex compositions of A site and B site. Although there is no cations ordering happened, the peak at high temperature which may be resulted from oxygen vacancy disappeared after annealing.

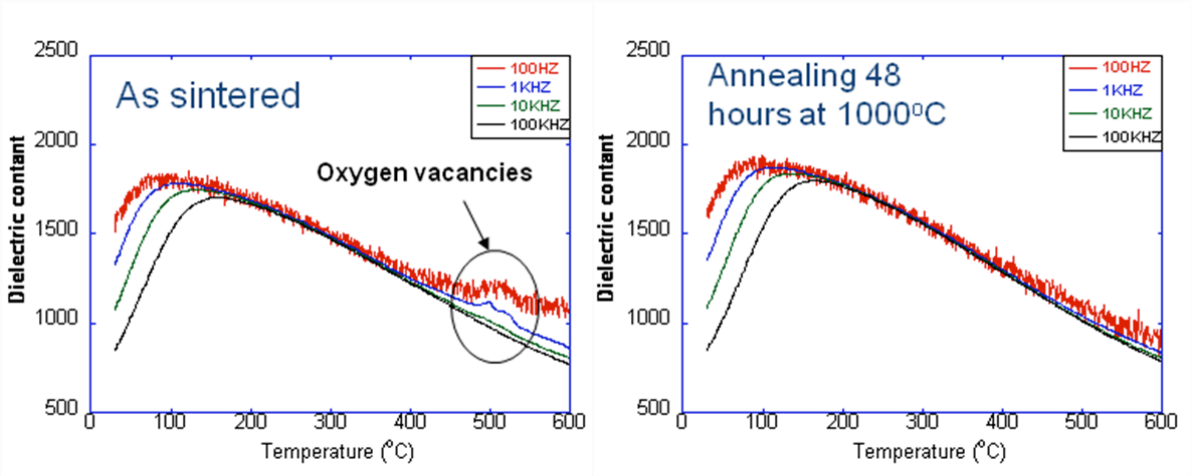

Figure 4.11 Annealing effect for 0.3BZT-0.7BT ceramics

4.4 Conclusions

Perovskite solid solutions based on $(1-x)Bi(Zn_{1/2}Ti_{1/2})O_3$-$xBaTiO_3$ with $x \geq 0.66$ were synthesized via conventional solid state processing techniques. A phase boundary between ferroelectric tetragonal and rhombohedral phases was observed close to x=0.99. The tetragonality decreased and the diffuseness of the phase transition increased with increasing BZT content. Measurement of the unit cell volume as a function of composition showed a linear dependence except for a peak near the MPB which can be attributed to the coexistence of the rhombohedral and tetragonal phases. The hystersis measurements revealed an improved P_r and E_c for x=0.95 compared to pure $BaTiO_3$. Due to the diffuseness of the phase transition, the dielectric constant remains stable and loss tangents remained small ($\tan\delta<0.01$) over a wide range of temperature ($T < 400°C$).

4.5 References

1. C. J, Stringer, T. R. Shrout and C. A. Randall, *J. Appl. Phys.* 99, 024106 (2006).
2. R. E. Eitel, C. A. Randall, T. R. Shrout, P. W. Rehrig. W. Hackenberger and S. -E. Park, Jap. *J. Appl. Phys*. 40, 5999 (2001).
3. R. E. Eitel, C. A. Randall, T. R. Shrout and S. -E. Park, Jap. *J. Appl. Phys*. 41, 2099 (2002).
4. M. R. Suchomel and P. K. Davies, *J. Appl. Phys* 96, 1489 (2004).
5. M. R. Suchomel and P. K. Davies, *Appl.Phys. Lett*. 86, 262905 (2005).
6. G. A. Smolenskii, V. A. Isupov, A. I. Agranovskaya, and N. N. Krainik, Sov. Phys. Solid State 2, 2651 (1961).
7. R. E. Cohen, *Nature* 358, 136 (1992).
8. C.-C. Huang, D.P. Cann, X. Tan, and N. Vittayakorn, *J. Appl. Phys*. 102, 044103 (2007). [10] R. E. Cohen, *Nature*358, 136 (1992).
9. O. Bidault, P. Goux, M. Kchikech, M. Belkaoumi, M. Maglione, Phys. Rev. B 49, 7868 (1994).
10. K. Uchino, S. Nomura, *Ferroelectrics Lett*. 44, 55 (1982).

CHAPTER 5

Structure and Ferroelectric Properties of $Bi(Zn_{1/2}Ti_{1/2})O_3$-$(Bi_{1/2}K_{1/2})TiO_3$ Perovskite Solid Solutions

Based on article submitted to IEEE Transactions on Ultrasonic, Ferroelectrics, and Frequency Control (June 2008)

Chien-Chih Huang, Naratip Vittayakorn and David P. Cann

Department of Mechanical Engineering, Oregon State University, Corvallis, OR 97331-6001, USA

Abstract

Lead-free piezoelectric ceramic $xBi(Zn_{1/2}Ti_{1/2})O_3$-$(1-x)(Bi_{1/2}K_{1/2})TiO_3$ were obtained via solid-state processing techniques. A single perovskite phase with tetragonal symmetry was obtained for $Bi(Zn_{1/2}Ti_{1/2})O_3$ substitutions up to 20 mole%. The maximum density was 97.1% at the composition of x=0.1. The dielectric measurement indicated that transition temperature decrease linearly with increasing BZT content. The P-E loops revealed the higher P_r with adding BZT. The piezoelectric coefficient, d_{33}, for x=0, x=0.05, x=0.1 were 110 pm/V, 185 pm/V and 235pm/V respectively. The dielectric and piezoelectric data showed the improvement of the properties of BKT when BZT was added.

5.1. Introduction

Lead zirconate titanate (PZT) and PZT-based solid solutions are widely used ferroelectric materials owing to their excellent piezoelectric, dielectric and pyroelectric properties.[1,2] However the toxicity of lead oxides and its high vapor pressure during processing has the potential for a negative impact on the environment. Materials based on the perovskite structure are excellent candidates for lead-free piezoelectric research due to the intrinsic versatility which can be achieved by chemical manipulation[3]. Bismuth potassium titanate, $Bi_{1/2}K_{1/2}TiO_3$ (BKT), is a well known ferroelectric material with the perovskite structure. BKT possesses tetragonal symmetry and has relatively high Curie temperature (T_c=380^{o}C)[4,5] which makes it suitable for the development of lead-free piezoelectric materials for wide temperature ranges. However the poor sinterability and poling difficulties have limited the application of this material. In order to improve the properties of BKT, Hiruma *et al.* reported the increase of the density of BKT ceramics through a hot pressing method[6]. Sasaki *et al.* reported the enhancement of piezoelectric and ferroelectric properties through solid solution with $Bi_{1/2}Na_{1/2}TiO_3$[7].

Recently the development of new bismuth-lead-based ferroelectric materials, $Bi(M)O_3$-$PbTiO_3$ (M=Zn^{2+}, Sc^{3+}, Fe^{3+} ,Ti^{4+}, e.q., $Bi(Sc^{3+})O_3$ or $Bi(Zn^{2+},Ti^{4+})O_3$),[8-11] has attracted a lot of attention. Due to the relative small size of Bi^{3+}, most $Bi(M)O_3$ compounds are not stable in the perovskite form and can only be synthesized under high pressures [12]. The smaller tolerance factor of $Bi(M)O_3$ and the highly polarizable Bi^{3+} ion can further enhance the transition temperature and piezoelectric effect in solid solutions with $PbTiO_3$[8].

Although the compositions of $Bi(M)O_3$-$PbTiO_3$ have been widely investigated, there are few reports on $Bi(M)O_3$ solid solutions with other non-lead perovskite end members. In this paper the structure, ferroelectric, and piezoelectric properties of the $Bi(Zn_{1/2}Ti_{1/2})O_3$-$(Bi_{1/2}K_{1/2})TiO_3$ (abbreviated BZT-BKT) solid solutions were studied. The effect of BZT on perovskite BKT in terms of density and transition temperature was also discussed. The purpose of this research is to improve the properties of BKT and find an alternative approach in the development of lead-free piezoelectric materials.

5.2 Experiment

The *x*BZT-(1-*x*)BKT ceramics were prepared using a conventional ceramic processing procedures. Reagent grade oxide powders of Bi_2O_3 (≥99.9%), ZnO (≥99%), TiO_2 (≥99.9%) and K_2CO_3 (≥99.5%) were weighted according to stoichiometric formulae and ball-milled with ethanol and yttrium-stabilized zirconia media for 6 h. The dried powders were calcined in crucibles at 920°C for 6 h and then ball-milled again for 6 h. The dried calcined powders were mixed with 3 wt% polyvinyl butyral (PVB) and then pressed into pellets with 12.7 mm diameter under 150 MPa. After burning out PVB binder at 400°C, the pellets were covered with extra powders and sintered in sealed crucibles between 1025°C-1045°C for 10 h. The densities of the sintered ceramics were obtained using the Archimedes method. The structure and lattice parameters for sintered ceramics were determined by x-ray diffraction (Bruker-AXS D8) in the 2θ scan range of 10°-80°. Prior to the measurement of the dielectric properties as a function temperature, a silver electrode

paste (Heraeus C1000) was applied to the ceramics and then fired at 650°C. An Agilent 4284A LCR meter was utilized to measure the dielectric properties over a wide temperature range using a NorECS ProboStat high temperature measurement cell. Polarization as a function of electric field (P-E loops) at 10 Hz on gold-sputtered samples was observed using a ferroelectrics test system (Precision LC; Radiant Technologies, Inc.). The electric-field induced strain was obtained at room temperature by using an optical displacement sensor (MTI-2100; MTI Instruments).

5.3 Resultsand Discussion

5.3.1 Structure and Physical properties of BZT-BKT

The x-ray diffraction patterns of sintered *x*BZT-(1-*x*)BKT ceramics at room temperature are shown in figure 5.1. Single phase perovskite structures with tetragonal symmetry were obtained for compositions with BZT contents lower than 20 mol%. Higher concentrations of BZT resulted in the formation of secondary phases. These results indicate that the presence of BZT in the solid solution decreases the structural stability of BKT perovskite phase. The lattice parameters were calculated based on XRD patterns and shown in Table 5.1. The c/a ratio showed little variation over the range in BZT content from $x = 0$ to $x = 0.2$. However, the unit cell volume increased linearly with increased BZT content. The densities of the ceramics as a function of BZT content are shown in figure 5.2. The density increased to the maximum value of 97.1% compared to theoretical density at 10 mol% BZT. Beyond 10 mol% BZT, the result was a decrease of the density. The decrease of density may come for Bismuth loss. From TGA data as shown in figure 5.3, the weight loss for

0.15BZT-0.85BKT at temperature 1020°C for 10 hours is 0.6%. Since the sintering temperature for 0.15BZT-0.85BKT is 1035°C, further weight loss which resulted in decrease of density can be expected.

Table 5.1 Physical properties of *x*BZT-(1-*x*)BKTceramic

x BZT	0	0.05	0.1	0.15	0.2
c/a ratio	1.019	1.013	1.015	1.014	1.015
Cell Volume(Å^3)	61.55	61.79	62.19	62.45	62.67
$\rho_{theoretical}$ (g/cm^3)	5.95	6.05	6.14	6.24	6.35
ρ (%)	92.4	94.8	97.1	95.2	94.6
T_m at 10KHz (°C)	374	340	313	304	293

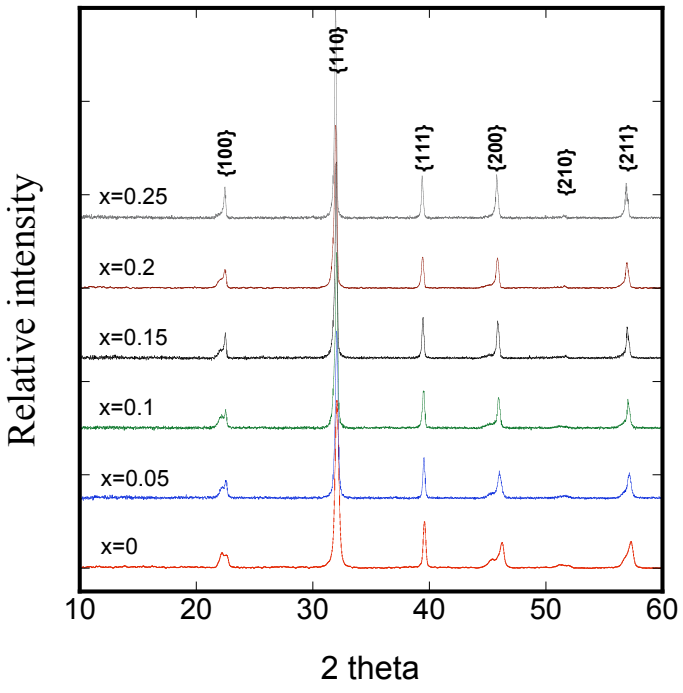

Figure 5.1 XRD diffraction patterns of sintered *x*(BZT)-(1-*x*)BKT ceramics.

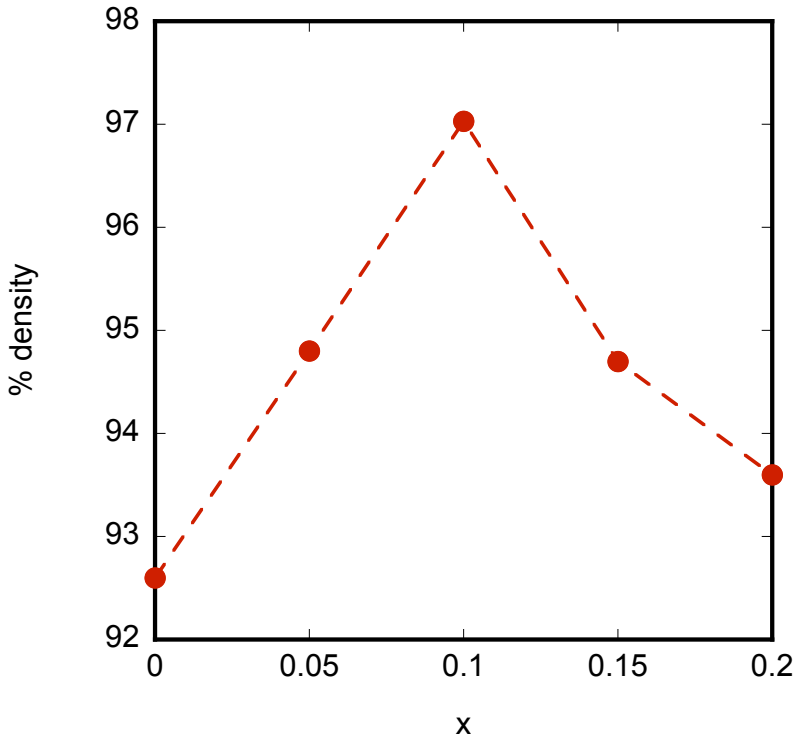

Figure5.2 Density as a function of BZT content

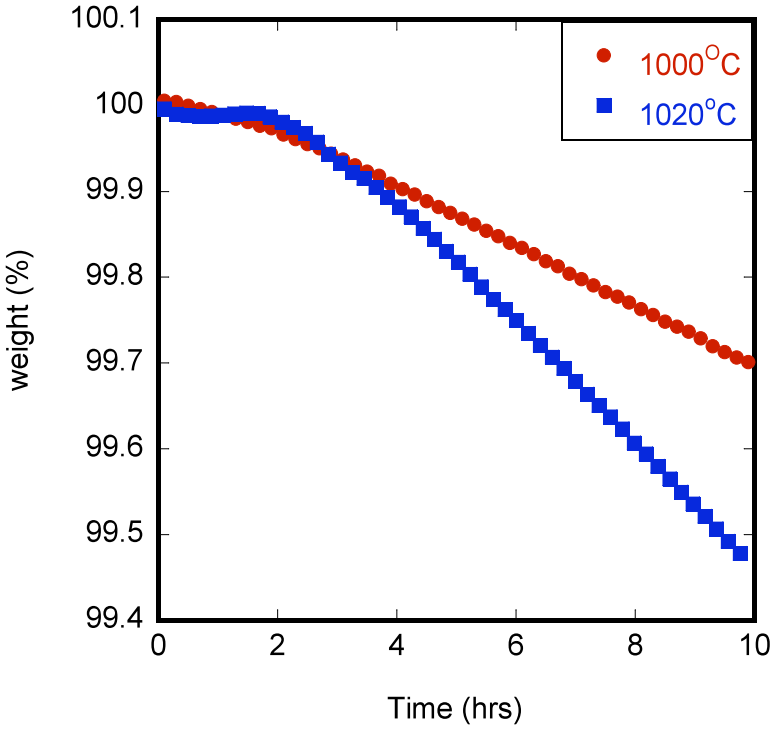

Figure 5.3 TGA data for 0.15BZT-0.85BKT measured at 1000°C and 1020°C for 10h

5.3.2 Dielectric Properties of BZT-BKT

The dielectric constant and dielectric loss (tan δ) for x=0 and x=0.1 measured from 100 Hz to 100 kHz as a function of temperature are shown in figure. 5.4. It was observed that the maximum dielectric constant increased and the phase transition became more diffuse with increasing BZT content. The increase in dielectric constant is at least partially related to the higher density and larger grain size [13-14]. The increased frequency dependence of the dielectric spectra below the transition temperature for x=0.1 indicates a diffuse transition in the BZT-BKT solid solution. Another feature in the dielectric spectra that can be noted is the suppression of the low frequency dielectric loss at high temperatures. This behavior is similar to that observed in the $BiScO_3$-$BiZnTiO_3$-$BaTiO_3$ ternary system [15]. The temperature at which maximum dielectric constant appeared, T_m, is listed in Table 5.1. The data clearly shows that T_m decreased monotonically with increasing BZT content.

Figure 5.5 shows the dielectric properties of 0.1BZT-0.9BKT ceramics sintered at 1040°C for 2h, 10h, 20h and 64h. The increase of dielectric constant and loss at T_m can be explained by grain growth due to longer sintering times. Moreover, it is well known that longer sintering times are also effective at increasing the chemical homogeneity which sharpens phase transitions. It is interesting to note that the high temperature tan δ decreased with increasing sintering hours possibly due to a reduction in oxygen vacancies.

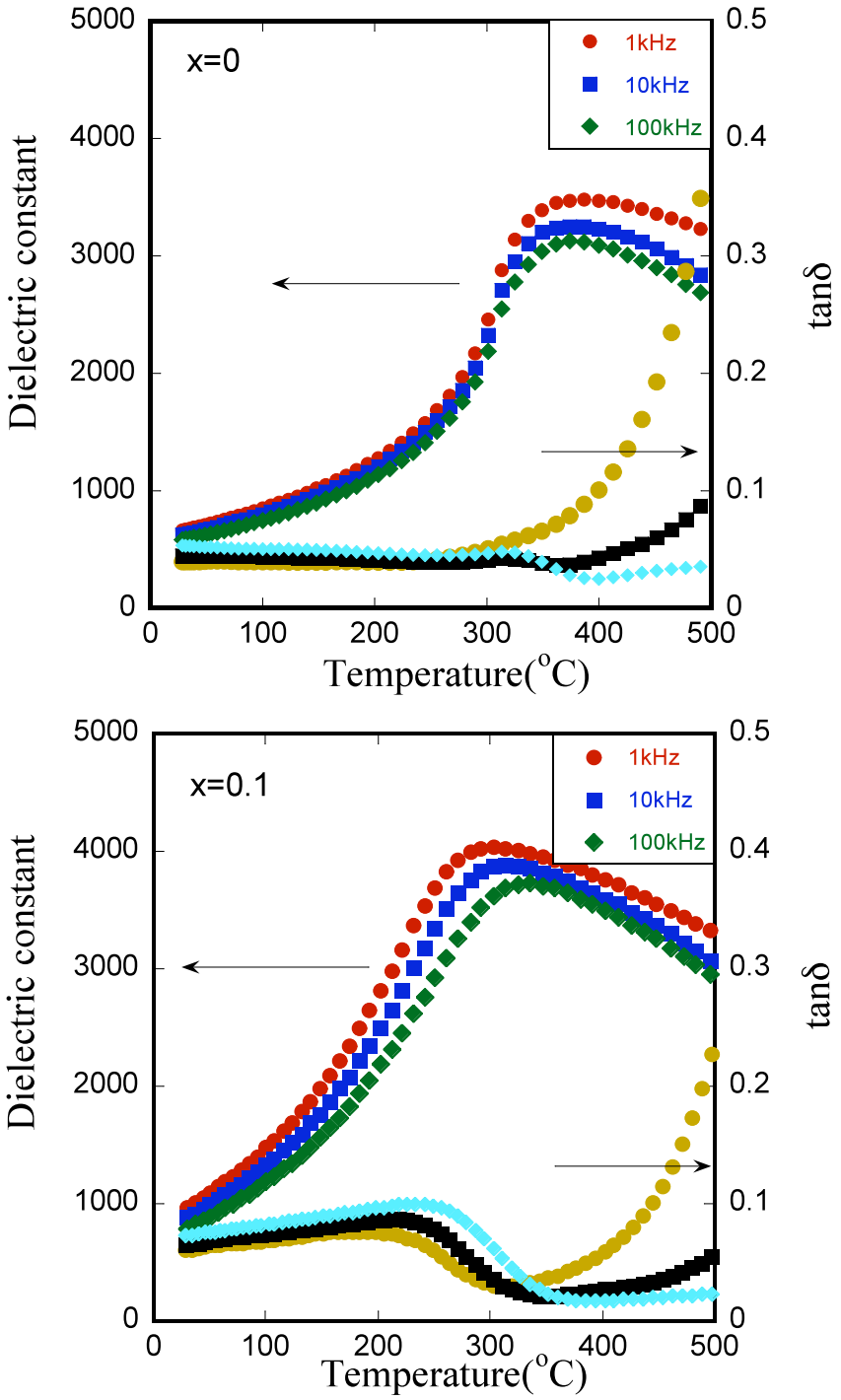

Figure 5.4 Dielectric constant and tanδ of *x*(BZT)-(1-*x*)BKT as a function of temperature

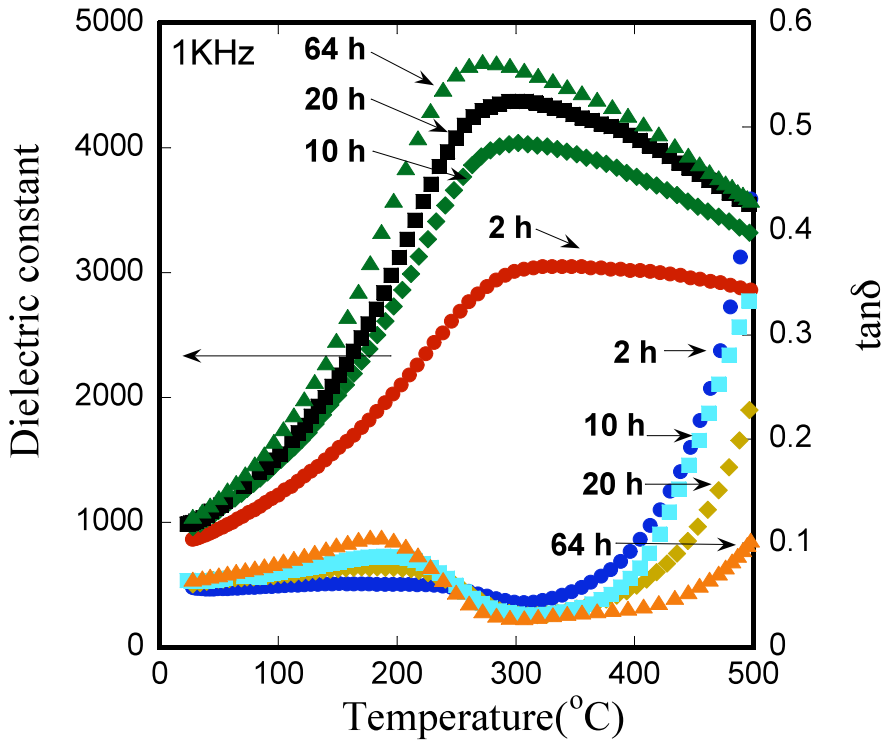

Figure 5.5 Dielectric properties of 0.1BZT-0.9BKT for different sintering time.

5.3.3 Ferroelectric and Piezoelectric Properties of BZT-BKT

The P-E loops for *x*BZT-(1-*x*)BKT ceramics were measured at 10Hz and are shown in figure 5.6a. The loops do not fully saturate up the maximum field levels of 100 kV/cm indicating a relatively hard ferroelectric state. With the addition of BZT, the hysteresis loops approach saturation with a significantly higher remnant polarization (P_r) increased from 6.1μC/cm to 11.8μC/cm. Figure 5.6b shows the strain behavior at room temperature under bipolar driving electric field from 0 to 80 kV/cm. The strain loops show the typical butterfly shape that is characteristic of ferroelectric piezoelectrics. It is clearly shown that the slope of the strain-electric field loop increased with the addition of x=0.1 BZT. Based on the P-E and strain data, it can be

observed that the addition of BZT to BKT enhanced the piezoelectric properties significantly. The P-E loop for 0.15BZT-0.85BKT as a function of temperature shown in figure 5.7 indicated the loss of ferroelectricity occurred at 200^{o}C. For pure BKT depolarization temperature is 270^{o}C which represents the transition from tetragonal to pseudocubic symmetry. Therefore, the increase of BZT content will result in decrease of depolarization temperature.

Finally, figure 5.8 shows the unipolar strain versus electric field data for xBZT-(1-x)BKT from 0 to 80 kV/cm. The longitudinal piezoelectric coefficient, d_{33}, was obtained from the ratio of maximum strain to maximum field. The d_{33} values for x=0, x=0.05, x=0.1 were calculated to be 110 pm/V, 185 pm/V and 235pm/V, respectively.

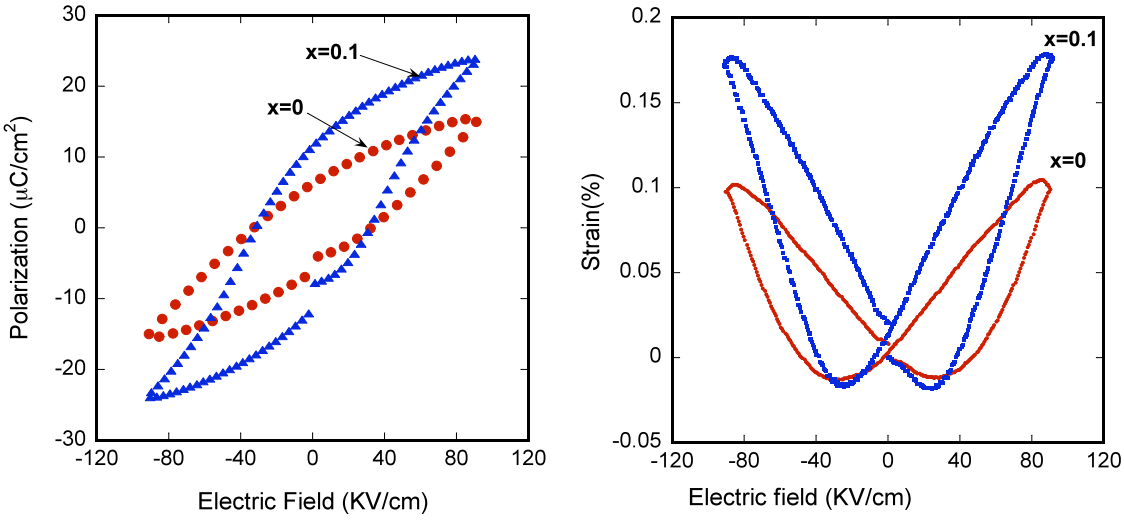

Figure 5.6 Polarization and strain as a function of electric field

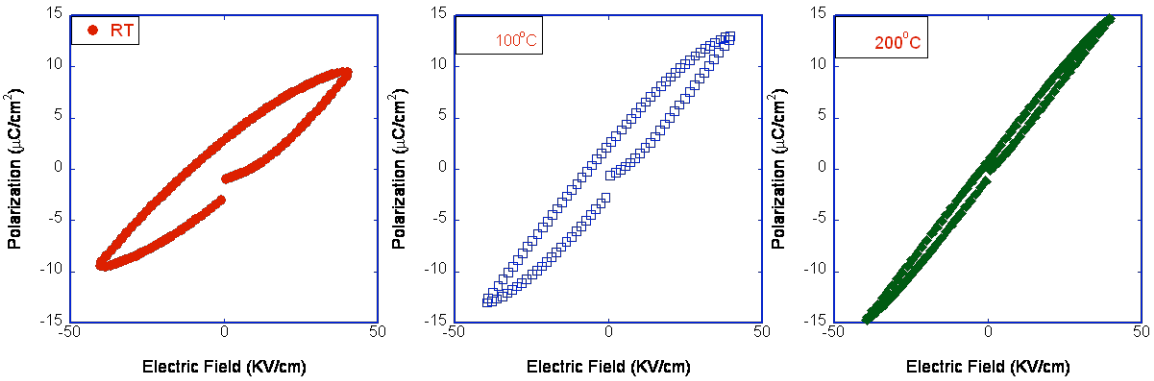

Figure 5.7 P-E loops for the composition of 0.15BZT-0.85BKT as a function of temperature.

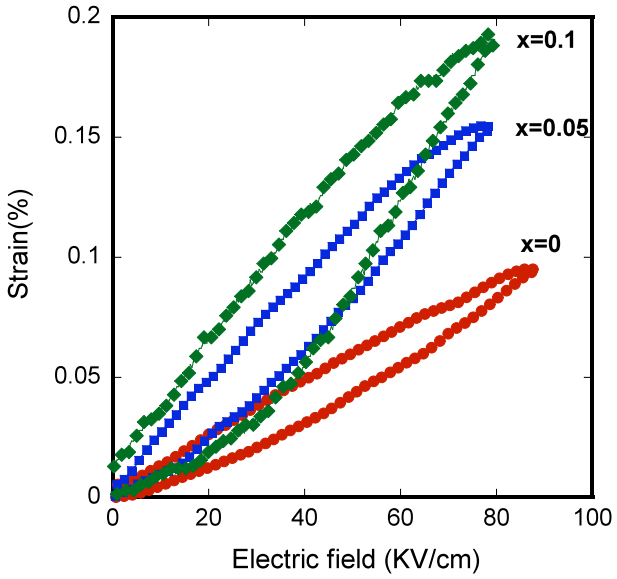

Figure 5.8 Longitudinal strain under unipolar driving electric field.

5.4. Conclusions

Single phase *x*BZT-(1-*x*)BKT perovskite solid solutions with $x \leq 0.2$ were obtained using conventional solid state processing. The XRD data indicated a perovskite phase with tetragonal symmetry for all of the single phase compositions. The c/a ratio remained nearly constant and T_m decreased linearly with increasing BZT

content. Optimized dielectric and piezoelectric properties were obtained for samples with maximum density of ρ=97.1% for the composition x=0.1. Longer sintering times were shown to result in lower tan δ values at high temperature. The piezoelectric coefficient, d_{33}, for x=0, x=0.05, x=0.1 were 110 pm/V, 185 pm/V and 235pm/V respectively. The dielectric and piezoelectric properties of BKT exhibited significant improvement with the addition of BZT.

5.5. References

1 B**.** Jaffe**,** W. R. Cook and H.Jaffe**:** Piezoelectric Ceramics (Academic. Press London, London) (1971)

2 S.-E. Park and T. R. Shrout, J. Appl. Phys. 82, 1804 (1997).

3 A. S. Bhalla, R. Guo, and R. Roy, Mat. Res. Innovat.4, 3(2000).

4 V. A. Bokov and I. E. Myl`nikova, Sov. Phys.-Solid state3, 631 (1961).

5 C. F. Buhrer, "Some Properties of Bismuth Perovskites," J. Chem. Phys., 36, 798(1962).

6 Y. Hiruma, R. Aoyagi, H. Nagata, and T. Takenaka, Jpn. J. Appl. Phys. 44, 5040 (2005).

7 A. Sasaki, T. Chiba, Y. Mamiya, and E. Otsuki, Jpn. J. Appl. Phys. 38, 5564(1999).

8 R. E. Eitel, C. A. Randall, T. R. Shrout, P. W. Rehrig, W. Hackenberger, and S.-E. Park,Jpn. J. Appl. Phys. 40, 5999(2001).

9 C. J. Stringer, T. R. Shrout, C. A. Randall, and I. M. Reaney,J. Appl. Phys. 99, 024106(2006).

10 M. R. Suchomel and P. K. Davies, J. Appl. Phys. 96, 4405(2004).

11 M. R. Suchomel and P. K. Davies, Appl. Phys. Lett. 86, 262905(2005).

12 M. R. Suchomel, A. M. Fogg, M. Allix, H. Niu, J. B. Claridge, and M. J. Rosseinsky, Chem. Mater. 18, 4987(2006).

13 Y. Hiruma, H. Nagata, and T. Takenaka, Jpn. J. Appl. Phys. 46, 1081(2007).

14 Z. Zhao, V. Buscaglia, M. Viviani, M. T. Buscaglia, L. Mitoseriu, A. Testino, M. Nygren, M. Johnsson, and P. Nanni, Phys. Rev. B.70, 024107 (2004).

15 C.-C. Huang, D. P. Cann, X. Tan, and N. Vittayakorn, J. Appl. Phys.102, 044103(2007).

CHAPTER 6

Phase Transitions and Dielectric Properties in $Bi(Zn_{1/2}Ti_{1/2})O_3$ - $NaNbO_3$ Perovskite Solid Solutions

Based on article submitted to Japanese Journal of Applied Physics (June 2008)

Chien-Chih Huang, Naratip Vittayakorn, Anurak Prasatkhetragarn, Brady J. Gibbons and David P. Cann

Department of Mechanical Engineering, Oregon State University, Corvallis, OR 97331-6001, USA

Abstract

Perovskite solid solutions based on the system $NaNbO_3$-$Bi(Zn_{1/2}Ti_{1/2})O_3$ were obtained via solid-state processing techniques. The crystal structure and ferroelectric phase transitions were studied by means of x-ray diffraction and dielectric measurements. A stable perovskite phase was obtained for $Bi(Zn_{1/2}Ti_{1/2})O_3$ substitutions up to 10 mole%. The dielectric characterization revealed that as $Bi(Zn_{1/2}Ti_{1/2})O_3$ content increased the transition temperature decreased and the transition peak became very diffuse. The P-E loop and strain measurement presented the induced ferroelectric phase with 1 mol% $Bi(Zn_{1/2}Ti_{1/2})O_3$ substitutions. As well as with substitution of Li for Na of $NaNbO_3$-$Bi(Zn_{1/2}Ti_{1/2})O_3$ system, the diffuseness of the transition peak decreased and transition temperature increased.

6.1 Introduction

Sodium niobate, $NaNbO_3$, is well-known perovskite material which possesses attractive dielectric properties and a complex series of phase transitions.[1-3] At room temperature, $NaNbO_3$ exhibits anti-ferroelectric behavior, however, by replacing Na with small amount of dopants (*e.g.* Li or K), the ferroelectric phase can be induced.[4-6] Since $NaNbO_3$ is known to exhibit a wide range of solid solutions with other ABO_3 perovskite, it would be good candidate for developing lead-free piezoelectric materials.

In studying past literature reports, the solid solution of $NaNbO_3$-ABO_3 can be divided into two groups.[7,8] In the first group, solid solutions with a small amount of a second component ABO_3 (*e.g.* $LiNbO_3$)[4] resulted in an intermediate pseudo-tetragonal ferroelectric phase and the shift in transition temperature is rather smooth. Otherwise, in the second group the ferroelectric orthorhombic phase replaces the anti-ferroelectric phase with a certain amount of the second component (*e.g.* $NaTaO_3$).[9] More importantly there is an abrupt change in the transition temperature at a specific composition.

There have been many efforts aimed at developing new lead replacement materials for piezoelectric applications. Bi is an excellent candidate for the substitution of Pb since Bi has a similar electronic structure to Pb and there are numerous Bi-based perovskite ceramics that can be used in solid solutions.[10-12] Recently, Suchomel *et al.* reported a new piezoelectric material based on $Bi(Zn_{1/2}Ti_{1/2})O_3$-$PbTiO_3$. Their research revealed that $Bi(Zn_{1/2}Ti_{1/2})O_3$ can increase the transition temperature and enhance the tetragonality of $PbTiO_3$.[12] However, due to the

smaller size of Bi^{3+} comparing to Pb^{2+}, $Bi(Zn_{1/2}Ti_{1/2})O_3$ is unstable in its pure perovskite form.

In previous work, solid solutions within the ternary perovskite system $Bi(Zn_{1/2}Ti_{1/2})O_3$-$BiScO_3$-$BaTiO_3$ were explored. A stable perovskite phase was obtained for all compositions with a $BaTiO_3$ content greater than 50 mole percent. Furthermore, a change in symmetry from pseudo-cubic to tetragonal was observed as the mole fraction of $BaTiO_3$ increased (figure 6.1).[13] Dielectric measurements show a dielectric anomaly associated with a phase transformation over the temperature range of 30 to 210°C for all compositions. Examination of the polarization hysteresis behavior revealed weakly non-linear hysteresis loops. With these data, ferroelectric phase diagrams were derived showing the transition between the pseudo-cubic relaxor behavior to the tetragonal normal ferroelectric behavior. This transition was also correlated to changes in the diffuseness parameter.

In order to develop lead-free piezoelectric materials, $NaNbO_3$ (NN) was used for this research due to its stable perovskite phase and high solubility with other perovskite end members. In this paper, the phase equilibria and dielectric properties of the binary solid solution $Bi(Zn_{1/2}Ti_{1/2})O_3$- $NaNbO_3$ (BZT-NN) was examined. The doping effect was also studied examining the effects of substituting Li for Na in the BZT-NN solid solutions. The purpose of this research is focus on the influence of BZT on the perovskite end member $NaNbO_3$ in terms of the transition temperature and its ferroelectric and dielectric properties.

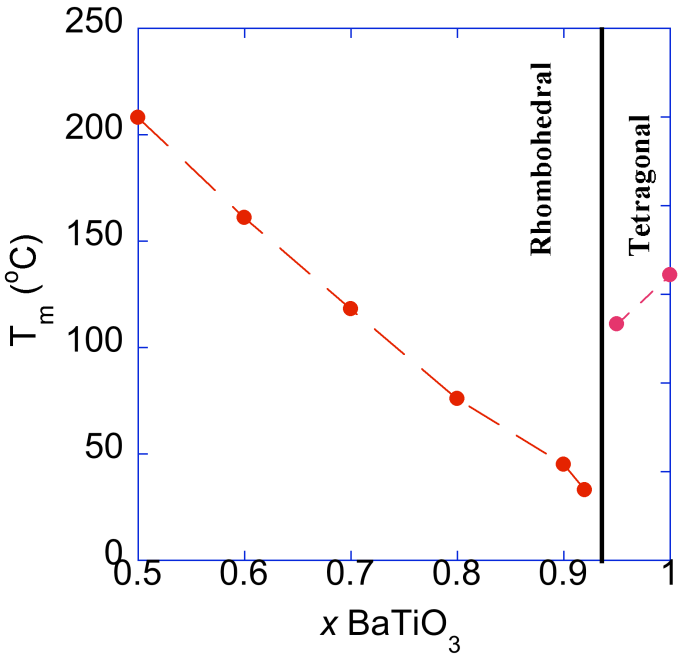

Figure 6.1 The (1-*x*)(Bi($Zn_{1/2}Ti_{1/2}$)O_3-$BiScO_3$)-*x*$BaTiO_3$ system.[13]

6.2 Experiment

The synthesis of *x*Bi($Zn_{1/2}$ $Ti_{1/2}$)O_3-(1-*x*)$NaNbO_3$ ceramics followed the conventional ceramic processing procedures. Reagent grade oxide powders of Bi_2O_3 (≥99.9%), ZnO(≥99%), TiO_2 (≥99.9%), Na_2CO_3(≥99.5%), and Nb_2O_5(≥99.9%) were batched in stoichiometric amounts and ball-milled with ethanol and yttrium-stabilized zirconia media for 6h. The dried powders were calcined in open crucibles at 920°C for 6h followed by an additional milling and drying step. The calcined powders were mixed with 3 wt% polyvinyl butyral (PVB) and then uniaxially cold-pressed at 150 MPa into 12.7 mm diameter pellets. Following binder burnout at 400°C, the pellets were sintered in sealed crucibles between 1110°C-1150°C for 2h. For phase

determination, x-ray diffraction (Bruker-AXS D8) was utilized in the 2θ scan range of 10°-80° using sintered pellets.

Prior to the electrical measurements, the pellets were polished to obtain smooth and parallel surfaces. After polishing, a silver electrode paste (Heraeus C1000) was applied and then fired at 650°C. An Agilent 4284A LCR meter was used to measure the dielectric properties over a wide temperature range using a NorECS ProboStat high temperature measurement cell. Polarization hysteresis measurements (P-E) were determined at a frequency of 4Hz using a ferroelectrics test system (Radiant). The strain as a function of applied electric field was obtained by using an optical displacement sensor (MTI-2100).

6.3 Results and Discussion

6.3.1 Crystal structure of BZT-NN Solid Solutions

The XRD patterns of sintered xBZT-(1-x)NN ceramics shown in figure 6.2a revealed that the perovskite phase was retained up to 10 mole% BZT added. Higher concentrations of BZT resulted in the formation of secondary phases. Initially, compositions rich in $NaNbO_3$ show peak splitting consistent with orthorhombic symmetry as expected. However, with increasing BZT content the separation between diffraction peaks corresponding to the orthorhombic phase becomes narrower and eventually merges into single broaden peaks at about x =0.05. The merging of peaks indicates a decrease in the tilt angle within the monoclinic system.

Figure 6.2b shows a close up of the diffraction peaks illustrating the evolution of the structure as a function of composition. The data clearly shows that the

orthorhombic structure is maintained, though the decrease in peak intensity suggests that the orthorhombic distortion is vanishingly small. The following section presents data on the phase transition via dielectric measurements, and it is clear that as the BZT content increases the phase transition approaches room temperature and becomes diffuse. For these reasons, it is not unexpected that the diffraction data is somewhat ambiguous.

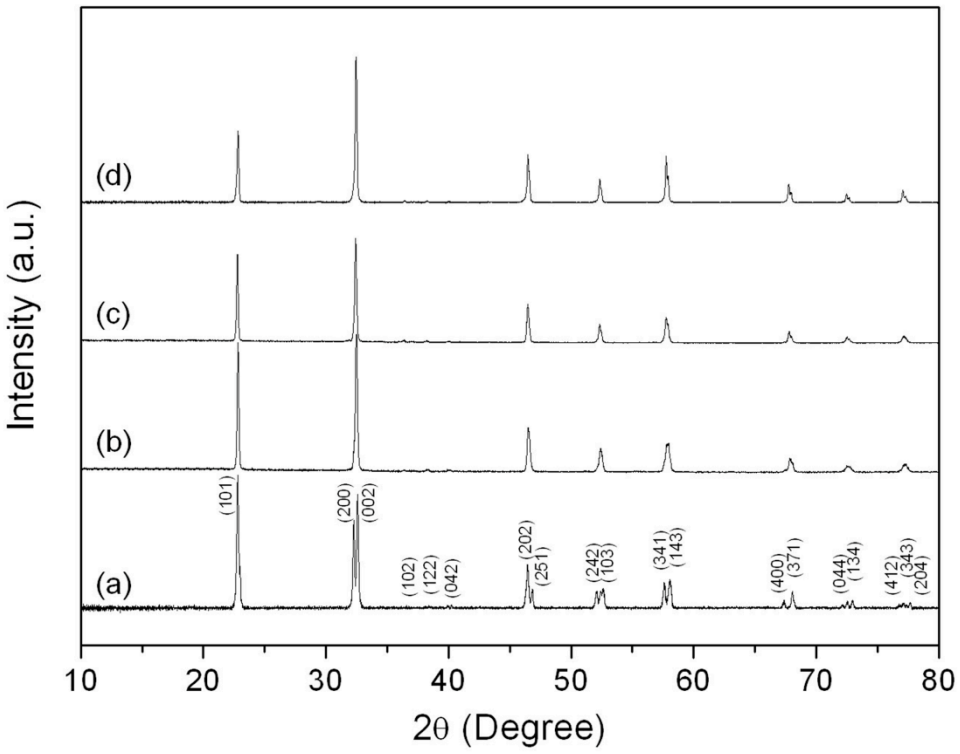

Figure 6.2aXRD data for xBi($Zn_{1/2}Ti_{1/2}$)O_3-(1-x)$NaNbO_3$ (a) x=0.01 (b) x=0.05 (c) x=0.075 (d) x=0.1.

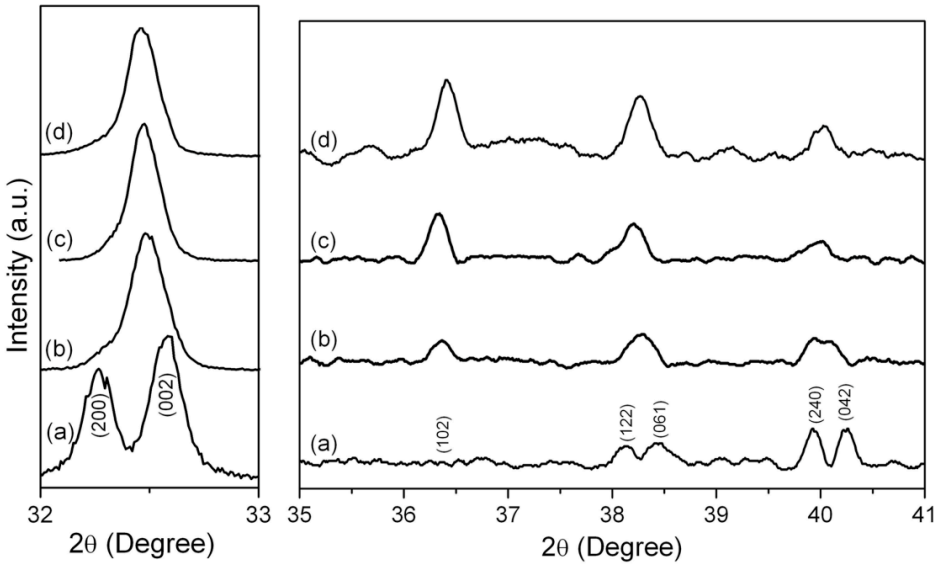

Figure 6.2b XRD data for xBi($Zn_{1/2}Ti_{1/2}$)O_3-(1-x)$NaNbO_3$ (a) x=0.01 (b) x=0.05 (c) x=0.075 (d) x=0.1.

6.3.2 Dielectric properties of BZT-NN Solid Solutions

The dielectric constant plotted against temperature for xBi($Zn_{1/2}Ti_{1/2}$)O_3-(1-x)$NaNbO_3$ from x=0.01 to x=0.1 is presented in figure 6.3a. It is shown that the maximum permittivity, ε_m, retained similar values for all compositions. However, a diffuse phase transition was observed for compositions where x>0.05 and the transition became more diffuse with increasing BZT content. Figure 6.3b revealed the dielectric loss as a function of temperature. It is very clear to see that the appearance of a peak at the composition of 0.9BZT-0.1NN. However as increasing the content of BZT, this peak disappeared. Addition of BZT also resulted in the decrease of high temperature dielectric loss which is very similar to other BZT system[13].

The temperature at which maximum dielectric constant appeared, defined as T_m, is plotted as a function of composition in figure 6.4. It is clear that for small

amounts of BZT in the solid solution, a decrease in T_m was observed with increasing BZT content. At BZT concentrations greater than x=0.05, T_m dramatically decreased. The trend of the transition temperature as a function of composition matches the description of the second group of $NaNbO_3$-ABO_3 solid solutions in which the antiferroelectric phase transfers to a ferroelectric phase with the addition of second component.[6] The general trend is also similar to that observed in the ternary $Bi(Zn_{1/2}Ti_{1/2})O_3$-$BiScO_3$-$BaTiO_3$ system. Based on these reports, ferroelectric properties can be expected for $Bi(Zn_{1/2}Ti_{1/2})O_3$-$NaNbO_3$ solid solution.

The dielectric properties as a function of frequency for the $0.1Bi(Zn_{1/2}Ti_{1/2})O_3$-$0.9NaNbO_3$ composition is shown in figure 6.5. With only 10% BZT introduced into the solid solution the maximum dielectric constant shifted to below room temperature indicating a significant destabilization of the ferroelectric phase. This is confirmed in the x-ray diffraction data where room temperature measurements indicate a weakly orthorhombic distortion.

The increase in permittivity and dielectric loss at higher temperatures is most likely not due to a phase transition but rather due to the onset of conduction losses presumably tied to non-stoichiometry. A strong frequency dependence characteristic of relaxor ferroelectric behavior was observed in the vicinity of the dielectric maximum.

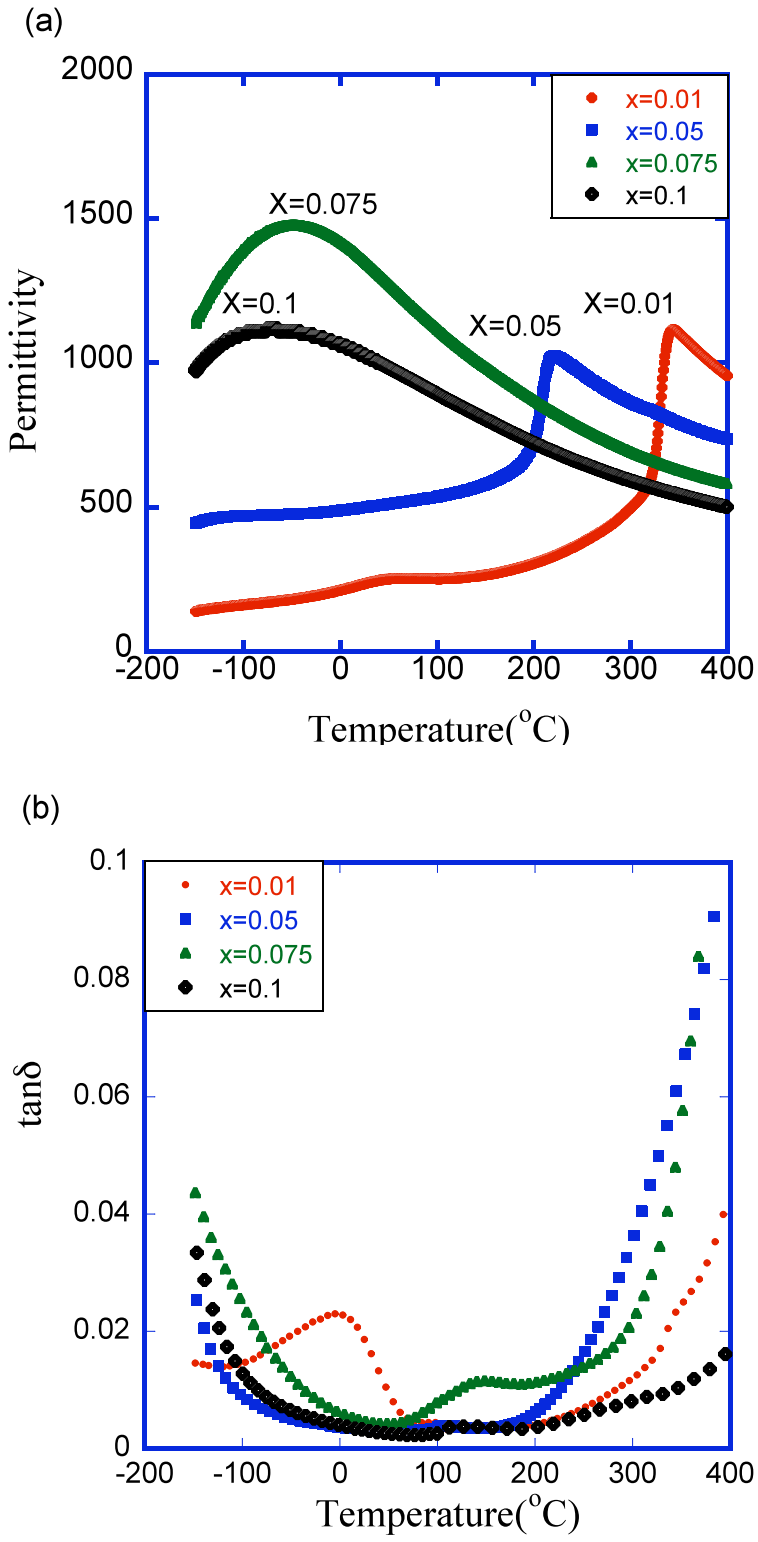

Figure 6.3 (a) Permittivity and (b) tanδ as a function of temperature for *x*BZT-(1-*x*)NN at a measuring frequency of 10 KHz

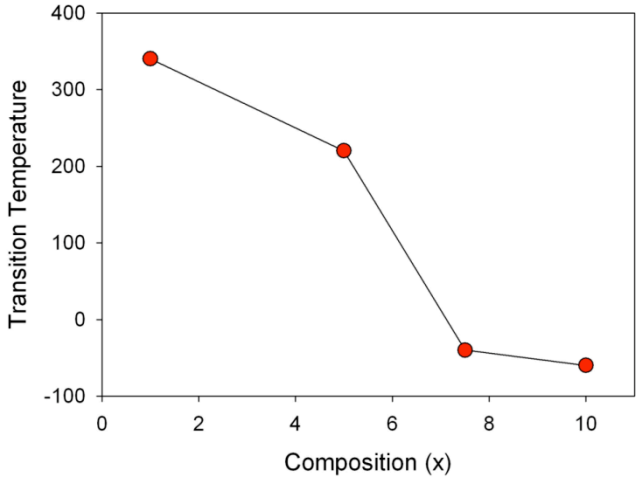

Figure 6.4 Concentration dependencies of the transition temperature for $x\mathrm{Bi}(\mathrm{Zn}_{1/2}\mathrm{Ti}_{1/2})\mathrm{O}_3$ - $(1\text{-}x)\mathrm{NaNbO}_3$

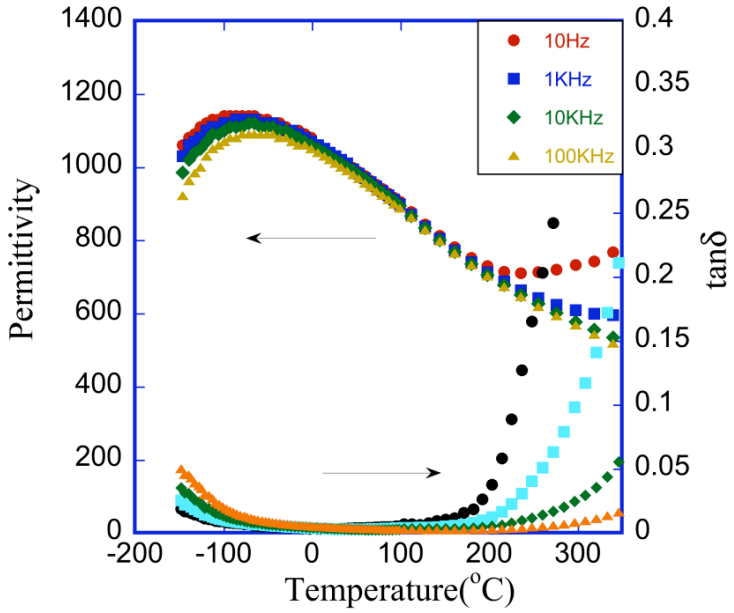

Figure 6.5 Permittivity and tanδas a function of frequency for the $0.1\mathrm{Bi}(\mathrm{Zn}_{1/2}\mathrm{Ti}_{1/2})\mathrm{O}_3$ - $0.9\mathrm{NaNbO}_3$

6.3.3 Ferroelectric and Piezoelectric Properties of BZT-NN

The polarization and strain as a function of applied electric field measured at room temperature for BZT-NN solid solutions are shown in figure 6.6. The broaden area of hysteresis loop which indicated the induced ferroelectric behavior is observed for 1mol% BZT substitution. The strain loop confirmed the existence of ferroelectric behavior. However when more BZT was added, the P-E loop become linear. The loss of hysteresis behavior can be explained by the decrease of transition temperature and increase of cations disorder with higher BZT concentrations.

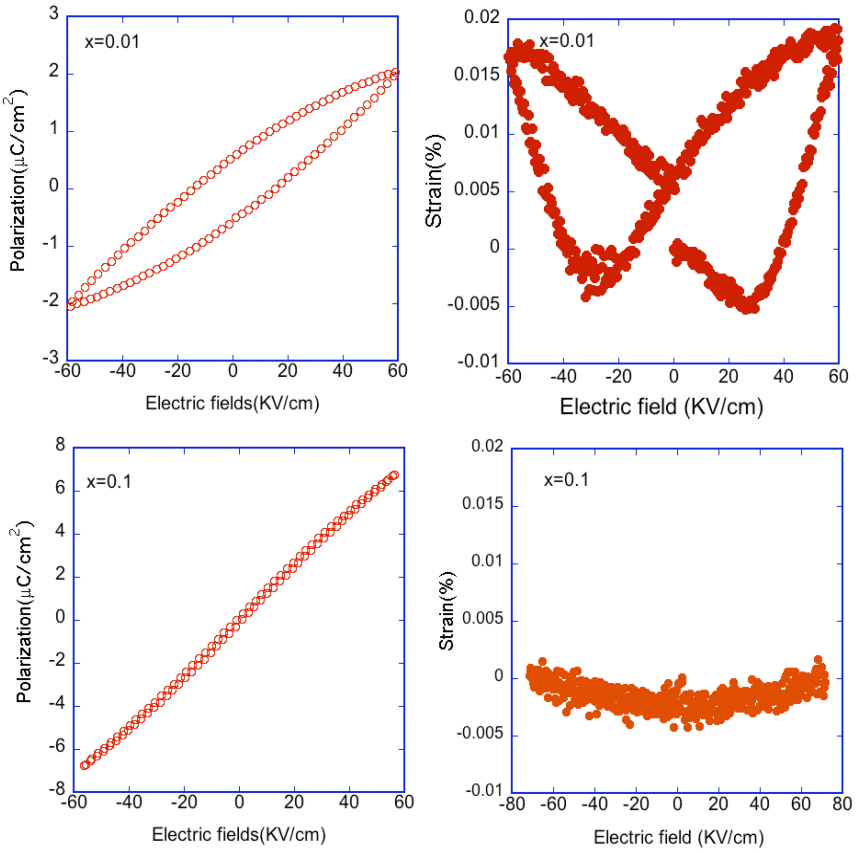

Figure 6.6 Polarization and strain versus electric field for $xBi(Zn_{1/2}Ti_{1/2})O_3$-(1-x)$NaNbO_3$ at 4Hz at room temperature

Figure 6.7 illustrated the resistivity of (1-*x*)BZT-*x*NN ceramics. The resistivity increased with increasing BZT content and to the maximum value of $10^{14}\Omega\cdot$cm at x= 0.925. The increased resistivity may be related to higher density for BZT-NN solid solutions.

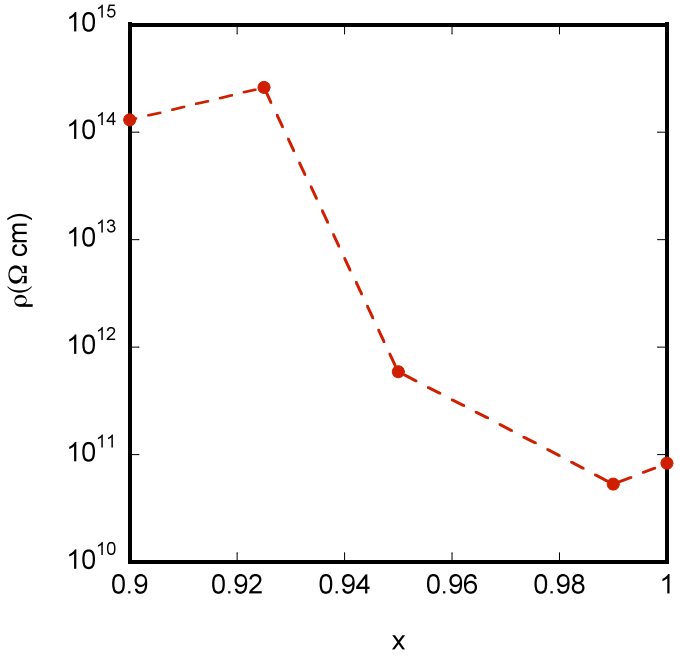

Figure 6.7 Concentration dependencies of the resistivity for xBi($Zn_{1/2}Ti_{1/2}$)O_3 - (1-x)$NaNbO_3$

6.3.4 Doping Effects in BZT-NN

In order to investigate the effect of doping within the $NaNbO_3$-ABO_3 solid solution, $LiNbO_3$ was substituted for $NaNbO_3$. The Li ion is approximately 20% smaller than Na and has been found to introduce an instability into the structure. The effects of replacing Li^+ for Na^+ in the composition 0.1Bi($Zn_{1/2}Ti_{1/2}$)O_3-0.9$NaNbO_3$ is shown in figure 6.8 and figure 6.9. The perovskite structure remained stable with up to 10 mole% Li added. At higher concentrations secondary phases appeared in the

diffraction data. As can be seen in the dielectric and P-E hysteresis loop data, the addition of Li had two effects. First, it increased T_m from below room temperature to nearly 100°C for 10% Li added. This indicates that the stability of the ferroelectric phase was enhanced with the addition of Li which corresponds to a broadening of the ferroelectric hysteresis loops as shown in figure 6.9. In addition, the phase transition sharpened with the addition of Li as the system shifted from relaxor to normal ferroelectric behavior. Room temperature x-ray diffraction measurements are mostly inconclusive because the phase transition is in the vicinity of room temperature. Temperature dependent diffraction measurements are currently underway to track the change in symmetry as a function of temperature. These results are very different than observations in the $NaNbO_3$-$LiNbO_3$ and $NaNbO_3$-$KNbO_3$ binary system,[4,6] where a pseudo-tetragonal phase transition was not observed in XRD and dielectric data.

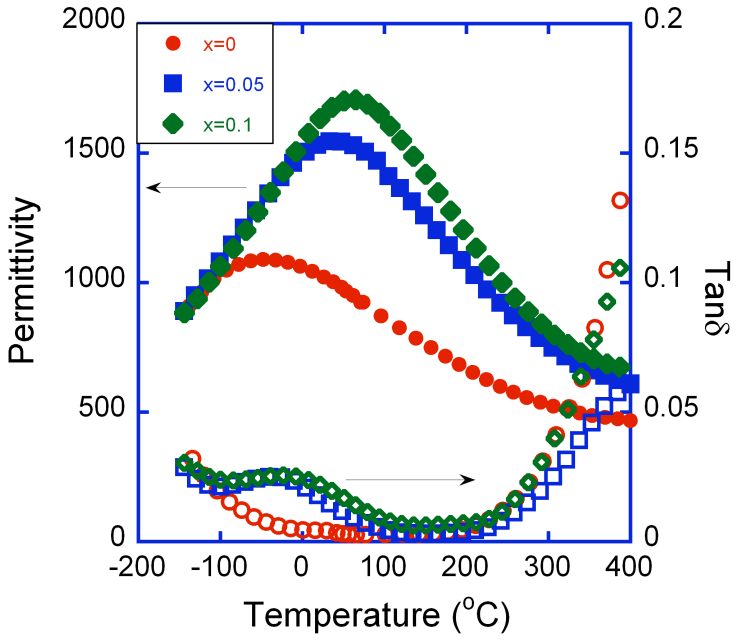

Figure 6.8 Permittivity and tanδas a functionof temperature for $0.1Bi(Zn_{1/2}Ti_{1/2})O_3$-$0.9Na_{1-x}Li_xNbO_3$

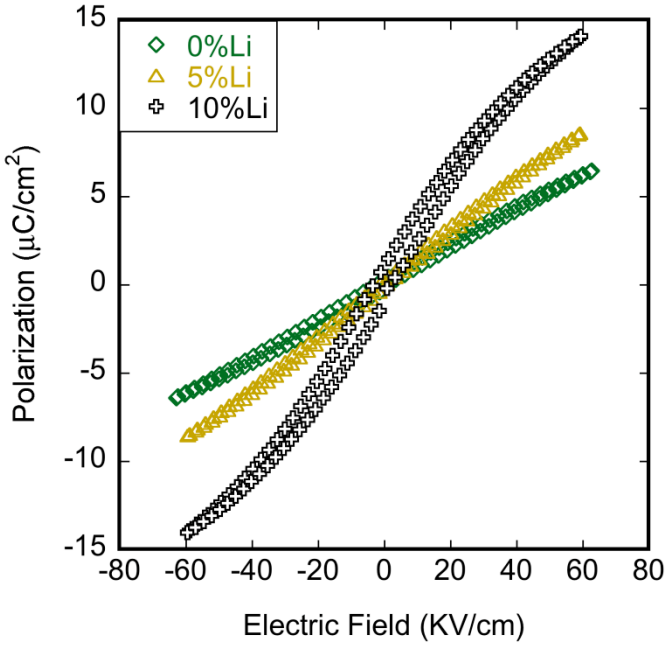

Figure 6.9 Polarization versus electric field for $0.1Bi(Zn_{1/2}Ti_{1/2})O_3$-$0.9Na_{1-x}Li_xNbO_3$at 4Hz at room temperature.

6.4. Conclusions

In this work, the phase equilibria and dielectric properties of the binary solid solution $Bi(Zn_{1/2}Ti_{1/2})O_3$- $NaNbO_3$ (BZT-NN) were examined. A combination of XRD and dielectric data indicated that a stable perovskite phase with orthorhombic symmetry was observed for compositions rich in $NaNbO_3$. As the BZT concentration increased the transition temperature dropped below room temperature and correspondingly the orthorhombic distortion weakened. The abrupt decrease of the transition temperature indicates the formation of ferroelectric phase which was confirmed by P-E loop and strain measurements. Through substitution of Li with Na for NN-BZT solution, diffuseness of the transition peak decreased and transition temperature increased.

6.5 REFERENCES

1 H. D. Megaw, Ferroelectrics 7, 87 (1974).

2 C. N. W. Darlington and K.S. Knight: ActaCryst. B55, 24 (1999).

3 S. Lanfredi, M. H. Lente and J. A. Eiras: Appl. Phys. Lett. 80, 2731 (2002).

4 T. Nitta: J. Am. Ceram. Soc. 51, 626 (1966).

5 M. A. L. Nobre and S. Lanfredi: J. Appl. Phys. 93, 5557 (2003).

6 G. Shirane, R. Newnham and R. Pepinsky: Phys. Rev. 96, 581 (1954).

7 G.A. Smolenskii, V.A. Bokov, V.A. Isupov, N.N. Krainik, R.E. Pasynkov, A.I. Sokolov: Ferroelectrics and Related Materials, (Gordon & Breach, New York, 1984) p. 634.

8 I.P Raevski, A.A. Prosandeev: J. Phys. Chem. Sol. 63, 1939 (2002).

9 H. Iwasaki and T. Ikeda: J. Phys. Soc. Jap. 18, 157 (1963).

10 R. E. Cohen, Nature 358, 136 (1992).

11 M. R. Suchomel and P. K. Davies, J. Appl. Phys. 96, 1489 (2004).

12 M. R. Suchomel and P. K. Davies, Appl. Phys. Lett. 86, 262905 (2005).

13 C.-C. Huang, D.P. Cann, X. Tan, and N. Vittayakorn: J. Appl. Phys. 102 044103 (2007).

CHAPTER 7

Phase transitions and ferroelectric properties in $BiScO_3$-$Bi(Zn_{1/2}Ti_{1/2})O_3$-$BaTiO_3$ solid solutions

Based on article published in Journal of Applied Physics **102**, 044103 (2007)

Chien-Chih Huang, Naratip Vittayakorn Xiaoli Tan, and David P. Cann

Materials Science, Department of Mechanical Engineering, Oregon State University, Corvallis, Oregon 97331

Abstract

Ceramics solid solutions within the ternary perovskite system $Bi(Zn_{1/2}Ti_{1/2})O_3$-$BiScO_3$-$BaTiO_3$ were synthesized via solid-state processing techniques. The crystal structure of sintered ceramics was analyzed by x-ray diffraction. A stable perovskite phase was obtained for all compositions with a $BaTiO_3$ content greater than 50 mol %. Furthermore, a change in symmetry from pseudocubic to tetragonal was observed as the mole fraction of $BaTiO_3$ increased. Dielectric measurements show a dielectric anomaly associated with a phase transformation over the temperature range of 30 °C–210 °C for all compositions. Examination of the polarization hysteresis behavior revealed weakly nonlinear hysteresis loops. With these data, ferroelectric phase diagrams were derived showing the transition between the pseudocubic relaxor behavior to the tetragonal normal ferroelectric behavior. This transition was also correlated with changes in the diffuseness parameter.

7.1 Introduction

Perovskite $Pb(Zr,Ti)O_3$ (PZT) ceramics are widely used for many industrial applications due to their superior performance in piezoelectric, dielectric and pyroelectric applications. However, recently there have been environmental concerns with PZT related to the toxicity of lead oxides which are volatile during processing. Consequently, this has motivated the search for lead free piezoelectric materials with piezoelectric properties comparable to PZT with a reduced environmental impact.

The origin of the enhanced piezoelectric response in perovskite PZT is the result of lone pair electrons in the Pb^{2+} hybrid orbitals[1] and the existence of a morphotropic phase boundary (MPB) between two ferroelectric phases.[2] Therefore, Bi^{3+} is an excellent candidate for the substitution of Pb in the PZT system since it has a similar electronic structure and there are already numerous Bi-based perovskite ceramics that can be used in solid solutions[3-8]. Through systematic research, a number of MPB systems based on $Bi(M)O_3$-$PbTiO_3$ ($M=Ti^{4+}$, Sc^{3+}, Zn^{2+}, Nb^{5+}…) has been discovered.[6,8] Recently, $BiScO_3$ (BS) perovskite has drawn attention due to its high Curie temperature (T_c=450°C) and its excellent piezoelectric properties at the MPB with $PbTiO_3$.[6] Another Bi-based perovskite,$Bi(Zn_{1/2}\ Ti_{1/2})O_3$ exhibits a high T_c with an enhanced tetragonality through solid solution with $PbTiO_3$.[8,9] However, both $BiScO_3$ and $Bi(Zn_{1/2}\ Ti_{1/2})O_3$ are unstable in their pure form and can only be stabilized under high pressures[10,11] or in solid solutions with other perovskite end members[6,8]. In order to develop lead-free piezoelectric materials, $BaTiO_3$ (BT) was used for this research in order to stabilize the BZT and BS perovskite phases in a solid solution.

Recently, Tinberg *et al.* reported ferroelectric thin films based on the $BiScO_3$-$BaTiO_3$ binary system[12]. Similar to the $BiScO_3$-$PbTiO_3$ system, when $PbTiO_3$ was replaced with $BaTiO_3$, the perovskite structure was stabilized and an MPB was observed. Although there are no reports related to the $Bi(Zn_{1/2}\ Ti_{1/2})O_3$-$BaTiO_3$ system, an increased transition temperature can be expected for this system.

In this work, the phase equilibria and dielectric properties of the ternary solid solution $BiScO_3$-$Bi(Zn_{1/2}\ Ti_{1/2})O_3$-$BaTiO_3$ (BS-BZT-BT) was examined. This report may provide an alternative approach for lead-free piezoelectric materials development.

7.2 Experiment

Solid solutions of $(1-x)(0.5BiScO_3$-$0.5Bi(Zn_{1/2}\ Ti_{1/2})O_3)$-$xBaTiO_3$ (BS-BZT-BT) were prepared by the conventional ceramic processing. Reagent grade oxides powders of Bi_2O_3 (≥99.9%), ZnO(≥99%), TiO_2 (≥99.9%) and $BaCO_3$(≥99.5%) were batched in stoichiometric amounts and ball-milled with ethanol and yttrium-stabilized zirconia media for 6h. The dried powders were double calcined in open crucibles between 800°C-950°C for 24h and followed by an additional milling and drying step. The calcined powders were mixed with 3 wt% polyvinyl alcohol (PVA) and then uniaxially cold-pressed at 150 MPa into 12.7mm diameter pellets. Following binder burnout at 500°C, the pellets were sintered in sealed crucibles between 850°C-1200°C for 2h. For phase determination, x-ray diffraction (Siemens D5000 diffractometer) was utilized in the 2θ scan range of 20°-60° for calcined powders and sintered pellets.

Prior to the electrical measurements, the pellets were polished to smooth and parallel surface. After polishing, a silver electrode paste (Heraeus C1000) was applied

and then fired at 600°C. An Agilent 4284A LCR was used to measure the dielectric properties over a wide temperature range using a NorECS ProboStat high temperature measurement cell. The polarization vs. electric field hysteresis loops of selected compositions were recorded at room temperature and -50ºC, respectively, with a RT66A standard ferroelectric test system (Radiant Technologies).

7.3 Results and Discussion

7.3.1 Phase of BS-BZT-BT

Figure 7.1a displays the XRD patterns for calcined powders of (1-x)(BS-BZT)-xBT. Perovskite phases were obtained for compositions containing at least 50 mol% $BaTiO_3$. For compositions below this amount, a complex mixture of phases was observed. Based on the {111} and {200} peak splittings shown in figure 1b, the composition with x=0.5 correspond to a pure rhombohedral symmetry. Compositions above x=0.95 stabilized in a pure tetragonal symmetry. The peaks between these two compositions indicated the coexistence of rhombohedral and tetragonal phases. The XRD patterns of sintered (1-x)(BS-BZT)-xBT pellets shown in figure 7.2 confirm that the samples retained phase pure perovskite for all compositions with 50 mol% and above $BaTiO_3$. In contrast to the calcined powders, in the sintered pellets the tetragonal perovskite phase was only present for compositions with x=0.95 to x=1. The remainder of the compositions $x \leq 0.9$ exhibited a rhombohedral symmetry. These results indicate that the MPB in this system may be located between x=0.9 to 0.95. This shift in symmetry between the calcined and sintered samples may be due to a number of factors. The observation of the coexistence of two perovskite phases in

calcined powders is likely the result of the relatively low processing temperature. The limited reaction kinetics may have resulted in an incomplete reaction between BT, BS and BZT. In addition, both Bi_2O_3 and ZnO have some degree of volatility at this temperature that may have caused a slight change in composition. Upon sintering, homogenization occurred leading to a clearly observed single perovskite phase.

The lattice parameters were calculated from XRD patterns shown in Table 7.1. Although Bi^{3+} is slightly smaller than Pb^{2+} based on 12-fold coordination, the unit cell volume increased with decreasing $BaTiO_3$ content due to substitution of larger size B-site cations Zn^{2+} (0.88 Å) and Sc^{3+} (0.885 Å) for Ti^{4+} (0.745 Å). Comparing the tetragonal structure for x=1 and x=0.95, the results show that the c:a ratio increased with $BaTiO_3$ content. This may be due to the phase transition for x=0.95 that occurs close to room temperature which results in the formation of a pseudo-cubic phase.

X Mole % BT	0.5	0.6	0.7	0.8	0.9	0.92	0.95	1
Structure	Rhombohedral						Tetragonal	
Lattice parameter (Å)	4.046	4.040	4.030	4.022	4.014	4.009	a: 3.997 c: 4.023	a: 3.992 c: 4.034
T_m (°C)	208	161	118	76	45	33	111	134
ε_m at T_m	1100	1170	1240	1360	2570	3960	3520	9740
δ	587.5	210.3	143.1	70	61.4	57.3	16.3	3.4
γ	1.99	1.74	1.65	1.67	1.66	1.44	1.38	1.11

Table 7.1 Room temperature structure and dielectric data for BZT-xBT at 10 KHz

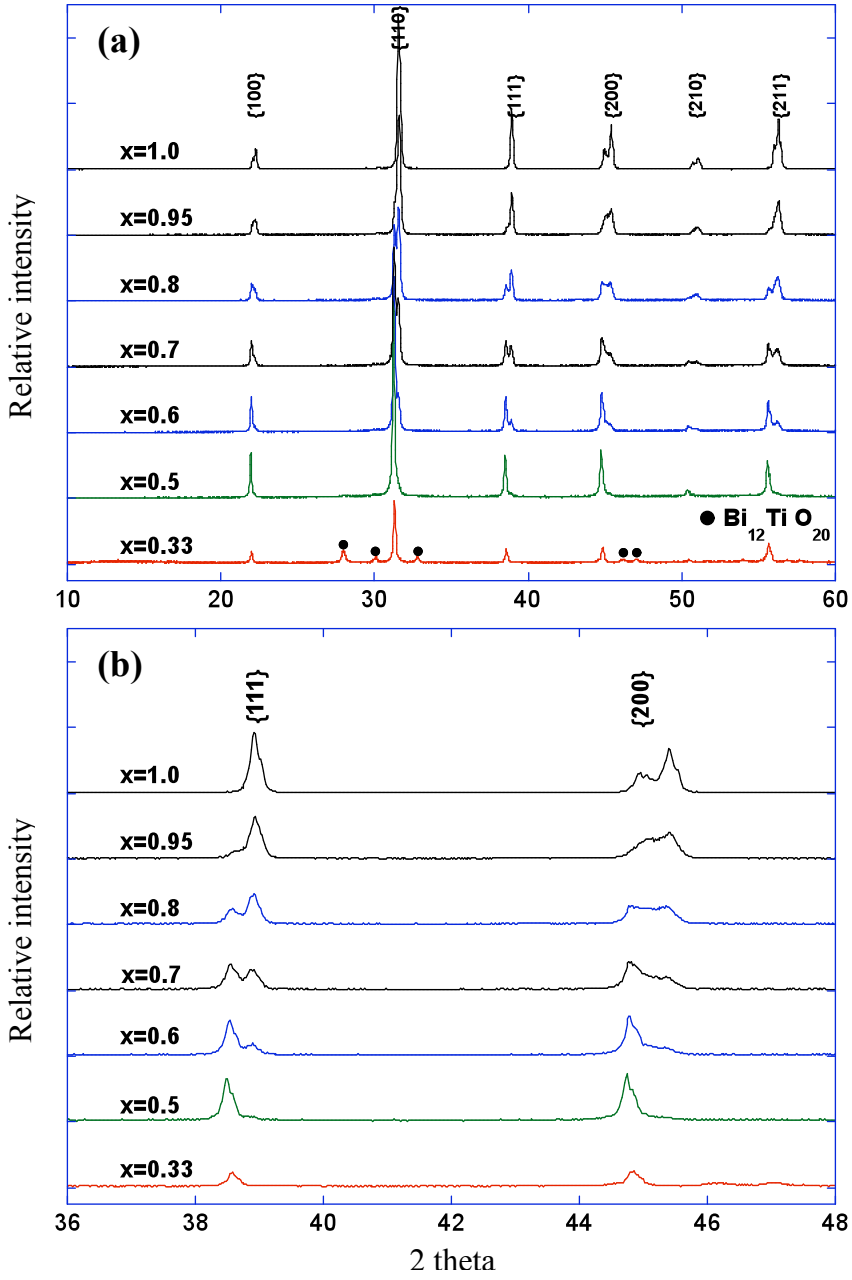

Figure 7.1 XRD diffraction pattern of calcined (1-x)(BS-BZT)-xBT powders

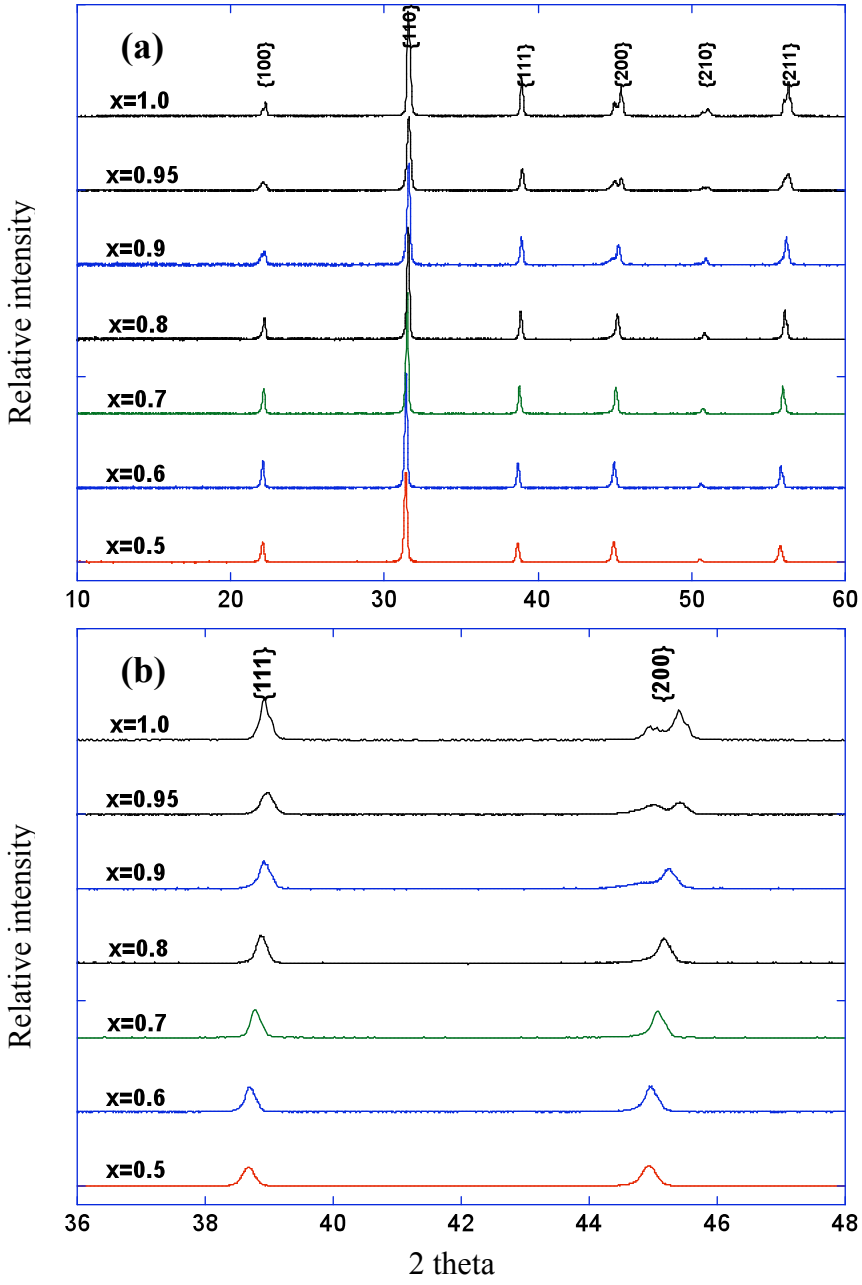

Figure 7.2 XRD diffraction pattern of calcined (1-x)(BS-BZT)-xBT sintered pellets

7.3.2 Dielectric Behavior of BS-BZT-BT

The dielectric constant and dielectric loss were measured from 100 Hz to 100 KHz as function of temperature. The room temperature dielectric properties for all of the compositions in this study are listed in Table 7.1. Figure 7.3 shows the permittivity versus temperature at 10KHz for (1-x)(BS-BZT)-xBTfrom x = 0.5 to 1.0. It was observed that the maximum permittivity, ε_m, increased with increasing $BaTiO_3$ content. However, temperature at which maximum permittivity appeared, T_m, exhibited a more complex trend. It is very clear from the data that while pure $BaTiO_3$ exhibited a strong first order phase transition, the addition of BS+BZT caused a shift towards relaxor ferroelectric behavior. It is well known that perovskite $BaTiO_3$ has three phase transitions within a wide range of temperature[13]. According to our XRD data in figure 7.2, when mixed with more than 10 mole% BS-BZT, all of three transition temperature merged into one diffuse transition which is also reflected in the XRD data. This kind of phenomena has also been noted when $BaTiO_3$was mixed with $BaZrO_3$.[14] In Table I, the data clearly shows that T_m decreased with increasing $BaTiO_3$ content for $x \leq 0.9$. On the contrary, T_m increased with $BaTiO_3$ content for $x \geq 0.95$.

For a diffuse phase transition, the degree of diffuseness can be obtained from the parameter δ_r derived via the following expression[15].

$$\frac{\varepsilon_m^{'}}{\varepsilon^{'}(f,T)} = 1 + \frac{(T - T_m(f))^{\gamma}}{2\delta_{\gamma}^2} (1 \leq \gamma \leq 2) \qquad 7.1$$

The parameter of γ is degree of dielectric relaxation, where $\gamma = 1$ corresponds

to a normal first-order ferroelectric phase transition. Larger values of γ express more relaxor-ferroelectric behavior of transition. The value of δ_r represents degree of diffuseness for transition peaks. Both γ and δ_r were determined from the slope and intercept of $\ln(\varepsilon/\varepsilon')$ versus $\ln(T-T_m)$. According to Table 7.1, a greater percentage of BS and BZT resulted in a higher degree of diffuseness and stronger relaxor behavior. This can be explained by the increased cation disorder due to the substitution on A-site by Bi and on the B-site by Sc and Zn.

The dielectric property as a function of frequency for (1-x)(BS-BZT)-xBT is shown in figure 7.4. A strong frequency dependence characteristic of a relaxor ferroelectric was observed. The peaks appear around 600^{o}C for x=0.8 are likely the result of oxygen vacancies.[16] Moreover, these compositions possess a stable dielectric constant of approximately 1000 and low loss tangent (tan δ< 0.01) up to high temperatures (T < 400^{o}C). It may have great potential for high temperature applications.

The polarization versus electric field measurements at 4 Hz for the x=0.5 and x=0.7 are shown in figure 7.5. The samples used in this study were sintered without being covered which due to the loss of Zn and Bi resulted in a slight upwards shift in T_{max} (i.e. on the order of 10-20°C). The loop from the ceramic of x=0.5 exhibits a weak non-linearity at room temperature which is not unexpected given that the measurements were taken at a temperature in the vicinity of T_m. At T = -50°C the slope of the loop decreased as expected due to the decrease in dielectric permittivity below T_m. Figure 7.6 displays room temperature P-E data for x=0.5 as a function of electric field. As the E-field increased a clear elliptical rotation is observed which is

another indication of non-linear behavior. The x = 0.7 sample exhibited a narrow, weakly non-linear loop at room temperature which broadened at lower temperatures corresponding to the increased tan δ below the transition temperature (Figure 7.4). It is interesting to note that even at relatively high fields up to 60 kV/cm all the loops were weakly non-linear with relatively low polarization values.

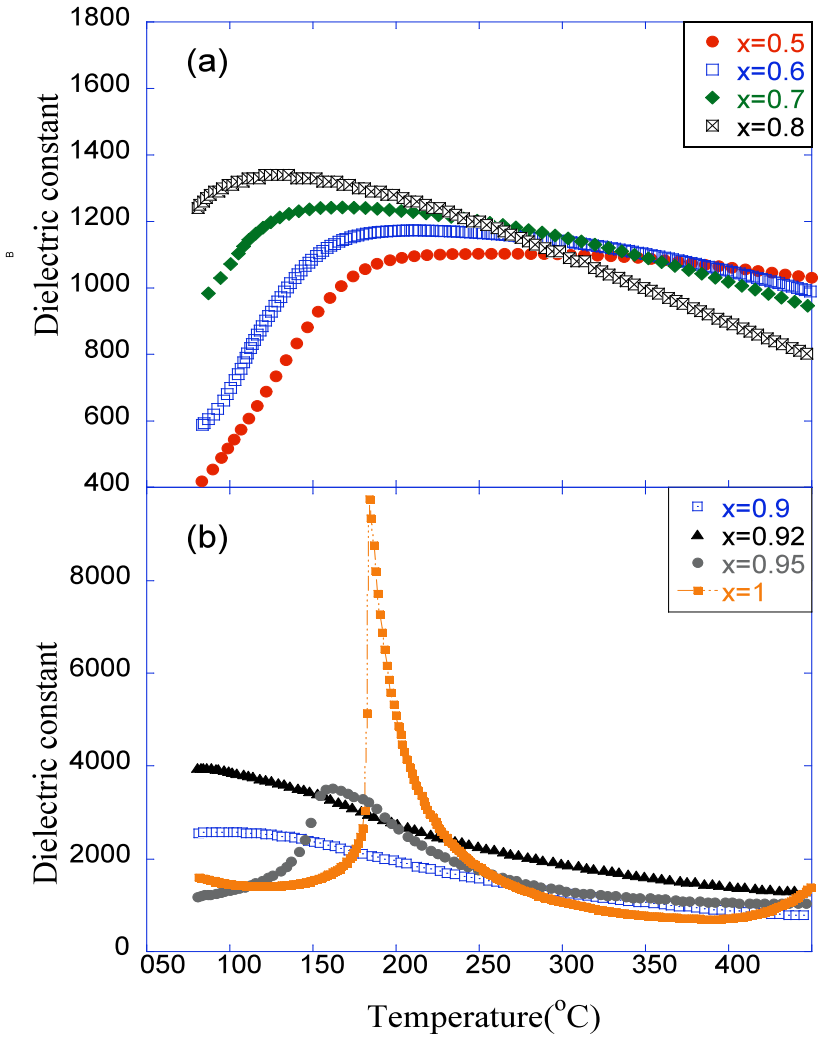

Figure 7.3 Dielectric constant of (1-x)(BS-BZT)-xBT as a function of temperature at measuring frequency of 10 kHz.

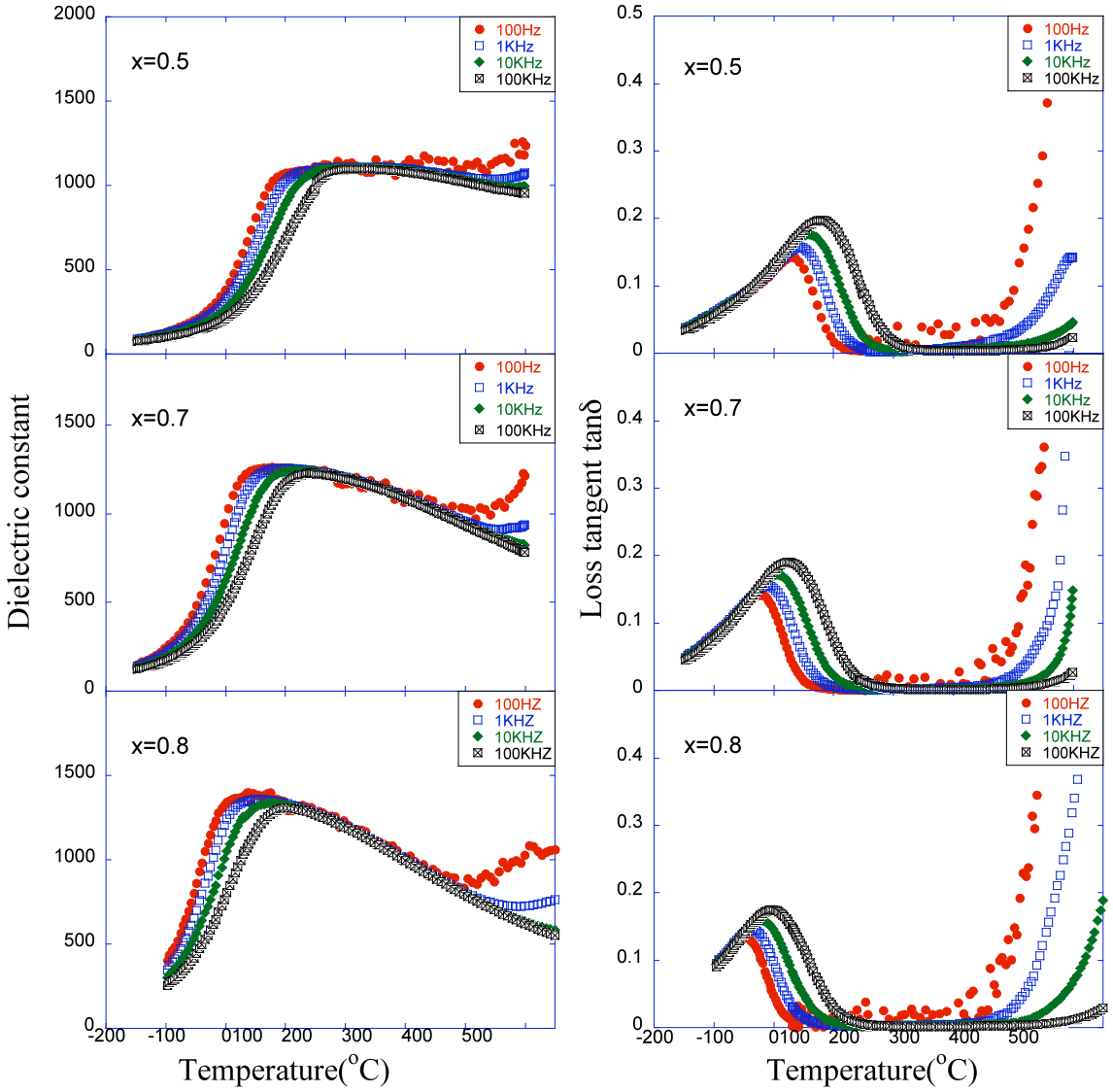

Figure 7.4 Dielectric constant and loss tangent of (1-x)(BS-BZT)-xBT with x=0.5, 0.7 and 0.8 as a function of temperature.

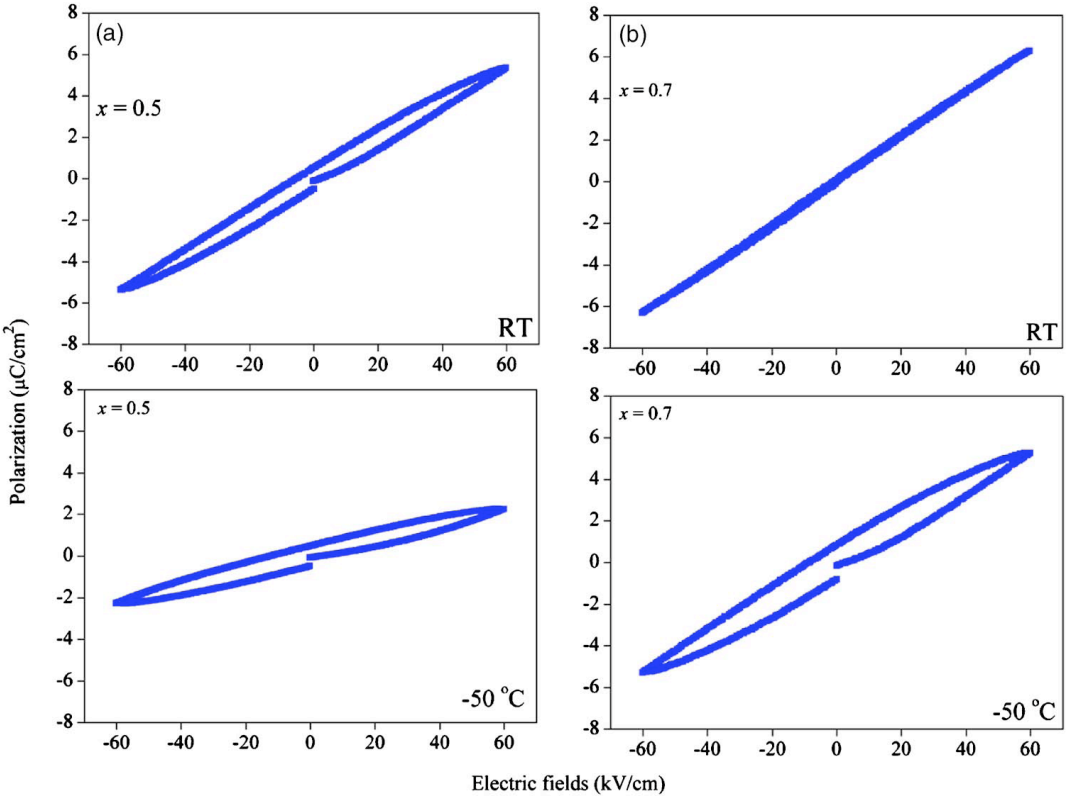

Figure 7.5 Polarization data on (1-x)(BS-BZT)-xBT ceramics at 4 Hz for (a) x=0.5 and (b) x=0.7.

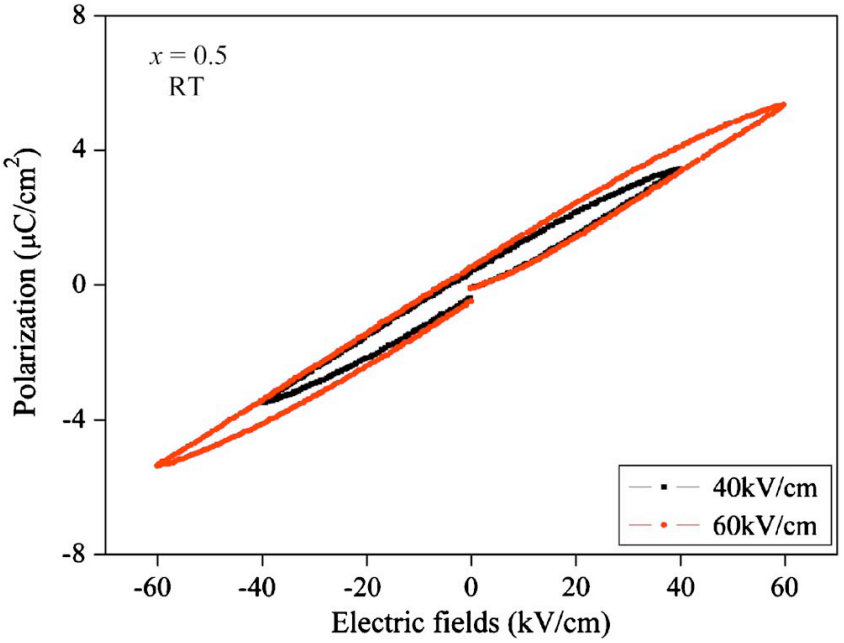

Figure 7.6 P~E hysteresis loop measured from the ceramic of x=0.5 at 4Hz at room temperature.

7.3.3 Phase transformations in the (1-x)(BS-BZT)-xBT system

Figure 7.7 presents data on the phase transformation in the (1-x)(BS-BZT)-xBT system obtained from the dielectric data. Starting from pure $BaTiO_3$ the phase transition decreases as the (BS-BZT) content increases to a minimum of 33°C at x=0.92. At higher (BS-BZT) concentrations the transition temperature then increases up to x=0.5. Also plotted in Figure 7.7 is the diffuseness parameter δ as a function of composition. Pure $BaTiO_3$ exhibits a sharp first-order phase transition, but as the (BS-BZT) content increases a monotonic increase in δ is observed owing to increased relaxor behavior.

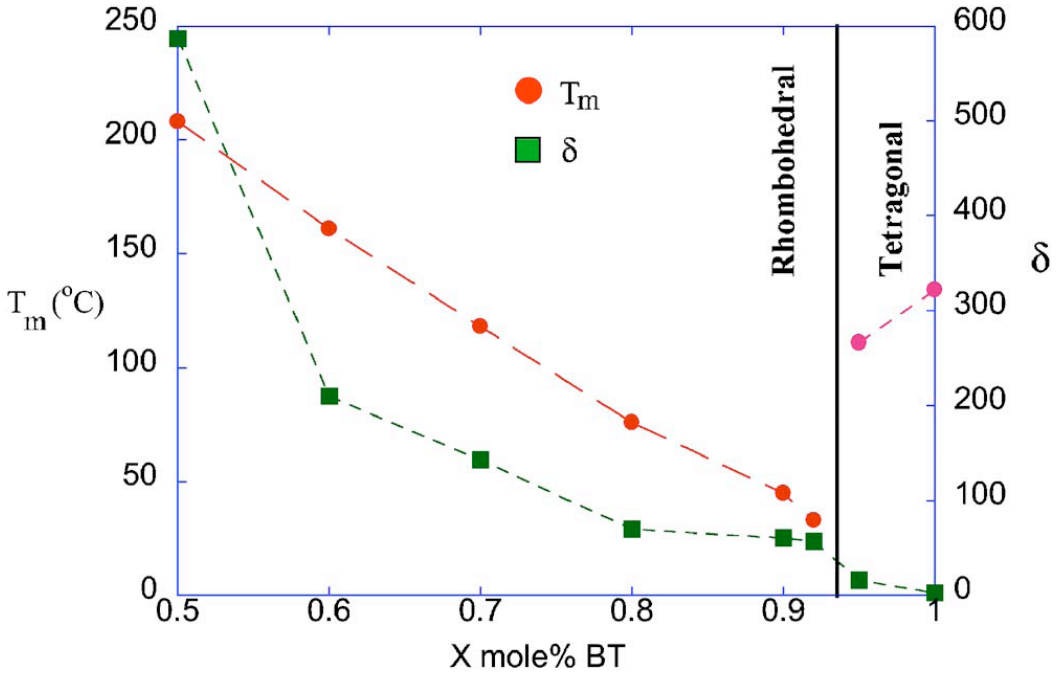

Figure 7.7 T_{max} and diffuseness δ as a function of $BaTiO_3$ content

7.3.4 Doping Effects in BS-BZT-BT

In order to investigate the effect of doping within the (1-x)(BS-BZT)-x$BaTiO_3$ solid solution, 1wt% of Zr, Cr and Mn was substituted for ($Zn_{1/2}Ti_{1/2}$) within B site. At this research, x=0.7 was selected since this composition revealed strong relaxor behavior which is suitable for ferroelectric instability study. Figure 7.8 showed dielectric constant and loss tangent of 0.3(BS-BZT)-0.7BT doped with Zr^{4+}, Cr^{3+} and Mn^{3+} ions. It is very clear to see dielectric constant decrease with Zr^{4+} doped but increase with Cr^{3+} and Mn^{3+} content. The dielectric loss showed that Zr^{4+} doped system has lowest loss at high temperature. The transition temperature increased with Cr^{3+} and Mn^{3+} doped. These results may indicate stability of ferroelectric was induced with doping Cr^{3+} and Mn^{3+}.

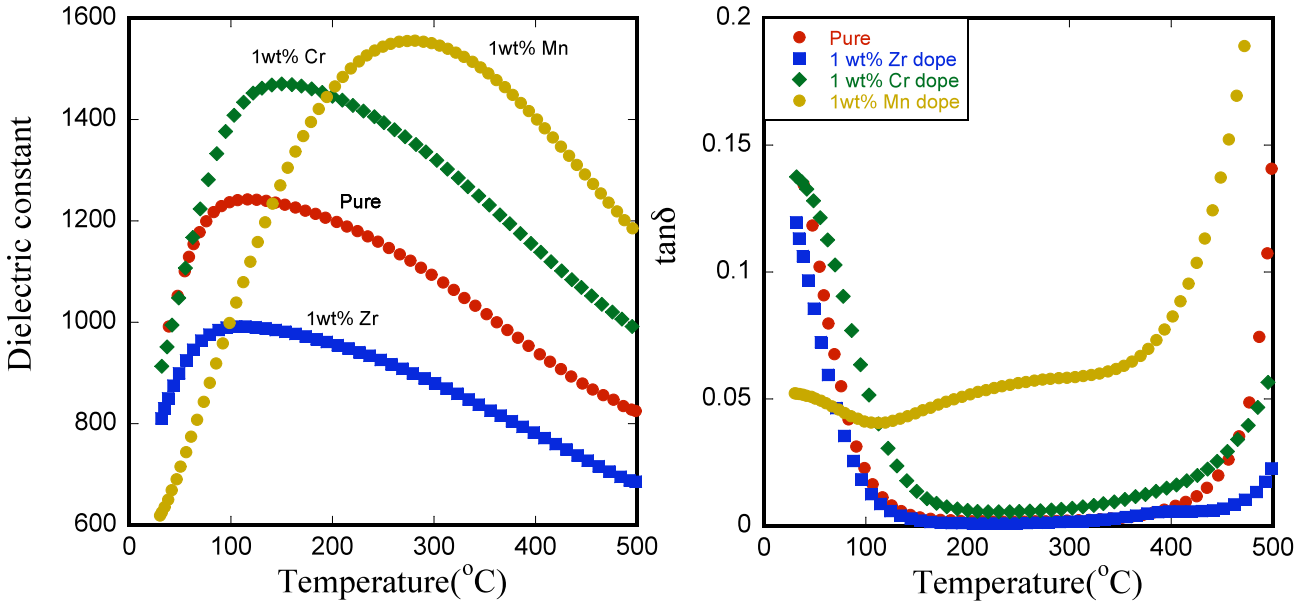

Figure 7.8 Dielectric constant and loss tangent of 0.3(BS-BZT)-0.7BT doped with Zr^{4+}, Cr^{3+} and Mn^{3+}.

7.4 Conclusion

Single phase perovskite was obtained for (1-x)(BS-BZT)-xBT for compositions containing at least 50 mole% $BaTiO_3$. The XRD data revealed that a MPB may exist between 5-8 mole% BS-BZT added to $BaTiO_3$. The dielectric characterization revealed that as BS-BZT was added to $BaTiO_3$ the phase transition become very diffuse. The relaxor ferroelectric behavior was likely due to complex cation ordering on the A-site and on the B-site. Due to the diffuseness of the phase transition, the compositions in this study exhibited a very stable dielectric constant greater than 1000 and low loss tangents (<0.01) over a wide range of temperature (T < 400°C).

7.5 Reference

1. R. E. Cohen, *Nature*358, 136 (1992).

2. R. Guo, L. E. Cross, S. -E. Park, B. Noheda, D. E. Cox and G. Shirane, *Phys Rev. Lett.*84, 5423 (2000).

3 C. F. Buhrer, *J. Chem. Phys*. 36, 798 (1962).

4 T. Takenaka, K. Maruyama and K. Sakata, *Jpn. J. Appl. Phys*. 30, 2236 (1991).

5 A. Sasaki, T. Chiba, Y. Mamiya and E. Otsuki, *Jpn. J. Appl. Phys*. 38, 5564 (1999).

6 R. E. Eitel, C. A. Randall, T. R. Shrout, P. W. Rehrig. W. Hackenberger and S. -E. Park, Jap. *J. Appl. Phys*. 40, 5999 (2001).

7 M. R. Suchomel and P. K. Davies, *J. Appl. Phys* 96, 1489 (2004).

8 M. R. Suchomel and P. K. Davies, *Appl.Phys. Lett*. 86, 262905 (2005).

9 I. Grinberg, and M. R. Suchomel, W. Dmowski, S. E. Mason, Hui Wu, P. K. Davies, and Andrew M. Rappe, *Phys.Rev. Lett*. 98, 107601 (2007).

10 Y. Y. Tomashpol'skii, E. V. Zubova, K. P. Burdina and Y. N. Venevtsev, *Soviet Phys*13, 859 (1969).

11 M. R. Suchomel, A. M. Fogg, M. Allix, H. Niu, J. B. Claridge and M. J. Rosseinsky, Chem. Mater. 18, 4987 (2006).

12 D. S. Tinberg and S. Trolier-McKinstry, *J. Appl. Phys*101, 024112 (2007)

13 B. Jaffe, W Cook, and H. Jaffe, *Piezoelectric Ceramics* (Academic, London, 1971).

14 Z. Yu, C. Ang, R. Guo, and A. S. Bhalla*, J. Appl. Phys* 92, 1489 (2002).

15 A. A. Bokov, Z. -G. Ye, *Solid State Commun.*116 ,105 (2000).

16 B. S. Kang, S. K. Choi, *Solid State Commun.*121, 441(2002).

CHAPTER 8

Summary and Future Work

8.1 Summary

In this chapter, the solubility, transition temperature, MPB compositions, ferroelectric/piezoelectric properties and annealing/doping effect of Bi-based perovskite will be summarized based on results outlined in the previous chapters.

8.1.1 Solubility of Bi(B'B")-ABO_3 Binary Compounds in the Perovskite Structure

Based on the results from former chapters, the relations of the perovskite phase stability for Bi(B'B")-ABO_3 (B'=Zn^{2+}, Ni^{2+}, Sc^{3+}, Y^{3+}, Ga^{3+}; B"=Ti^{4+}, Nb^{5+}, Ta^{5+}) to tolerance factor (t), equation 2.9, and the electronegativity difference between the cation and anion (EN), equation 2.10, were discussed.

Figure 8.1 summarizes the solubility of (a) $xBi(Zn_{1/2}Ti_{1/2})O_3$-$(1-x)ABO_3$ and (b) xBi(B'B")-$(1-x)BaTiO_3$ in terms of tolerance factor and electronegativity difference. The ABO_3 refers to a stable perovskite end member and Bi(B'B")O_3 indicates unstable Bi-based perovskite end members. The meshed area denotes that the solubility of $Bi(Zn_{1/2}Ti_{1/2})O_3$ is lower than 10mole%.

It is very clear to see that as the tolerance factor of ABO_3 increased, the solubility of $Bi(Zn_{1/2}Ti_{1/2})O_3$ also increased. It is also interesting to note that only alkaline-based ABO_3 compounds followed this rule. There is no clear trend for solubility as a function of electronegativity difference. Furthermore, from Figure 7.1b one can conclude that the solubility is less relevant with the tolerance factor of

unstable end member of $Bi(B'B'')O_3$ and only can be related to tolerance factor of the stable perovskite compound ABO_3.

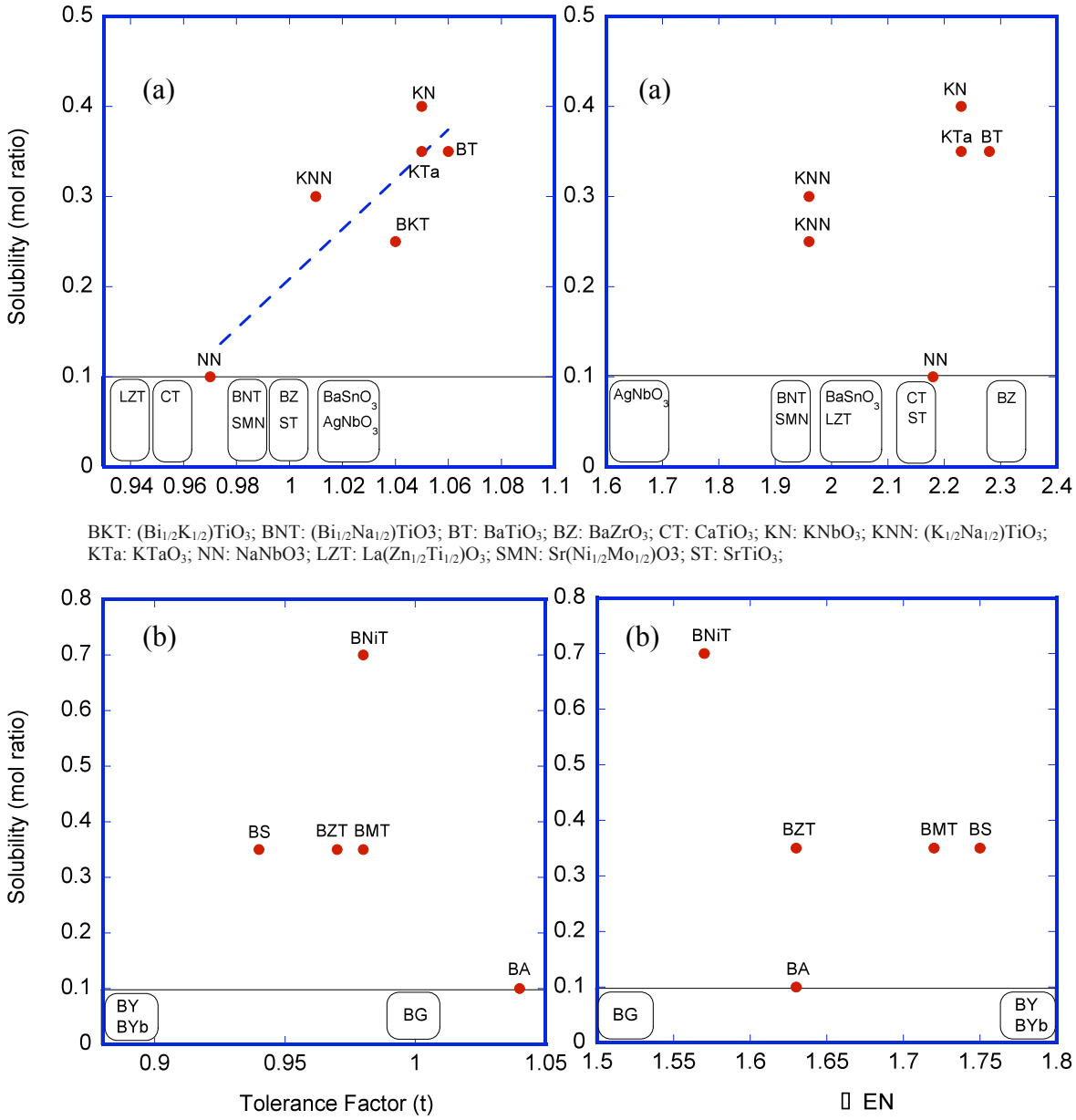

BKT: $(Bi_{1/2}K_{1/2})TiO_3$; BNT: $(Bi_{1/2}Na_{1/2})TiO3$; BT: $BaTiO_3$; BZ: $BaZrO_3$; CT: $CaTiO_3$; KN: $KNbO_3$; KNN: $(K_{1/2}Na_{1/2})TiO_3$; KTa: $KTaO_3$; NN: NaNbO3; LZT: $La(Zn_{1/2}Ti_{1/2})O_3$; SMN: $Sr(Ni_{1/2}Mo_{1/2})O3$; ST: $SrTiO_3$;

BNiT: $(Bi(Ni_{1/2}Ti_{1/2})O_3$; BZT: $(Bi(Zn_{1/2}Ti_{1/2})O_3$; BMT: $(Bi(Mg_{1/2}Ti_{1/2})O_3$; BS: $BiScO_3$; BY: $BiYO_3$; BYb: $BiYbO_3$;BG: $BiGaO_3$;

Figure 8.1 Solubility of (a) $xBi(Zn_{1/2}Ti_{1/2})O_3$-(1-x)ABO_3 and (b) xBi(B'B")-(1-x)$BaTiO_3$ in terms of tolerance factor and electronegativity difference.

8.1.2 Phase Transition for (1-x)Bi(B'B")O_3-xABO_3

Determined by dielectric data, the phase transition temperature as a function of Bi(B'B")O_3 content is plotted in figure 8.2. The trends in transition temperature can be classified into three groups. The transition temperature in group (I) decreased first until a phase transition appeared and then increased again. Examples of group (I) compositions in this study are (1-x)Bi(B'$_{1/2}$Ti$_{1/2}$)-x$BaTiO_3$ where B'=Zn^{2+}, Mg^{2+} and Ni^{2+}. The transition temperature in group (II) decreased linearly with increasing Bi(B'B")O_3 content until a second phase appeared. An example of a group (II) system is (1-x)Bi($Zn_{1/2}Ti_{1/2}$)O_3-x($Bi_{1/2}K_{1/2}$)TiO_3. The group (III) compounds showed a non-linear decrease in transition temperature as a function of Bi(B'B")O_3 content. Some examples of group (III) are (1-x)Bi($Zn_{1/2}Ti_{1/2}$)-xABO_3 where ABO_3=$KNbO_3$, $KTaO_3$ and $NaNbO_3$.

The absence of MPB compositions in groups (II) and (III) is due to the lack of phase transitions with compositional manipulation. Based on the data from this research, the trend of transition temperature depends on the ABO_3 stable perovskite instead of Bi(B'B")O_3 end members.

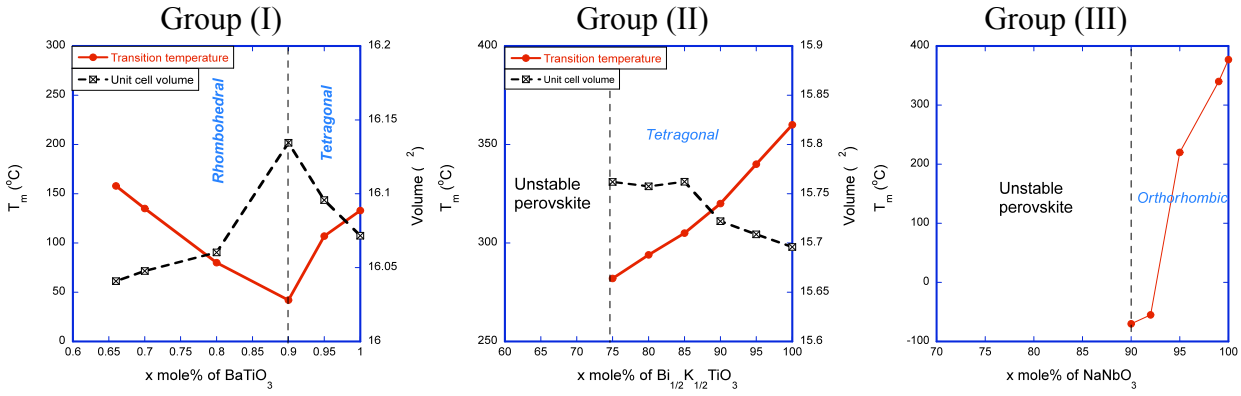

Figure 8.2 Transition temperature as a function of composition of (1-x)Bi($Zn_{1/2}Ti_{1/2}$)O_3-xABO_3

8.1.3 MPB Compositions

The MPB compositions in this study appeared in (1-x)$Bi(Zn_{1/2}Ti_{1/2})O_3$-x$BaTiO_3$ (BZT-BT) binary and (1-x)($Bi(Zn_{1/2}Ti_{1/2})O_3$-BiScO3)-x$BaTiO_3$(BS-BZT-BT) ternary system.

According to x-ray diffraction data, a morphotropic phase boundary (MPB) between tetragonal and rhombohedral perovskite phases was observed at x≈0.9. The phase relationship of the $Bi(Zn_{1/2}Ti_{1/2})O_3$-BiScO3-$BaTiO_3$ ternary system including MPB compositions is shown in figure 8.3. For compositions rich in $BaTiO_3$, the symmetry of the perovskite phase was tetragonal but with increased $Bi(Zn_{1/2}Ti_{1/2})O_3$and $BiScO_3$content the rhombohedral phase appeared. The dielectric characterization revealed that as $Bi(Zn_{1/2}Ti_{1/2})O_3$ content increased to the MPB composition, the transition peak became very diffuse and this system transferred from normal ferroelectric to relaxor ferroelectric behavior.

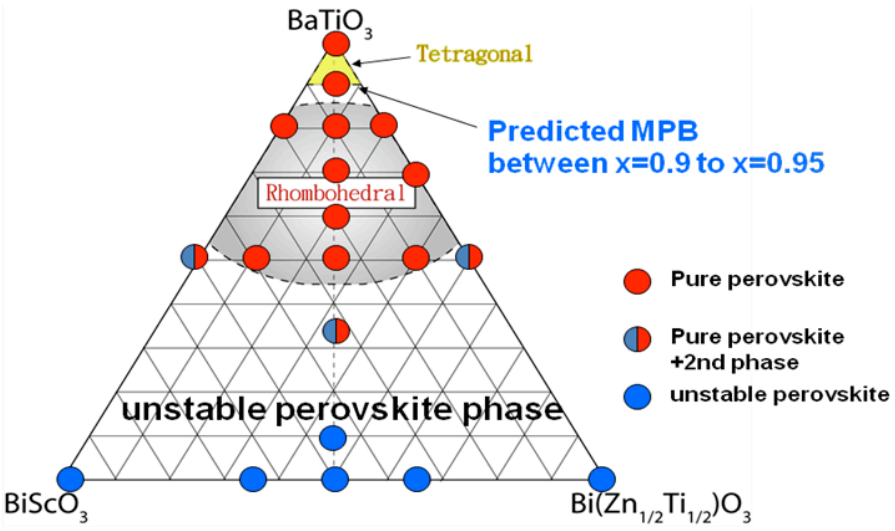

Figure 8.3 The phase relationship of the $Bi(Zn_{1/2}Ti_{1/2})O_3$-$BiScO_3$-$BaTiO_3$ ternary system including MPB compositions.

8.1.4 Ferroelectric and Piezoelectric Behaviors for (1-x)Bi(B'B")O_3-xABO_3

The discussions of ferroelectric and piezoelectric properties will be focused on $Bi(Zn_{1/2}Ti_{1/2})O_3$-xABO_3(BZT-ABO_3) perovskite since this system has higher break down voltage and higher resistance,which can broaden the measurement range, than other Bi(B'B")O_3-ABO_3compositions.

The polarization hysteresis data (P-E loops) at room temperature for *x*$Bi(Zn_{1/2}Ti_{1/2})O_3$-*(1-x)*$BaTiO_3$ indicated the remnant polarization (P_r) and coercive field (E_c) increased to 10.2 μC/cm and 11.3 KV/cm for 0.05BZT-0.95$BaTiO_3$ compared to pure $BaTiO_3$. However, when more BZT was added the area of hysteresis loops decreased dramatically. The absence of clear hysteresis behavior for higher BZT contents can be related to a decreased transition temperature. Although T_m increased for *x*>0.1, the relaxor behavior due to rhombohedral symmetry and possibly degree of higher disorder in the structure resulted in the disappearance of hysteresis loop.

The P-E loops for *x*$Bi(Zn_{1/2}Ti_{1/2})O_3$-(1-*x*)$(Bi_{1/2}K_{1/2})TiO_3$ revealed an increase in remanent polarization from 6.1μC/cm^2 to 11.5μC/cm^2 with the addition of 10 mole% BZT. The high electric field piezoelectric coefficient, d_{33}, for *x*=0, *x*=0.05, *x*=0.1 were 110 pm/V, 185 pm/V and 235pm/V, respectively. Overall, the dielectric and piezoelectric properties for $(Bi_{1/2}K_{1/2})TiO_3$ system showed significant improvement when BZT was added.

For the solid solutions of *x*$Bi(Zn_{1/2}Ti_{1/2})O_3$-(1-x)$NaNbO_3$the P-E loop and strain measurement presented the induced ferroelectric phase with 1 mol% $Bi(Zn_{1/2}Ti_{1/2})O_3$ substitutions. The piezoelectric coefficient, d_{33}, for the *x*=0.01 composition was 35 pm/V. However with more BZT added the result was a dramatic

decrease in ferroelectric and piezoelectric properties. Like the BZT-BT system, the absence of hysteresis behavior for higher BZT contents can be related to a decreased transition temperature and higher degree of disorder for cations.

Based on the results for all of the BZT-ABO_3 compositions, one can conclude that the ferroelectric behavior will be induced by very small amount of BZT added. However, a higher ratio of BZT will result in loss of ferroelectric and piezoelectric behavior except BZT-BKT system.

8.1.5 Annealing and Doping Effect

Based on XRD and dielectric data, no significant long range ordering appeared after 64 hours annealing for BZT-BT, BZT-BKT, BZT-NN and BZT-BS-BT solid solutions. This may due to the complex structure which has at least two cations in A site and two cations in B site. However the high temperature tan δ decreased with increasing sintering hours which may indicate the reduction in oxygen vacancies.

Although there is no long range ordering observed from XRD for all of doped samples, the increase of cation order region still can be described by the increased transition temperature and wider P-E loops. The effects of replacing Li^+ for Na^+ in the composition $0.1Bi(Zn_{1/2}Ti_{1/2})O_3$-$0.9NaNbO_3$ resulted in higher transition temperature and wider P-E hysteresis loop. This indicates that the stability of the ferroelectric phase was enhanced with the addition of Li. For 0.3(BS-BZT)-0.7BT solid solutions, 1wt% of Zr^{4+}, Cr^{3+} and Mn^{3+} was substituted for $(Zn_{1/2}Ti_{1/2})$ within B site. The phase transition peaks became more diffuse with Zr^{4+} doping but became sharper with Cr^{3+} and Mn^{3+} doping. The dielectric loss showed that Zr^{4+} doped compositions had the

lowest loss at high temperatures. The transition temperature increased with Cr^{3+} and Mn^{3+} doping. These results may indicate that the stability of the ferroelectric was induced with Cr^{3+} and Mn^{3+}doping for the relaxor BS-BZT-BT system.

8.2 Future Work

8.2.1 Enhancement of Piezoelectric Properties in Lead-Free Bi(B'B")-ABO_3

According to the experimental data obtained from this research, the piezoelectric and ferroelectric properties Bi(B'B")-ABO_3 still cannot compare with lead-based piezoelectric ceramics. All of the transition temperatures decreased with increasing Bi(B'B")O_3 content. Furthermore, the system transferred from the normal ferroelectric state to a relaxor ferroelectric state with just small amount of Bi(B'B")O_3. This represents a significant obstacle in developing a good piezoelectric material since the ferroelectric behavior is very essential.

In order to investigate the enhanced properties piezoelectric, the stable ferroelectric behavior must be maintained. There are two possible ways to develop ferroelectric properties in Bi(B'B")-ABO_3 system. First, there still many stable ABO_3 perovskite that have not yet been used for Bi(B'B")-ABO_3 solid solutions. As mentioned from the former conclusions, the phase transition temperature and ferroelectric behavior are strongly related to the stable ABO_3 perovskite. These stable ABO_3 perovskites are not necessarily ferroelectrics since the experimental data already proved that ferroelectric properties can be induced from an anti-ferroelectric with BZT substitution. Second, as mentioned in the discussion of the BZT-NN system in chapter 6 and the BS-BZT-BT ternary system in chapter 7, the ferroelectric

behavior can be induced or enhanced by small amount dopant. BKT may be a good candidate for doping since the transition temperature still remains high after substitution BZT. Further, the density of BKT can be enhanced by substitution of BZT which is suitable for high electric field measurements.

There is no long-range ordering confirmed by XRD for Bi(B'B")-ABO_3 system, however the sharper transition peaks and higher transition temperature may indicate the growth of polar nano-region. In order to investigate the degree of order within these regions, the Raman spectroscopy will be employed to measure doping and annealing effect in terms of cations short-range ordering.

8.2.2 Application in other fields

It was observed that Bi(B'B")-ABO_3 solid solutions, especially in $Bi(Zn_{1/2}Ti_{1/2})O_3$-based system, have very stable dielectric constants and low losses at high temperatures. For most stable perovskites in this research the density was increased when BZT was added. It makes this kind of materials very desirable for high temperature capacitance applications. Furthermore, the high electric field P-E loops for 0.15BS-0.15BZT-0.3BT revealed an unsaturated permittivity which is shown in figure 8.4. The dielectric constant can be expressed by the slope of P-E loop. In most ferroelectric materials the dielectric constant will dramatically decrease due to saturation at relatively low electric fields, e.q. $BaTiO_3$ and $Pb(ZrTi)O_3$. In Bi(B'B")-ABO_3 solid solutions, it may be useful to explore high energy density applications since this system has a relatively high dielectric constant under high electric field. Quantitatively, the stored energy density is given by:

$$U = \frac{1}{2}\varepsilon_0 \varepsilon_r E^2 \qquad (8.1)$$

Where ε_o is the permittivity of free space, ε_r is the relative dielectric constant, and E is the electric field applied to the samples. In order to increase the break down voltage of Bi(B'B")-ABO_3 system, the samples must be made into thin films to minimize the defects within the samples.

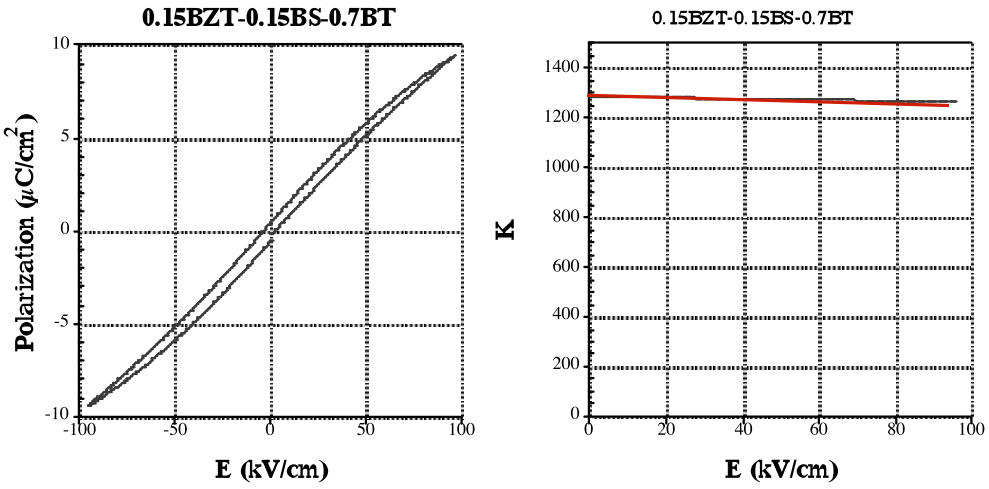

Figure 8.4 P-E loop and dielectric constant as a function of applied electric field for 0.15BZT-0.15BS-0.7BT solid solution.

Another application for Bi(B'B")-ABO_3 may be as a long-term actuator. From dielectric data for 0.1BZT-0.9BKT solid solutions, the decrease in the high temperature dielectric loss may indicate the suppression of defects in this system. The reason for fewer defects existing within this system may due to the relative low sintering temperatures. In most cases, the fatigue failure for actuators comes from

point defects, e.g. oxygen vacancies. Therefore, lead free Bi(B'B")-ABO_3 materials may be suitable for developing durable actuators.

Bibliography

1. Z. Yu, C. Ang, R. Guo, and A. S. Bhalla, J. Appl. Phys 92, 1489 (2002).

2. R. J. Cava, T. Siegrist, W. F. Peck, Jr., J. J. Krajewski, B. Batlogg and J. Rosamilia, Appl. Rev. 44, 9746 (1991).

3. I. P. Raevski and S. A. Prosandeev, J. Phys. Chem. Solids 63, 1939 (2002).

4. C. F. Buhrer, J. Chem. Phys. 36, 798 (1962).

6. Y. Hiruma, R. Aoyagi, H. Nagata and T. Takenaka, Jpn. J Appl. Phys. 44, 5040 (2005).

7. H. Nagata, T. Takenaka, Jpn. J Appl. Phys. 36, 6055 (1997)

8. A. Sasaki, T. Chiba, Y. Mamiya and E. Otsuki, Jpn. J. Appl. Phys. 38, 5564 (1999).

9. Y. Y. Tomashpol'skii, E. V. Zubova, K. P. Burdina and Y. N. Venevtsev, Soviet Phys 13, 859 (1969).

10. Curie & J. Curie, "Developement by Pressure of Polar Electricity in Hemihedral Crystals with Inclined Faces," Bulletin de la SocieteMineralique de France, 3 90 (1880).

11. K. Uchino, Ferroelectric Devices, Marcel Dekker,Inc., New York (2000).

12. A. S. Bhalla, R. Guo, R. Roy, Mat. Res. Innovat. 4 3 (2000).

13. S. O. Kasap, Electronic Materials and Devices, McGraw-Hill, New York (2006).

14. B. Jaffe, W. R. Cook, H. Jaffe, Piezoelectric Ceramics, Academic Press, New York, (1971).

15. J. Valasek, Phys. Rev. 17, 475 (1921).

16. V. K. Pecharsky and P. Y. Zavalij, Fundamentals of Powder Diffraction and Structure Characterization of Materials, Kluwer Academic, Boston (2003).

17. W. D. Kingary and W. R. Cook, Introduction to Ceramics, Wiley and Son Inc., New York, (1976).

18. G. A. Smolenskii and A. L. Agranovskaya, Sov. Phys.-Tech. Phys.,1380 (1958).
19. C. A. Randall, A. S. Bhalla, T. R. Shrout, and L. E. Cross, J. Mater. Res. 5, 829 (1990).
20. B. S. Kang, S. K. Choi, Solid State Commun. 121, 441 (2002).
21. A. A. Bokov, Z.-G. Ye, J. Mater. Sci. 41, 31(2006).
22. G. A. Samara and E. L. Venturini, Phase Transitions 79, 21 (2006).
23. A. Navrotsky, Physics and Chemistry of Earth Materials, Cambridge University, Cambridge (1994).
24. O. Muller, R. Roy, The Major Ternary Structural Families, Springer-Verlag, New York (1974).
25. A. Halliyal, T. R. Gururaja, U. umar and A. Safari, IEEE 6th International Sympoosium on Application of Ferroelectrics, 437 (1986).
26. N. Wakiya, N. Ishizawa, K. Shinozaki and N. Mizutani, Mater. Res. Bull. 30, 1121 (1995).
27. A. Simon, J .Ravez and M. Maglione, J. Phys.:Condens.Matter16, 963 (2004).
28. N. Yasuda, H. Ohwa and S . Asano, Jpn. J. Appl. Phys. 35, 5099 (1996).
29. G. A. Smolenskii, Jpn. J. Appl. Phys. 28 (1970).
30. D. Viehland, S. J. Jang, L. E. Cross and M. Wuttig, J. Appl. Phys. 68, 2916 (1990).
31. C. A. Randall and A. S. Bhalla, Jpn. J. Appl. Phys. 29, 327 (1990).
32. P. K. Davies and M. A. Akbas, J. Phys. Chem. Solids 61, 159 (2000).
33. R. Tarvin, P. K. Davies, J. Am. Ceram. Soc. 87,859 (2004).
34. V. A. Isupov, Ferroelectrics 315, 123 (2005).
35. R. Guo, L. E. Cross, S. -E. Park, B. Noheda, D. E. Cox and G. Shirane, Phys Rev. Lett. 84, 5423 (2000).
36. S. W. Choi, T. R. Shrout, S. J. Jang & A. S. Bhalla, Ferroelectrics100, 29 (1989).

37. C. Duran, S. Trolier-McKinstry and G. L. Messing, Journal of Electroceramics 10, 47 (2003).

38. R. E. Cohen, *Nature* 358, 136 (1992).

39. F. Sugawara, S. Iida, Y. Syono, and S. Akimoto, J. Phys.Soc. Jpn. 25, 1553 (1968).

40. T, Atou, H. Chiba, K. Ohoyama, Y. Yamaguchi. Y. Syono, J.Solid State Chem. 145, 639 (1999).

41. L.E. Orgel, J. Chem. Soc. 1959, 3815 (1959).

42. G.W. Watson, S.C. Parker, G. Kresse, Phys. Rev. B, 8481 59 (1999).

43. R. Seshadri and N. A. Hill Chem. Mater.13, 2892 (2001).

44. G. A. Smolenskii, V. A. Isupov, A. I. Ggranovskaya and N. N. Krainik, Soviet Physics Solid State 2, 2651 (1961).

45. K. Prasad, Lily, K. Kumari and K.L. Yadav, J. Phys. Chem. Solids 68, 1508 (2007).

46. J.-H. Park, P. M. Woodward, J. B. Parise, R. J. Reeder, I. Lubomirsky and O. Stafsudd, Chem. Mater. 11, 177 (1999).

47. T. Takenaka, K. Maruyama, K. Sakata, Jpn. J. Appl. Phys. 30 Part 1 (9B), 2236 (1991).

48. Y. Hiruma, H. Nagata, T. Takenaka, J. Ceram. Soc Jpn, S. 112(5), S1125 (2004).

49. H. Nagata, M. Yoshida, Y. Makiuchi, T. Takenaka, Jpn. J. of Appl. Phys. 42(12), 7401 (2003).

50. J. A. Zvirgzds, P. P. Kapostins, J. V. Zvirgzde, T. V. Kruzina, Ferroelectrics 40, 75 (1982).

51. East, J.; Sinclair, D. C. J. Mater. Sci. Lett. 16, 422 (1997).

52. T. Takenaka, H. Nagata, J. Eur. Ceram. Soc. 25, 2693 (2005).

53. S. Zhao, G. Li, A. Ding, T. Wang, Q. Yin, J. Phys. D: Appl. Phys.39, 2277 (2006).

54. Y. Yuan, S. Zhang, X. Zhou, J. Liu, Jpn. J. Appl. Phys. 45, 831 (2006).

55. Thomas R. Shrout&Shujun J. Zhang, J Electroceram 19, 111 (2007).

56. T. Wada, K. Toyoike, Y. Imanaka and Y. Matsuo, Jpn. J. Appl. Phys. 40, 5703 (2001).

57. V. V. Ivanova, A. G. Kapyshev, Y. N. Venevtsev and G. S. Zhdanov, Izv. Akad. Nauk SSSR 26, 354 (1962).

58. R. C. Turner, P. A. Fuierer, R. E. Newnham, T. R. Shrout, Appl. Acoust. 41, 299 (1994).

59. R. E. Eitel, C. A. Randall, T. R. Shrout, P. W. Rehrig, W. Hackenberger, and S. -E. Park, Jpn. J. Appl. Phys. 40, 5999 (2001).

60. C. A. Randall, R. Eitel, B. Jones and T. R. Shrout, J. Appl. Phys.95, 3633 (2004).

61. D. I. Woodward, I. M. Reaney, R. E. Eitel and C. A. Randall, J.appl. phys. 94, 3313 (2003).

62. S. M. Choi, C. J. Stringer, T. R. Shrout and C. A. Randall, J. Appl. Phys. 98, 034108 (2005).

63. C. J. Stringer, R. E. Eitel, T. R. Shrout and C.A. Randall, J. Appl. Phys. 97, 024101 (2005).

64. M. R. Suchomel and P. K. Davies, Appl. Phys. Lett. 86, 262905 (2005).

65. D. M. Stein, M. R. Suchomel and P. K. Davies, Appl. Phys. Lett. 89, 132907 (2006).

66. C. J. Stringer, T. R. Shrout, C. A. Randall, I. M. Reaney, J. Appl. Phys. 99, 024106 (2006).

67. I. Grinberg, M. R. Suchomel, W. Dmowski, S. E. Mason, Hui Wu, P. K. Davies and A. M. Rappe. Phys. Rev. Lett.98, 107601 (2001).

68. J. S. Reed, Principles of Ceramics Processing, Wiley Interscience, New York (1995).

69. D. C. Sinclair and A. R.West, J. Appl. Phys. 66, 3850 (1989).

70. Electrical Measurement Method for Piezoelectric Ceramic Elements (Standards of Electronic Materials Manufacturers Association of Japan, April 1993) EMAS-6100.

71. R. E. Eitel, C. A. Randall, T. R. Shrout and S. -E. Park, Jap. J. Appl. Phys. 41, 2099 (2002).

72. M. R. Suchomel and P. K. Davies, J. Appl. Phys 96, 1489 (2004).

73. C.-C. Huang, D.P. Cann, X. Tan, and N. Vittayakorn, J. Appl. Phys. 102, 044103 (2007).

74. O. Bidault, P. Goux, M. Kchikech, M. Belkaoumi, M. Maglione, Phys. Rev. B 49, 7868 (1994).

75. K. Uchino, S. Nomura, *Ferroelectrics Lett*. **44**, 55 (1982).

76. S.-E. Park and T. R. Shrout, J. Appl. Phys. 82, 1804 (1997).

77. V. A. Bokov and I. E. Myl`nikova, Sov. Phys.-Solid state 3, 631 (1961).

78. M. R. Suchomel, A. M. Fogg, M. Allix, H. Niu, J. B. Claridge, and M. J. Rosseinsky, Chem. Mater. 18, 4987 (2006).

79. Y. Hiruma, H. Nagata, and T. Takenaka, Jpn. J. Appl. Phys. 46, 1081 (2007).

80. Z. Zhao, V. Buscaglia, M. Viviani, M. T. Buscaglia, L. Mitoseriu, A. Testino, M. Nygren, M. Johnsson, and P. Nanni, Phys. Rev. B. 70, 024107 (2004).

81. H. D. Megaw, Ferroelectrics 7, 87 (1974).

82. C. N. W. Darlington and K.S. Knight: ActaCryst. B55, 24 (1999).

83. S. Lanfredi, M. H. Lente and J. A. Eiras: Appl. Phys. Lett. 80, 2731 (2002).

84. T. Nitta: J. Am. Ceram. Soc. 51, 626 (1966).

85. M. A. L. Nobre and S. Lanfredi: J. Appl. Phys. 93, 5557 (2003).

86. G. Shirane, R. Newnham and R. Pepinsky: Phys. Rev. 96, 581 (1954).

87. G. A. Smolenskii, V. A. Bokov, V. A. Isupov, N. N. Krainik, R. E. Pasynkov, A. I. Sokolov: Ferroelectrics and Related Materials, (Gordon & Breach, New York, 1984) p. 634.

88. H. Iwasaki and T. Ikeda: J. Phys. Soc. Jap. 18, 157 (1963).

89. I. Grinberg, and M. R. Suchomel, W. Dmowski, S. E. Mason, Hui Wu, P. K. Davies, and Andrew M. Rappe, Phys.Rev. Lett. 98, 107601 (2007).

90. D. S. Tinberg and S. Trolier-McKinstry, J. Appl. Phys101, 024112 (2007).

91. A. A. Bokov, Z. -G. Ye, Solid State Commun.116 ,105 (2000).

Appendix

Complete ionic radius, electronegativity and atomic mass of the element used in this research

A site	Radius[1]	EN[2]	Mass[2]
Li+	1.24	0.98	6.9
Na+	1.39	0.93	23
K+	1.64	0.82	39.1
Rb+	1.72	0.82	85.5
Cs+	1.88	0.79	132.2
Ag+*	1.53	1.93	107.9
Ca2+	1.34	1	40.1
Sr2+	1.44	0.95	87.6
Pb2+	1.49	2.33	207.2
Ba2+	1.61	0.89	137.3
Ce3+	1.34	1.12	140.1
La3+	1.36	1.1	138.9
Bi3+*	1.45	2.02	209

B site	Radius[1]	EN[2]	Mass[2]
Mg2+	0.72	1.31	24.3
Mn2+	0.67	1.55	54.9
Ni2+	0.69	1.91	58.7
Zn2+	0.74	1.65	65.4
Fe3+	0.645	1.83	55.9
Al3+	0.535	1.61	27
Ga3+	0.62	1.81	69.7
In3+	0.8	1.78	114.8
Mn3+	0.58	1.55	54.9
Sc3+	0.745	1.36	45
Y3+	0.9	1.22	88.9
Yb3+	0.868	1.1	173.04
Ti4+	0.605	1.54	47.9
Sn4+	0.69	1.96	118.7
Zr4+	0.72	1.33	91.2
Hf4+	0.71	1.3	178.5
V5+	0.54	1.63	50.9
Nb5+	0.64	1.6	92.9
Ta5+	0.64	1.5	181
Mo6+	0.61	2.16	95.9
W6+	0.6	2.36	74

O	Radius	EN
O2-	1.4	3.44

Reliable data

Based on calculation

*extropolation

Radius for A site is based on 12-fold correction,
B site is based on 6-fold correction.

1. Radius data are based on R. D. Shannon, Acta Cryst. A32, 751 (1976)

2. Electronegativity and Mass are based on http://www.webelements.com/

Complete perovskite tolerance factor, electronegativity and atomic mass difference between A site and B site used in this research

None Bi End member	t[1]	EN[2]	MA-MB
$AgNbO_3$	1.02	1.68	15
$BaTiO_3$	1.06	2.23	135.76
$BaSnO_3$	1.02	2.02	18.6
$BaZrO_3$	1.00	2.33	46.1
$(BiNa)TiO_3$	0.99	1.93	68.1
$(BiK)TiO_3$	1.04	1.96	76.15
$CaTiO_3$	0.97	2.17	-7.8
$CsNbO_3$	1.14	2.25	39.3
$KNbO_3$	1.05	2.23	-53.8
$KTaO_3$	1.05	2.28	-141.9
$La(ZnTi)O_3$	0.94	2.09	82.25
$NaNbO_3$	0.97	2.18	-69.9
$(NaK)NbO_3$	1.01	1.96	-61.85
$PbTiO_3$	1.02	1.51	159.3
$PbZrO_3$	0.96	1.61	116
$RbNbO_3$	1.08	2.23	-7.4
$RbTaO_3$	1.08	2.28	-95.5
$Sr(NiMo)O_3$	0.98	1.95	10.3
$SrTiO_3$	1.00	2.20	39.7

Bi-based End member			
$Bi(ZnTi)O_3$	0.97	1.63	152.35
$BiScO_3$	0.94	1.75	164
$Bi(NiTi)O_3$	0.98	1.57	155.7
$Bi(MgTi)O_3$	0.98	1.72	172.9
$BiAlO_3$	1.04	1.63	182
$BiGaO_3$	1.00	1.53	139.3
$Bi(MgW)O_3$	0.96	1.64	172.275
$Bi(MgZr)O_3$	0.95	1.51	151.25
$BiInO_3$	0.92	1.54	94.2
$BiYO_3$	0.88	1.82	120.1

Illuminite
Perovskite is not available

1. Radius data are based on R. D. Shannon, Acta Cryst. A32, 751 (1976)
2. Electronegativity and Mass are based on http://www.webelements.com/